UNIVERSITY OF CALIFORNIA
RIVERSIDE

The Role of the Energy-Sensing AMP-Activated Protein Kinase in Intestinal Epithelial Physiology and Pathophysiology

A Dissertation submitted in partial satisfaction
of the requirements for the degree of

Doctor of Philosophy

in

Biomedical Sciences

by

Stephanie J. King

December 2019

Dissertation Committee:

Dr. Declan F. McCole, Chairperson
Dr. Christian Lytle
Dr. Frances Sladek

The Dissertation of Stephanie J. King is approved:

Committee Chairperson

University of California, Riverside

Acknowledgments

I have heard School of Medicine Dean Deborah Deas quote this African proverb many times over my graduate education, "If you want to go fast, go alone. If you want to go far, go together." Completion of this dissertation is a shining example of this wise proverb. The work presented herein would not have been possible without 'my village' - people who have supported me educationally, emotionally, mentally, financially, and socially.

I would first like to thank the wonderful members of the McCole Laboratory for all of their help, patience, and support these past few years. Rosie Alvarez taught me how a lab runs and how to manage and perform animal experiments. Dr. Ali Shawki taught me the intricacies of data analysis and at times provided much needed advice. Dr. Moorthy Krishnan taught me patience and how to work with others. My undergraduate mentees Kyrillos Girgis and Destani Ross taught me how to teach and were of considerable help maintaining the lab, preparing samples, and running experiments. Vinicius Canale, Alina Santos, Dr. Marianne Spalinger, and Pritha Chatterjee were supportive peers and I thank them for sharing all of the growing pains of a Ph.D. and the celebrations of our successes.

I would like to thank my collaborators Dr. Hashini Batugedara, Dr. Meera Nair, Dr. Christian Lytle, Dr. Nancy Lainez, Dr. Djurdjica Coss, and Dr. Russell Jones for teaching me, troubleshooting experiments with me, and kindly sharing resources.

I have a number of mentors who deserve mention as their guidance and advice kept me motivated during trying times. I thank my dissertation committee members, Dr. Frances Sladek and Dr. Christian Lytle, who helped guide my research, provided invaluable feedback, and supported my research career. Dr. Djurdjica Coss, Dr. David Lo, Dr. Monica

Carson, Dr. Emma Simmons, and Dr. Shaun Bowler for their encouragement and career advice. Dr. Kim Barrett for coaching my writing and professional development. Dr. Emma Wilson for helping me face hard truths to change for the better and being my cheerleader as I did. For all of the support I received in the context of my work, there was just as much in the way of friends of family. To my fur therapists, here and gone, thank you for your cuddles and unconditional love. Thank you to my team of graduate advocacy heroes Maiko Le Lay, Shawn Ragan, Siddharth Agarwal, and Arielle Manganiello for helping me see how we can make this journey better for others and fighting for it. To Tim Ngo, who was a friend, a scientist, and a teacher. To my Lil' Sibs Anthony Perez and Jessica Noll, thank you for your encouragement and company. Thank you to Dr. Jessica Jang and Dr. Marcy Martin for listening to my whinging and making it better with food, travel, bingewatching, and giraffes & rhinoes.

A very special thank you to Anica Sayoc for being the realest and the kindest. You are extraordinary and I would have had a much tougher time without your shoulder to lean on.

To my mentor and advisor Dr. Declan McCole, a very sincere thank you for taking me under your wing and never losing hope. You taught me the ups and downs and the sometimes down again of science. I am truly grateful for the opportunity you gave me, your unwavering support, and your example. You made graduate school what it should be for all students, a positive place to challenge yourself intellectually and personally, pursuing knowledge for the sake of curiosity. Thank you.

Finally to my Family. Thank you to my brother for reminding me there is life outside the lab and fun to be had. Thank you to my grandparents for homecooked meals

and love. Thank you to my parents for teaching me to believe in the impossible and giving me the persistance to chase it. Thank you to my husband Chris for being my perfect foil and my partner.

The text of this dissertation, in part or in full, is a reprint of the material as it appears in the *American Journal of Physiology - Gastrointestinal and Liver Physiology* 2019 (Chapter 2, Chapter 3). The co-author Declan F. McCole listed in that publication directed and supervised the research which forms the basis for this dissertation.

To my husband and my parents for all the support and love.

ABSTRACT OF THE DISSERTATION

The Role of the Energy-Sensing AMP-Activated Protein Kinase in Intestinal Epithelial Physiology and Pathophysiology

by

Stephanie J. King

Doctor of Philosophy, Graduate Program in Biomedical Sciences
University of California, Riverside, December 2019
Dr. Declan F. McCole, Chairperson

AMP-Activated Protein Kinase (AMPK) is a cellular energy sensor that regulates metabolic processes. The downstream effects of AMPK activation differ by type of stimulation, cell type or tissue, and state of the microenvironment. Various groups have suggested AMPK plays a protective role in the intestinal epithelium during both homeostasis and inflammation, however these studies have overlooked the need for increased specificity in order to definitively determine the effects of AMPK. In this study, I used *in vitro* and tissue-specific *in vivo* model systems to test the impact of AMPK activity at baseline and in different models of inflammation. I observed changes in intestinal permeability, protein and gene expression, transporter responses, and inflammatory signaling using molecular and physiological methodologies. I confirmed that AMPK does regulate intestinal barrier function during homeostasis, but that loss of these actions does not confer increased susceptibility to experimental colitis or pathogenic enteric infection. AMPK promotes barrier function through expression of the barrier-forming tight junction protein Claudin-4 and acts as an inhibitor of calcium-dependent electrogenic ion transport through repression of

expression of the basolateral $Na^+/K^+/2Cl^-$ cotransporter 1 (NKCC1). In addition, the regulatory effects of AMPK are maintained during oxidative stress where calcium-dependent electrogenic ion transport is suppressed due to AMPK-dependent phosphorylation and decreased activity of NKCC1. Loss of epithelial AMPKα resulted in decreased cell death during experimental colitis, however this did not ultimately impact course and severity of the disease as measured through histological scoring, colon shortening, and intestinal permeability. Finally, epithelial AMPKα-deficiency did not render mice more sensitive to infection with the murine enteric pathogen *Citrobacter rodentium* as they displayed similar levels of bacterial burden. These data suggest AMPK plays a minor role in maintenance of the intestinal epithelium and that its association with protection in models of colitis could in part be due to other signaling molecules or AMPK activity in other cell types. Further work to more specifically modulate AMPK activity in the intestinal epithelium is needed to confirm if AMPK is anti- or pro-inflammatory in various contexts within the intestinal epithelium.

Contents

List of Figures

List of Tables

1 | Introduction

1.1 AMP-Activated Protein Kinase

AMP-Activated Protein Kinase (AMPK) is a master regulator of cellular energy levels whose canonical function is to relieve energetic stress (decreased availability of ATP) by modulating cellular metabolic pathways. It is a highly conserved heterotrimeric protein expressed ubiquitously in eukaryotic tissues. For example, AMPK orthologues have been identified in *Saccaromyces cerevisiae*, *Drosophila melanogaster*, *Caenorhabditis elegans*, and *Arabidopsis thaliana*, demonstrating its importance across phyla [1–4]. The function of AMPK has been well-studied in diseases such as obesity, diabetes, cardiovascular disease, metabolic syndrome, and cancer [5–7]. However, little is known about the role of this kinase at the main site of nutrient assimilation in the body: the gastrointestinal tract.

1.1.1 Activation and Regulation

Canonical activation of AMPK occurs through phosphorylation of a specific Threonine residue within the activation loop of the α catalytic subunit (hereafter activation loop Threonine) resulting in >100-fold increase in kinase activity in response to intracellular increases in AMP, ADP and/or Ca^{2+} [8]. Phosphorylation of the activation loop Threonine

is performed by upstream kinases, the most prominent of which is Liver kinase B1 (LKB1) encoded by *STK11*. LKB1 is a tumor suppressing kinase whose gain-of-function germline mutation is known to cause Peutz-Jeghers syndrome in humans, characterized by non-cancerous hamartomatous polyps in the gastrointestinal tract and increased risk of tumor development. Twelve AMPK-related kinases have been identified, all of which are activated by LKB1 [9]. LKB1 is constitutively active and its activity is regulated by posttranslational modifications [10]. Preferential activation by LKB1 has been shown in skeletal muscle and heart where loss of LKB1 reduced AMPKα2 activity, with little effect on AMPKα1 [11, 12]. Binding of AMP and ADP to the γ subunit of AMPK causes a conformational change that promotes phosphorylation of the activation loop Threonine and may discourage dephosphorylation by PP2Cα while ATP binding antagonizes these actions [8, 13–18]. In addition to changes in energy status, increases in intracellular calcium can also activated AMPK via the Ca^{2+}/Calmodulin-dependent Kinase Kinase β (CaMKKβ) [19–22]. Activation by CaMKKβ is LKB1- and AMP/ADP-independent, although AMPK still retains sensitivity to the levels of adenine nucleotides [23]. Activation of AMPK by CaMKKβ typically occurs during cellular stress such as hypoxia, loss of cell-cell contacts or detachment, and amino acid starvation [24–27].

1.1.2 Subunits and Structure

Each AMPK subunit exists as multiple isoforms and each isoform is encoded by a distinct gene. These are expressed in a tissue-specific manner and, in some cases, display preference in subcellular localization. In addition, various heterotrimeric complexes appear to be regulated uniquely. For example, only 3 of the possible 12 complexes are present in skeletal

muscle and their activation is dependent on exercise intensity and duration [28–30]. Here I describe each subunit and the differences between each subunit isoform, as depicted in Figure 1.1.

The α catalytic subunit

Beginning from the N-terminus, the α catalytic subunit contains the catalytic kinase domain followed by the auto-inhibitory domain (AID). The kinase domain consists of N- and C-lobes and an activation loop containing the activating phosphorylation site (Threonine-172, although the exact location differs by species and isoform) [31]. The AID consists of a bundle of three helices capable of repressing AMPK activity at baseline by restricting movement of helix αC, of the kinase domain [17, 32, 33]. The auto-inhibitory domain is followed by two α-regulatory interacting motifs (α-RIMs) which bridge the auto-inhibitory domain with the regulatory core of the heterotrimeric complex [34]. As alluded to earlier, the two α catalytic subunit isoforms, α1 and α2, are expressed differently in various tissues. For example, the α1 isoform is exclusively expressed in certain cell types including T cells, macrophages, and erythrocytes. In the liver, the α1 and α2 isoforms account for an equal proportion of all AMPK activity. The α1 isoform is predominantly expressed in adipose tissue while in skeletal muscle and cardiac tissue the α2 isoform is dominant. Apart from expression, the α catalytic isoforms are also unique in their localization where the α2 subunit is present in both the nucleus and cytoplasm due to the presence of a functional nuclear export signal at the C-terminus [35–37]. In contrast, the α1 isoform is limited to the cytoplasm and has been shown to associate with the plasma membrane in airway epithelial cells [38]. Differences in isoform activity and specifity have been suggested through the use of whole-body transgenic

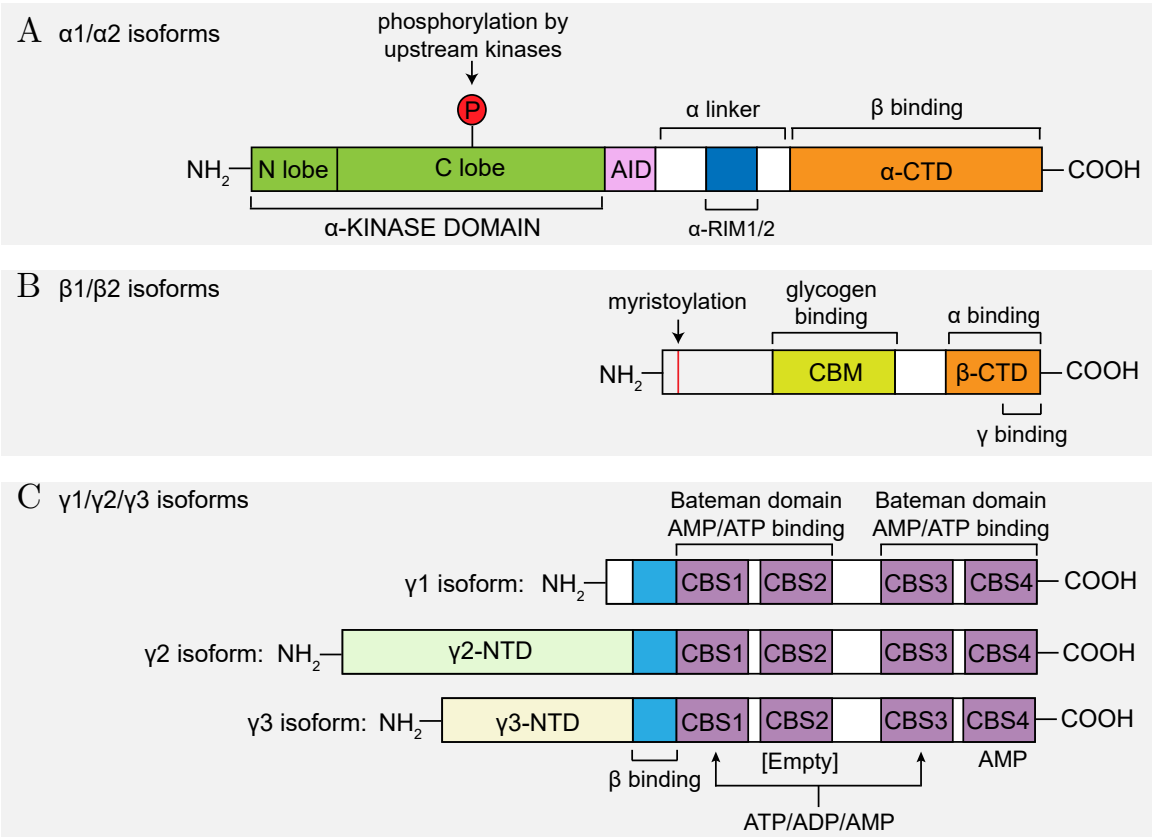

Figure 1.1: AMPK Subunit Isoforms and Domains

The alpha (A) and beta (B) subunit isoforms are of comparable length and structure, while the gamma (C) subunit isoforms have distinct N-terminal domains due to alternative splicing. Binding sites of the subunits in the heterotrimeric structure and regulatory sites are indicated. The α catalytic subunits contain the kinase domain and bind to the β subunits via the C-terminal domain. The β subunit is capable of myristoylation to facilitate AMPK association with lipid bilayers and the glycogen binding domain allows for carbohydrate regulation of the protein. The γ subunits function in nucleotide binding and vary in their sensitivity to this event. AID = autoinhibitory domain, RIM = regulatory interacting motifs, CTD = C-terminal domain, CBM = carbohydrate-binding module, CBS = cystathione β-synthase motif, NTD = N-terminal domain.

knockout animals where initial metabolic testing revealed distinct responses. For example, AMPKα2 knockout mice do not develop AMPK agonist-induced hypoglycemia and have an overt metabolic phenoype (insulin resistance and reduced glucose tolerance) whereas AMPKα1 knockout mice do and display anemia and splenomegaly. As mentioned earlier, different specificity of upstream kinases for the catalytic isoforms has also been reported where lack of LKB1 abolished ischemia-mediated activation of α2 but not α1 [11, 12]. The isoforms have an overall sequence similarity of 77% which increases to 90% in the catalytic domain. It is therefore unsurprising that the α1β1γ1 and α2β1γ1 complexes have identical specific activity (~6μmol/min/mg) and similar sensitivity to AMP binding [14]. However the α2 isoform is more readily deactivated by the phosphatase PP2Cα compared to the α1 isoform [39].

The β regulatory subunit

Two isoforms of the β subunit exist, β1 and β2, and they are thought to exert inhibitory regulation of the complex [40–42]. The isoforms are similar in length, are the smallest subunit in the complex, and contain 80% sequence similarity within the carbohydrate-binding module. The β subunit contains a myristoylation site at the N-terminus followed by a glycine-rich domain and a carbohydrate-binding module. Myristoylation is proposed to facilitate localization of AMPK to lysosomes in response to glucose starvation and binding of AMPK to mitochondrial membranes to promote selective autophagy [40, 43, 44]. The carbohydrate-binding module binds glycogen, allowing the kinase to sense sugar levels and modulate its activity accordingly [45–50]. In the heterotrimer, the carbohydrate-binding module sits atop the N-lobe of the catalytic α subunit [51–53]. The carbohydrate-binding

module is followed by a unique C-interacting helix. This structure associates with the B- and C-helices in the kinase domain of the α catalytic subunit and secures the nucleotide-binding domain of the γ subunit to the C-terminal domain of the α catalytic subunit [53].

The γ regulatory subunit

The γ subunit is largely composed of a region of motif repeats known as the cystathionine β-synthase motif. Pairs of these motifs form Bateman domains that have an ATP-binding cleft. The γ subunit contains four of the cystathionine β-synthase motifs that form a flat four-pointed surface, with one motif repeat located in each quadrant. This conformation creates four potential ligand-binding sites, however only three sites are occupied at any time [17, 53, 54]. Studies of the mammalian γ subunit determined that site 1 remains empty, site 4 is strongly bound to AMP, and sites 2 and 3 bind AMP and ADP competitively. There are three isoforms of the γ subunit and they differ in structure and sensitivity to nucleotide-binding. The γ1 isoform is largely composed of the nucleotide-binding domain alone while the γ2 and γ3 isoforms possess long N-terminal extensions with unknown structure and function. The nucleotide-binding domain is only 60% similar across all three isoforms, due to alternative splicing that generates the γ2 and γ3 isoforms [55]. Activity and sensitivity of isoforms are distinct and can be tissue-dependent. For example, the γ1 isoform has the highest activity of all the isoforms in most tissues, with the exception of the brain which has equal activity of all three isoforms. In addition, the γ2 isoform has the greatest sensitivity to AMP concentration in the brain while the γ3 subunit is the least sensitive [31, 56]. AMP binding to the γ2 and γ3 isoforms has little effect on Threonine-172 phosphorylation, however AMP binding to the γ1 subunit stimulates phosphorylation of Threonine-172 by

LKB1. Binding of AMP or ADP in all γ isoforms is protective against dephosphorylation of Threonine-172, although the γ2 isoform is the most sensitive to ADP binding.

1.1.3 Transgenic Knockout Animals

A major technical resource in advancing our understanding of the role(s) of AMPK *in vivo* has been the generation of transgenic animals lacking one or multiple AMPK subunit isoforms. However, complete loss of both α catalytic isoforms or β isoforms renders an embryonic lethal phenotype at ~10.5 days post-conception demonstrating the importance of AMPK activity during embryogenesis [57, 58]. Instead, animals lacking one catalytic isoform were initially generated. As mentioned previously, AMPKα2 knockout mice have a phenotype resembling Type 2 Diabetes although these mice lack a number of molecular features of the disease such as decreased insulin secretion by pancreatic islets, decreased glucose uptake in muscle and increased muscle lipid availability, and uptake of free fatty acids [59]. In contrast, AMPKα1 knockout mice display enlarged spleens and anemia, in part due to the exclusive expression of AMPKα1 in red blood cells that is critical for autophagy-dependent clearance during differentiation [60, 61]. Despite these advances, use of single-isoform knockout mice has been discouraged as previous work has shown compensatory increases in expression and activity of the remaining isoform, complicating conclusions drawn from these mice. For example, skeletal muscle from AMPKα2 knockout mice has increased expression of the α1 isoform yet a significant reduction in ACC phosphorylation persists, and this phenomenon is not observed in the liver from these mice [59]. In addition, muscle contraction in both AMPKα1 and AMPKα2 knockout mice increased AMPK activity to similar levels as wild-type mice, accompanied by increased expression of

the remaining catalytic isoform in both knockout mouse models [62]. This was also observed in kidney proximal tubules lacking either AMPKα1 or AMPKα2 and by lack of phenotype in mice with a chondrocyte-specific deletion of AMPKα1 [63, 64]. Further complicating matters, there does not seem to be any difference in substrate specificity in the catalytic isoforms [65]. For these reasons, researchers have turned to tissue-specific knockout models that allow ablation of multiple isoforms without a loss in viability.

1.1.4 Pharmacological Regulators

Due to its role in mediating metabolic homeostasis, there has been much work on the use of AMPK activation to combat symptoms and features of metabolic syndromes and oncogenic signaling. The majority of these studies have utilized pharmacological manipulation of AMPK activity, however some of these drugs have AMPK-independent effects that preclude researchers from specifically confirming if effects are directly downstream of AMPK. The type 2 Diabetes biguanide therapy, Metformin, is an AMPK activator used in many studies due to its clinical relevance. AMPK activation due to Metformin is indirect and occurs by inhibition of mitochondrial respiratory-chain complex 2 that increases the AMP:ATP ratio [66–69]. This was further confirmed when the mitochondrial respiratory-chain complex 2 inhibitor R419 was found to indirectly activate AMPK [70, 71]. However as alluded to earlier, Metformin can act independently of AMPK such as in its inhibition of hepatic gluconeogenesis [72, 73]. In addition, these effects can be context-dependent. For example, Metformin suppression of adipogenesis does not require AMPK and is instead mediated by mTOR/p70-S6K signaling in C3H10T1/2 mouse mesenchymal stem cells while AMPK activation in mouse embryonic fibroblasts potentiated this effect [74]. Another activator

of AMPK, 5-Aminoimidazole-4-carboxamide ribonucleotide (AICAR) is phosphorylated to ZMP, an AMP mimetic that can activate AMPK allosterically. AICAR has been used experimentally as a specific AMPK activator, however similar to Metformin it can also have AMPK-independent effects. AICAR can inhibit cytokine production and T cell activation in an mTOR-dependent manner in T cells and induce IL-6 secretion in mouse muscle independently of AMPK [75, 76]. Compound C, or Dorsomorphin ($C_{24}H_{25}N_{50}$; 6-[4-(2-piperidin-1-ylethoxy) phenyl]-3-pyridin-4-ylpyrazolo [1, 5-a] pyrimidine), is a selective AMPK inhibitor whose mechanism of AMPK activation has remained elusive [77]. Despite initial understanding of its specificity, Compound C has since been reported to inhibit a number of kinases to a similar degree or more efficiently than AMPK [78, 79]. To this end, a number of off-target effects of Compound C have also been observed [80, 81]. While these pharmacological agents can be used to understand AMPK function, it is essential to form conclusions cognizant of the limitations of these drugs.

1.2 Gastrointestinal Physiology

1.2.1 Anatomy and Functional Organization

The gastrointestinal tract consists of epithelia and its associated tissues beginning from the oral cavity and ending at the anus. Each organ of the gastrointestinal tract is responsible for a unique function. Within the intestine each segment also has a specialized function which is supported by distinct epithelial and tissue structure, composition of epithelial and immune cell subtypes, and other properties. For the purposes of this dissertation, our discussion will focus on the intestine. The small intestine is the main site of nutrient absorption and

includes the duodenum, jejunum and ileum. Its organization is highly specialized to increase the absorptive area. It consists of finger-like extensions known as villi that are covered by a single layer of columnar epithelial cells that are surrounded by 5-7 crypts known as the crypts of Lieberkühn. In addition, villus enterocytes have apical microvilli structures that form a brush border membrane to increase the surface area for absorption. The duodenum is the initial site of contact with chyme from the acidic environment of the stomach and thus has chemo- and mechanosensitive nerve endings that sense the composition of luminal contents and bicarbonate-secreting glands to protect the epithelia [82]. The jejunum is the longest intestinal segment where a majority of nutrient absorption occurs. The ileum has shorter villi than other segments of the small intestine and is the site of conjugated bile acid absorption. The ileum also has a large capacity for absorption in the event jejunal nutrient absorption is impaired. As a result, clinical nutrient malabsorption is unlikely. In the colon, villi disappear in favor of long colonic crypts and large folds of the tissue known as haustrae (plicae in mice) increase the absorptive area. The ascending colon (proximal colon in mice) is also the largest site of gut microbiota colonization, which plays an important role in the metabolism and absorption of certain nutrients, as well as maintenance of the intestinal barrier. Finally, the colon is a major site of fluid reabsorption that serves to restrict fluid loss by dehydrating fecal contents thereby initiating stool formation in advance of excretion and storage of fecal waste (descending colon and rectum). The intestinal epithelium is highly dynamic and composed of a number of specialized cell types critical for its function. These include differentiated secretory (Paneth, goblet, enteroendocrine, and secretory enterocytes) and absorptive cell lineages. Enterocytes refer to intestinal epithelial cells that can be secretory or absorptive in the small intestine while colonocytes refer to the

intestinal epithelial cells residing in the colon. Intestinal stem cells at the base of the crypt maintain a regenerative niche that supports complete turnover of the intestinal epithelium every 5 days. Newly divided intestinal epithelial cells at the crypt base have a secretory character that differentiates into a more absorptive character as they migrate towards the villus tip. It was previously thought that absorptive enterocytes had similar expression of macromolecule transporters, however recent work by Moor et al. has demonstrated there are regions of the villus where expression of certain macromolecule transporters is segregated, although how this is accomplished is still unknown [83]. Cells fated to become Paneth cells first migrate towards the lumen similar to enterocytes, however as they terminally differentiate they return to the crypt base where they secrete a number of antibacterial components such as antimicrobial peptides. Paneth cells are long-lived (>30 days) and are usually restricted to the small intestine, though they may develop in the colon during chronic inflammation [84, 85]. Enteroendocrine cells contain secretory granules of peptide hormones that are released into the lamina propria where they can access and enter the circulation. Underneath the intestinal epithelium, layers of circular and longitudinal muscle aid in the digestion process and move luminal contents distally for eventual excretion. Contractions of the smooth muscle are controlled by hormone release and the autonomic and enteric nervous systems. Innervation of the intestines is largely parasympathetic from the vagus nerve (small intestine to transverse colon) and pelvic nerve (from descending colon onward).

1.2.2 Functions of the Intestinal Tract

Digestive Functions

The primary purpose of the intestine is to facilitate recovery of nutrients from the diet and prepare waste for excretion. This process largely occurs passively and efficiently through coupled transport. In addition, fluid secretion and reabsorption by the intestines aids in nutrient absorption and excretion of waste. In the midst of these processes, there is also modulation of the immune system through interactions with environmental factors, host behavior such as diet, and host-pathogen communication. To accomplish these functions, the intestine is highly specialized with respect to cell populations, expression of proteins, and spatial organization. In this section, I briefly describe how these adaptations support intestinal function.

Nutrient Absorption and Fluid Dynamics In general, secretory intestinal epithelial cells reside in the intestinal crypts while absorptive cells are present in the surface epithelium. Absorption of macromolecules is largely mediated by sodium (Na^+)-coupled transport that occurs passively down its concentration gradient. This electrolyte movement across epithelia is driven by the electrochemical gradient established by the Na^+-K^+-ATPase that moves 2 potassium (K^+) ions into the cell and 3 Na^+ ions out of the cell, along with the actions of apical and basolateral K^+ channels that allow net movement of potassium into the gut lumen. A normal human colon absorbs 1.5 - 2.0 liters of fluid a day, a process driven by the movement of Na^+ and Cl^- across the epithelia. In addition to fluid absorption, fluid secretion in the colon also occurs albeit to a lesser extent. In pathophysiological conditions such as secretory diarrhea, fluid secretion in the colon outweighs absorption leading to net

fluid loss. In addition, in patients with Inflammatory Bowel Diseases (IBD) such as Ulcerative colitis (UC), diarrhea is the predominant symptom resulting from a loss of Na^+ and Cl^- absorption [86, 87]. Movement of Cl^- into the cell with Na^+ and K^+ by the Na^+-K^+-Cl^- cotransporter 1 (NKCC1) occurs electrogenically down the concentration gradients as described earlier. NKCC1 is a basolateral membrane protein and acts as the main mediator of Cl^- accumulation within the cell [88, 89]. Following stimulation, increases in intracellular cAMP and/or Ca^{2+} inhibit Na^+ and Cl^- influx and activate apical chloride secretion into the lumen through the Cystic Fibrosis Transmembrane Conductance Regulator (CFTR) and Ca^{2+}-activated Cl^- channels (CaCCs).

1.2.3 The Intestinal Barrier

Intestinal epithelial cells (IECs) stand at the interface of the external environment and the internal environment of the body. In order to protect the body from pathogens and commensal bacteria of the resident gut microbiome, these intestinal epithelial cells function as regulators of what is referred to as the intestinal barrier. This barrier is composed of the following components: the mucus layer, commensal bacteria of the gut microbiota, specialized intestinal epithelial cells such as Paneth cells and goblet cells that secrete antimicrobial peptides and mucins, enterocytes that regulate passage of molecules paracellularly, and the underlying immune cells which respond to changes in the luminal environment and failures of the barrier (Figure 1.2). The first of these, the mucus layers, create a physical deterrent to prevent bacterial adherence to intestinal epithelial cells. The mucus layer is formed by secretion of mucins and fluid from goblet cells and columnar intestinal epithelial cells, and contains antimicrobial peptides and secretory IgA secreted from Paneth cells and B cells,

respectively. The intestinal epithelial cells are the main physical blockade separating the external and internal environments. They are intimately associated through junctional proteins that regulate two methods of paracellular transport - the pore pathway and the leak pathway. The pore pathway is controlled largely by claudins and is charge and size-selective, while the leak pathway non-selectively allows passage of molecules 100 angstroms in diameter and is regulated by occludin and myosin light chain (MLC) phosphorylation [90–93]. Unregulated passage of macromolecules and bacteria can also occur following epithelial damage. Intestinal epithelial cells also monitor luminal microbes by continuous sampling and relay of the information to gut associated lymphoid tissue (GALT) where commensals can promote barrier function and pathogenic bacteria elicit inflammatory responses that can impair barrier function [94–96].

1.3 Inflammation in the GI Tract

The gastrointestinal tract is a unique site where balance of tolerogenic and immunogenic responses is necessary to maintain colonization of commensals but repress growth and invasion of pathogenic bacteria. To accomplish this, crosstalk between the gut microbiota, intestinal epithelial cells, and mucosal immune cells facilitates coordinated and complex processes of inflammation and wound healing. Microbes in the luminal environment are sensed by extracellular toll-like receptors (and intracellular NOD-like receptors) on intestinal epithelial cells that facilitate innate immune responses such as activation of Nuclear factor-kappa B (NF-$\varkappa$B) signaling and expression and secretion of the pro-inflammatory

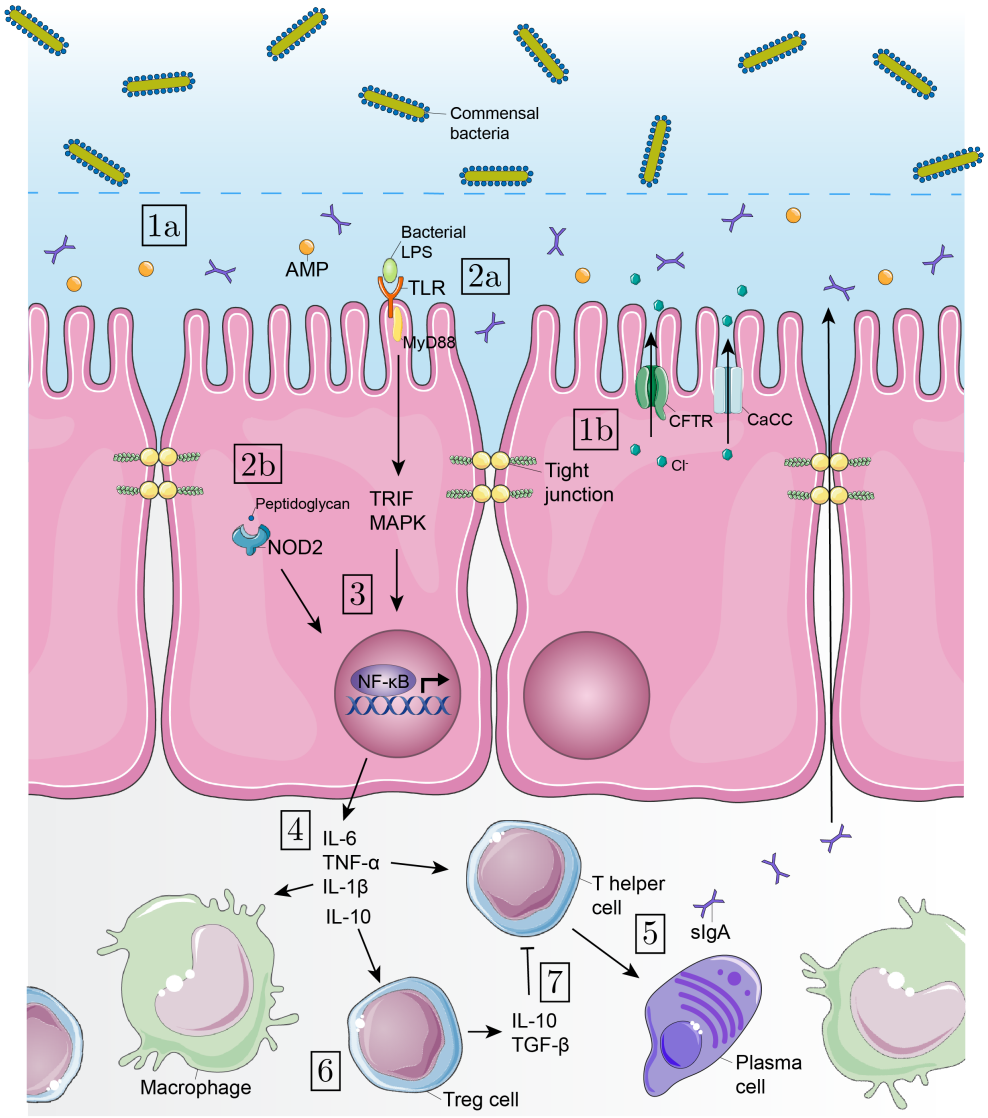

Figure 1.2: Homeostasis at the Intestinal Barrier

1a) The mucus layer consists of an inner dense layer containing secretory IgA (sIga) and antimicrobial peptides (AMP) (dashed line) and a loose outer layer where the microbiota reside. 1b) Apical chloride channels (CFTR, CaCC) drive fluid secretion to hydrate the mucus layer and tight junctions regulate selective paracellular transport across intestinal epithelial cells. 2a) Toll-like receptors (TLR) at the apical membrane sense microbial components such as lipopolysaccharide (LPS). 2b) Intracellular pattern recognition receptors such as NOD2 sense other microbial components like peptidoglycan. 3) Together, these receptors activate inflammatory signaling (MAPK) and induce pro-inflammatory gene expression via the Nuclear Factor-kappaB (NF-ϰB) transcription factor. 4) Secretion of cytokines activates inflammatory responses from myeloid cells and CD4+ T helper cells. 5) T helper cells support B cell differentiation to Plasma cells and production of sIgA. 6) Interleukin-10 (IL-10) promotes T regulatory (Treg) cell differentiation. 7) Activation of Treg cells increases secretion of IL-10 and transforming growth factor-β that inhibit CD4+ T cells and promote tolerogenic immunity.

cytokines interleukin-6 (IL-6), tumor necrosis factor-α (TNF-α), and interleukin-1β (IL-1β). These cytokines recruit leukocytes to the epithelium that in turn activate inflammatory responses such as production of reactive oxygen species and cytokine release. Antigen presentation to T cells induces adaptive immune responses such as secretory IgA production from B cells [97]. Expression of particular repetoires of cytokines leads to differention of leukocytes into specified subsets such as $CD4^+$ T cells to Th1, Th2, or Th17 cells. In coordination with the expression of pro-inflammatory mediators, intestinal epithelial cells also produce immunoregulatory molecules such as the anti-inflammatory cytokine interleukin-10 (IL-10) and transforming growth factor-β (TGF-β). These immunoregulatory mediators promote differentiation of T regulatory cells that repress pro-inflammatory signaling in order to prevent excessive inflammatory responses and promote wound healing. In healthy intestine, activation of fibroblasts and smooth muscle cells initiates the wound healing process where collagen deposition is accompanied by recruitment of monocytes and neutrophils that clear cell debris, and supports the expansion and migration of intestinal epithelial stem cells that re-populate the injured site [98, 99]. These processes are essential to healthy barrier function as evidenced by transgenic mouse models lacking expression of proteins important for bacterial-sensing and immunomodulation develop spontaneous colitis and a number of these same mediators are IBD risk genes [100–105]. It is therefore critical to understand these mechanisms in order to identify novel therapeutic opportunities for acute and chronic intestinal inflammation.

1.4 Project Proposal

Inital work in intestinal epithelia observed AMPK activation facilitated tight junction assembly and therefore intestinal barrier function [106–110]. Recent evidence by a number of groups has suggested activation of AMPK is protective in injury models of experimental colitis, however these studies have been correlative due to difficulties in specifically targeting AMPK activity [111–116]. Furthermore, a number of AMPK agonists and inhibitors have AMPK-independent effects and AMPK transgenic mouse models have limitations due to the expression of the remaining catalytic isoform, adding to the complexity of these conclusions. Previous work by our laboratory demonstrated knockdown of AMPKα1 by small-interfering RNA decreased the loss of intestinal barrier function induced by interferon-γ [117]. These data suggest AMPK mediates increased intestinal permeability downstream of interferon-γ rather than preserving barrier function as studies in experimantal colitis models have suggested. In agreement with this, IL-10-deficient mice that develop spontaneous colitis have increased AMPK activation compared to wild-type mice [118, 119]. In order to better understand these differences, I proposed to investigate the role of AMPK in homeostasis and in acute models of intestinal inflammation such as oxidative stress, injury-induced experimental colitis, and pathogenic infection. In order to determine the impact of AMPK activation on immune-related functions of intestinal epithelial cells, I utilized a number of model systems for this study. Mechanistic questions were answered using immortalized intestinal epithelial cell lines which can be manipulated in a more specific manner than *in vivo* systems. In order to observe the effects on the intestinal barrier as a whole, which includes not only epithelial cells but immune cells, the mucus layer and resident gut microbiota,

I employed a Villin-Cre intestinal epithelial-specific AMPKα knockout mouse model and challenged mice with different experimental models of colitis to observe if any effects were context-dependent.

2 | Materials and Methods

2.1 Materials and Buffers

All buffers utilized in the study were prepared according to standardized protocols and are listed in the appendix.

2.2 Cell Culture System

Cell culture maintenance

T_{84} colonic epithelial cells (generously provided by Dr. Kim Barrett, UCSD) were maintained in 50:50 Dulbecco's Modified Eagle Medium/Ham's F12 (DMEM/F12) media (Life Technologies) supplemented with 10% fetal bovine serum (Gibco #26140079, lot #1947391) and 1% Penicillin-streptomycin (Life Technologies) at 37°C in 5% CO_2 in 25 cm^2 or 75 cm^2 culture flasks (Corning) at 40-80% confluence until seeding. Cell growth media was replaced every other day, following 2-3 washes with pre-warmed 1X phosphate-buffered saline (1X PBS). HT-29.cl19A cells (from Dr. Kim Barrett, UCSD) were grown to confluence (~5 days) in DMEM supplemented with 10% FBS, 1% L-glutamine, and streptomycin (100

Table 2.1. Trans-Well® Permeable Supports

Plate Size	Insert Surface Area	Seeding Density	Insert Media Volume	Well Media Volume
6-well	4.67 cm^2	1 x 10^6	1.5 mL	2.6 mL
12-well	1.12 cm^2	5 x 10^5	0.5 mL	1.5 mL

µg/mL) in 75 cm^2 flasks. For seeding, cells were washed 3 times with pre-warmed 1X PBS to remove any traces of growth media and incubated in 1-2 mL 0.25% Trypsin + EDTA (Gibco) at 37°C until all cells became detached. The cell suspension was collected into a 15 mL conical tube with 8-9 mL of growth media and a single cell suspension was achieved by repeated pippetting using a serological pipet (~15 times). A 20 µL aliquot was diluted 1:2 in trypan blue and incubated for a few minutes. The stained aliquot was placed in a hemocytometer and cells were counted as described in standard protocols. Appropriate cell numbers (see 2.1) were seeded onto pre-warmed plates containing growth media and retuned to the incubator. Trans-well® Permeable Supports with polyester membranes and 0.4 µ m pore size were purchased from Corning® or Millicell® Cell Culture Inserts from EMD Millipore (for Ussing chambers) were utilized for all experiments. Cells cultured on permeable supports were fed every other day for 1 week, then fed every day until harvest.

2.3 Measurement of Transepithelial Electrical Resistance

Transepithelial electrical resistance (TEER) was measured using an EVOM voltohmmeter chopstick electrodes (World Precision Instruments) in triplicate per well. Plates were placed on a block heated to 37°C for measurements and temperature was allowed to stabilize for 10 minutes prior to measurement. Establishment of a semi-permeable and polarized

Table. 2.2 Transepithelial Electrical Resistance Measurement

Plate or Dish Size	Insert Membrane Growth Area (cm)	Insert Diameter (mm)	Polarized Range (Ohms)
6 well plate	4.67	24	214-535
12 well plate	1.12	12	893-2,232

monolayer was confirmed by TEER measurements greater than 1000 ohms $\bullet$ cm^2 (Table 2.2) and polarized monolayers were utilized for downstream experiments.

2.4 Cell Treatments

Hydrogen peroxide (H_2O_2, 30% w/v solution, Calbiochem purchasd from Millipore Sigma #7722-84-1) was utilized for oxidative stress experiments. T_{84} cells were treated basolaterally with H_2O_2 for the concentrations specified. The Ca^{2+}/Calmodulin Kinase Kinase β inhibitor STO-609-acetic acid (10 µM; Sigma-Aldrich #S1318) was applied bilaterally to T_{84} monolayers for 30 minutes prior to H_2O_2. The AMPK inhibitor Compound C or Dorsomorphin (50 µM, Millipore Sigma #P5499) was added bilaterally for 30 minutes prior to H_2O_2. The AMPK activator Metformin-hydrochloride (5 mM, Millipore Sigma #PHR1084) was applied bilaterally for 30 minutes. Capsaicin (20 µM, Sigma-Aldrich #M2028) was applied bilaterally for 30 minutes.

2.5 Human Subjects

Human subject experiments were performed at the University of California San Diego. Control patients (n = 3; 2 female & 1 male; age-range 52-71, mean: 61 ± 5 years) presenting for colon cancer screening were asymptomatic and showed no clinical or macroscopic signs of acute or chronic inflammation. Individuals with a history of inflammatory bowel disease,

or intestinal inflammation at the time of the study were excluded. With informed consent, mucosal punch biopsies (approximately 2 mm^2 surface area) were taken using a reusable round cup jumbo biopsy forceps Olympus FB-25 K-1 from macroscopically normal appearing regions of the sigmoid colon. Tissue biopsies were placed in cold, oxygenated Ringer's solution for transportation from the endoscopy suite to the laboratory. Tissues were allowed to equilibrate at 37°C in Ringer's for 20 minutes prior to incubation in test solutions for the indicated time points. Biopsies were then washed in ice-cold Ringer's (3 times) prior to tissue homogenization in lysis buffer for Western blot analysis (described below). The protocol was evaluated and approved by the University of California San Diego Institutional Review Board.

2.6 Protein Expression Analysis

2.6.1 Sample preparation from cell lysates

Cells were incubated with ice-cold Radio-immunoprecipitation assay (RIPA) lysis buffer (50 mM Tris-Cl pH 7.4, 150 mM NaCl, 1% NP-40, 0.5% sodium deoxycholate, 0.1% sodium dodecyl sulfate) containing protease and phosphatase inhibitors (2 mM sodium fluoride, 2 mM sodium orthovanadate, 1 μM phenylmethylsulfonyl fluoride, Roche cOmplete™, EDTA-free Protease Inhibitor Cocktail (Millipore Sigma #4693132001), Phosphatase Inhibitor Cocktail #2 and #3 (Millipore Sigma #5726 and #0044, respectively) for 10-15 minutes at 4°C before collection using a pipette or cell scraper. Whole cell lysates were immediately placed on ice. Whole cell lysates were sonicated to shear DNA using a QSonica Q125 Sonicator at 30% amplitude for 10 sec on/10 sec off for a total of 2 cycles followed by centrifuga-

tion at 13,000 rpm for 15 minutes at 4°C. Supernatants were placed in sterile, labeled 1.7 mL tubes on ice. Protein concentration in each sample was quantified using a Thermo Scientific™ Pierce™ BCA™ kit (Fisher Sci. #PI23228) according to the manufacturer's instructions. Protein concentration was measured in plastic cuvettes using a NanoDrop 2000c spectrophotometer in comparison to a standard curve. Gel loading samples were prepared with 20 μg of protein with 2X or 4X Laemmli loading buffer (BioRad) containing fresh β-mercaptoethanol (Sigma-Aldrich). Gel loading samples were stored at -20°C and stock whole cell lysates were stored at -80°C.

2.6.2 Sample preparation from isolated tissue

RIPA lysis buffer (see above) was added to flash frozen tissue and tissues were sonicated at 40% amplitude in short intervals until complete homogenization of the tissue. Lysates were centrifuged at 13,000 rpm for 15 minutes at 4°C. Protein samples were prepared as described above. Gel loading samples were stored at -20°C and stock whole cell lysates were stored at -80°C.

2.6.3 Immunoprecipitation

Following cell treatment and lysis (see above), whole cell lysate protein content was quantified and adjusted so that each sample contained an equal amount of protein. lysates were incubated with immunoprecipitating antibody, as per the manufacturer's instructions, for 1 hour at 4°C followed by another 1 hour incubation at 4°C with protein A-Sepharose. For NKCC1 immunoprecipitation, the goat polyclonal anti-Total NKCC1 (N-16) was used. Lysates were then centrifuged for 3 minutes at 21,000 x g and the supernatant was discarded.

The pellets were washed in ice-cold phosphate-buffered saline three times and resuspended in 2X gel loading buffer (50 mM Tris, pH 6.8, 2% SDS, 200 mM dithiothreitol, 40% glycerol, 0.2% bromophenol blue) and boiled prior to separation by SDS-polyacrylamide gel electrophoresis.

2.6.4 Electrophoresis, blotting and analysis

Gel loading samples were subjected to Sodium-dodecylsulfate polyacrylamide gel electrophoresis (SDS-PAGE) and proteins were transferred to polyvinylidine difluoride (PVDF) membranes using a wet transfer system (BioRad). Membranes were blocked for 1 hour at room temperature in 5% non-fat milk or bovine serum albumin in 1X Tris-buffered saline + 1% Tween-20 (TBST). Primary antibody incubations were conducted overnight at 4°C in blocking buffer. Membranes were washed with 1X TBST five times for 5 minutes. Secondary antibody incubations were conducted for 1 hour at room temperature in blocking buffer. Following secondary antibody, membranes were washed with 1X TBST five times for 5 minutes. Thermo Scientific™ SuperSignal™ West Pico PLUS Chemiluminescent Substrate (Fisher Sci. #PI34580) was applied to membranes for 5 minutes. Membranes were exposed to x-ray film in a dark room and films were developed immediately. Densitometry of protein bands was performed using FIJI (ImageJ) NIH imaging software.

2.6.5 Antibodies for western blotting

All phospho-antibodies were diluted 1:1000 in 5% BSA unless otherwise indicated. All other antibodies were diluted 1:1000 in 5% milk unless noted otherwise. AMPKα (Cell Signaling #2532) , Phospho(Thr172)-AMPKα (Cell Signaling #4OH9) , NKCC1 antibodies TEFS-2

and T4, α-Smooth Muscle Actin (Sigma-Aldrich #A2547) diluted 1:5000, E-cadherin (BD Transduction Labs #610181) diluted 1:4000, Occludin (Thermo Fisher Sci. #71-1500), Zonula occludens-1 (Invitrogen #61-7300), Claudin-2 (Invitrogen #32-5600), Claudin-4 (Invitrogen #32-9400), Claudin-15 (Invitrogen #32-9800), AMPKα1 (Abcam #ab3759), AMPKα2 (Abcam #ab3760), AMPKβ (Cell Signaling #57C12), Phospho(Ser79)-Acetyl-CoA Carboxylase (Cell Signaling #3661), Acetyl-CoA Carboxylase (Cell Signaling #3676), Cleaved caspase-3 (Cell Signaling #5A1E), Poly(ADP)ribose polymerase (PARP) (Cell Signaling #9542), β-Actin (Sigma-Aldrich #A5316) diluted 1:5000, Peroxidase-conjugated Goat Anti-Rabbit (Jackson ImmunoResearch Labs #111-036-045) diluted 1:5000, Peroxidase-conjugated Goat Anti-Mouse (Jackson ImmunoResearch Labs #115-036-062) diluted 1:10,000 for β-Actin or 1:5000 for all others.

2.7 Biotinylation Assay

The procedures for this experiment were adapted from [1]. Briefly, T_{84} cell monolayers were treated as described earlier. Following treatment, monolayers were washed twice with ice-cold 1X PBS pH 8.0. 10 μM of EZ-Link™ Sulfo-NHS-SS-biotin (Thermo Sci. #21331) was added basolaterally and incubated for 30 minutes at 4°C. Fresh biotin was added and incubated for an additional 30 minutes. Monolayers were washed twice with ice-cold 1X PBS pH 8.0 then incubated in quenching buffer (100 mM Glycine in 1X PBS pH 8.0) for 15 minutes. Quenching buffer was aspirated and 500 μL of RIPA lysis buffer was added to monolayers and incubated for 30 minutes at 4°C with gentle agitation. Cells were scraped and collected into 1.7 mL tubes. Cells were sonicated and centrifuged as

described earlier and supernatant was aspirated into new tubes. Protein quantification of supernatent was performed as described earlier. 50 µL of Pierce® Streptavidin-Agarose Resin (Thermo Sci. #20353) was placed in 1.7 mL tubes and washed according to the manufacturer's instructions. Equal concentrations of protein (~1 mg/mL) were added to respective streptavidin bead aliquots and incubated overnight at 4°C with rotation. The next day, samples were centrifuged according to streptavidin-agarose beads' manufacturer's instructions. Supernatants were aspirated into new tubes for total NKCC1 samples. Beads were washed twice with a high salt buffer (0.1% Triton X-100, 500 mM NaCl, 50 mM Tris, 5 mM EDTA at pH 7.5) for 10 minutes and once with a low salt buffer (0.1% Triton X-100, 100 mM NaCl, 50 mM Tris, 5 mM EDTA at pH 7.5) for 10 minutes. Biotinylated proteins were eluted from streptavidin beads using 50 µL Laemmli Sample Buffer (BioRad).

2.8 *In Vitro* Kinase Assays

Peptides were purchased from Peptide 2.0. Wild-type peptide sequence was RRAMATLLAKFRIDFSDIMVLGRR and Mutant peptide sequence was RRAMATLLAKFRIDFADIMVLGRR. SAMS peptide (Abcam #ab120182) was used as a postive control. The assay was performed as described previously [2]. Briefly, reactions were prepared in 1.7 mL tubes to the following final concentrations: 1 nM Recombinant human His-tagged AMPK (α2/β1γ1) (Sigma-Aldrich #A1733), 1 mM AMP, 2 mM peptide, 5 mM $MgCl_2$, and 50 mM HEPES pH 7.0. 0.2 mM AT-^{32}P (from 2 mCi/mL stock) was added last and reactions were incubated at 37°C for 20 minutes. Reactions were briefly centrifuged and 20 µL of each reaction was blotted onto a 2.5 cm circle P81-grade phosphocellulose Whatman paper. Papers were

allowed to dry for 5-10 minutes followed by washes with 1% phosphoric acid for 10 minutes (3 times). Papers were soaked briefly in acetone and allowed to dry. Each paper was placed in an individual scintillation tube and scintillating buffer was added to soak the paper. Counts per Million (CPM) of tubes were read on a Beckman LS 6500 scintillation counter.

2.9 Transgenic Animal Models

Animal lines and colony maintenance

Mice were maintained in a specific pathogen-free facility with access to standard chow (PicoLab® Rodent Diet 20 5053*) and water ad libitum. Density of housing was limited to 5 animals per cage. All mouse genotypes within a given mouse line were cohoused prior to experiments. Mice transferred to conventional housing were fed Laboratory Rodent Diet 5001*. AMPKα2 whole-body knockout mice first described by Viollet et al. in 2003 were generated on a C57BL/6J background by a Cre-loxP system where loxP sites flanked exon C which corresponds to amino acids 189-260 of the catalytic domain [3]. AMPKα intestinal epithelial cell-specific knockout mice have not been previously described and were generated by breeding AMPKα1α2 floxed mice with a Villin-Cre mouse (both lines kindly provided by Russell G. Jones, McGill University). These mice have a mixed background of C57BL/6JN.

2.9.1 Sacrifice and sample collection

Mice were anestherized using 4% isofluorane in an anesthesia chamber and kept under anesthesia until sacrifice using a nose cone. Blood was collected from the posterior vena cava using an insulin syringe into a 1.7 mL tube. Following blood collection, anesthetized

mice were sacrificed by cervical dislocation. Intestinal tissue was excised and immediately placed in 1X PBS on ice. Intestines were cut into intestinal segments (Duodenum, Jejunum, Ileum, Cecum, Proximal colon, Distal colon) and were utilized as follows: 0.5 cm each for paraffin and frozen sections and 0.25 cm each for protein and RNA expression analysis.

2.10 Ussing Chambers

2.10.1 Physiological solutions

The composition of the Kreb's Ringer's buffer used for Ussing chamber, Western blot studies, and $^{86}Rb^{+}$ uptake studies was (in mM): 140 Na^{+}, 120 Cl^{-}, 5.2 K^{+}, 25 HCO_3^{-}, 0.4 $H_2PO_4^{-}$, 2.4 HPO_4^{2-}, 1.2 Ca^{2+}, 1.2 Mg^{2+}, and 10 D-glucose.

2.10.2 Resistance and ion transport

Intestinal epithelial cells were seeded in Millicell® Cell Culture Inserts and grown until polarization was confirmed by TEER measurement (~10 days). Inserts were placed in sliders and mounted in Ussing chambers containing pre-warmed Kreb's Ringer's buffer. Mice were sacrified without isofluorance anesthesia by cervical dislocation and CO_2 asphyxiation. Intestinal tissues were excised onto a chilled platform, opened longitudinally and fecal matter removed gently with forceps. The serosal layer was stripped and epithelium was placed on inserts for mounting in Ussing chambers containing pre-warmed Krebs-Ringer's buffer (KBR) supplemented with glucose. For H_2O_2 experiments, excised mouse intestinal tissue was treated bilaterally with H_2O_2 (1-5 mM) for 30 minutes prior to transport stimulation and recording of resistance. Resistance was observed continuously once the tissues were mounted

and recorded after 10-15 minutes following stabilization of the tissue. To stimulate cyclic-AMP-dependent transport, 20 µM Forskolin (Sigma-Aldrich #F6886) was added bilaterally. Current and resistance was allowed to stabilize. To stimulate Ca^{2+}-dependent transport, 300 µM Carbachol (Carbamoylcholine chloride, Sigma-Aldrich #C4382) was added basolaterally. Change in short-circuit current (ΔIsc) was calculated from the difference of the peak of current following stimulation and baseline current immediately preceding stimulation.

2.10.3 Basolateral $^{86}Rb^{+}$ uptake studies

Basolateral K^{+} uptake was measured with $^{86}Rb^{+}$ as a tracer using an adaptation of a previously described method [4]. Confluent monolayers of T_{84} cells grown on 12mm Transwell® inserts were rinsed three times with warm Ringer's solution and incubated for 1 hour at 37°C. After 1 hour pre-incubation, cells were exposed bilaterally to H_2O_2 (500 µM) or vehicle control for 30 minutes on a warming plate at 37°C. Inserts were transferred to wells containing Ringer's solution with or without 100 µM Carbachol (CCh) for 1 minute, and then transferred to wells containing Ringer's with 1 µCi/mL $^{86}Rb^{+}$ and CCh, and maintained at 37°C for 3 minutes. $^{86}Rb^{+}$ uptake was terminated by immersing inserts several times in ice-cold 100 mM $MgCl_2$ containing 10 mM Tris-HCl, pH 7.5. Filters were immediately excised from the inserts, placed directly into 5 mL scintillation fluid, and $^{86}Rb^{+}$ content measured by standard scintillation methods. K^{+} influx was calculated as (cpm/g protein/min)/SA, where SA is the specific activity of the uptake buffer (cpm/µmol K+). Data were expressed as µmol of K^{+} influx/g protein/min.

2.10.4 *Ex vivo* intestinal permeability

Whole intestinal sections were mounted in Ussing chambers containing pre-warmed Krebs-Ringer's buffer (KBR) supplemented with either mannitol (small intestine) or glucose (large intestine). 4 kDa Fluorescein isothiocyanate (FITC)-dextran was added to the apical (luminal) side and both chambers were sealed with chamber caps to prevent evaporation. Buffer was collected from the basolateral (lamina propria) side at regular intervals and an equal volume was removed and discarded from the apical chamber to prevent a volume difference across the tissue. Fluorescence in each sample and a standard curve was measured using a GloMax®-Multi Detection System plate reader (Promega) at 490 nm. Liner regression was performed in GraphPad to interpolate sample concentrations from the standard curve.

2.11 Immunofluorescence

2.11.1 Tissue preparation, blocking and staining of slides

Isolated tissues from mice were immediately placed in 1.7 mL tubes containing 0.5 mL of 4% paraformaldehyde (PFA) on ice. Tubes were transferred to 4°C and incubated overnight. 4% PFA was aspirated as discarded in appropriate waste container. Tissues were washed three times with 1 mL of 1X PBS, aspirating and discarding PBS after each wash. After the final wash, tissues were stored in 30% sucrose in 1X PBS at 4°C. Tissues were blocked using Optimal cutting temperature (OCT) solution and plastic molds. Blocks were wrapped in foil and stored at -80°C. Tissues were cut into 4 µm sections using a Leica cryostat and placed on positively-charged glass slides. Slides were stored at -20°C or -80°C.

2.12 Intestinal Epithelial Cell Isolation

Intestinal tissue was excised from mice and stored temporarily in ice-cold 1X PBS during the procedure. Intestinal segments were separated (Duodenum, Jejunum, Ileum, Cecum, Proximal colon and Distal colon) and mesentery was carefully removed using fine forceps. Using a curved syringe, lumens were flushed with ice cold 1X PBS to remove any fecal matter or luminal contents. Using a 200 µL pipet tip and forceps, the intestinal segments were carefully inverted and placed in 1.7 mL tubes containing 500 µL of Corning® Cell Recovery Solution (Corning #354253) on ice. Samples were incubated for 2 hours at 4°C with rotation. Using forceps, intestinal segments were shaken in their tubes to release intestinal epithelial cells and remnant tissue was discarded. Samples were then washed three times as follows: centrifuged at 600 x *g* for 5-10 minutes, supernatent was aspirated and discarded, and the cell pellet was resuspended in ice cold 1X PBS. After the final wash, cell pellets were resuspended in RIPA lysis buffer for protein expression analysis.

2.13 *In Vivo* Intestinal Permeability

Mice were fasted overnight (8-12 hours) and orally gavaged with 10 mg/mL 4 kDa fluorescein (FITC)-dextran, according to their body weight. After four hours, mice were anesthetized using 4% isofluorane and blood was collected retro-orbitally (for baseline/survival experiments) or from the posterior vena cava. Blood was allowed to clot for 30 minutes at room temperature and centrifuged at 1,500 x *g* for 15 minutes at 4°C. Serum was aspirated and placed in a labeled tube on ice. Serum was diluted 1:5 in a black 96-well plate in techni-

cal duplicates. Fluorescence in each sample and a standard curve was measured using a GloMax®-Multi Detection System plate reader (Promega) at 490 nm. Duplicates were averaged and linear regression was performed in GraphPad to interpolate sample concentrations from the standard curve.

2.14 Models of Colitis and Assessment of Disease Severity

2.14.1 Dextran sulfate sodium (DSS)

Mice housed in a specific-pathogen-free facility were transferred to conventional housing and acclimated for 2 weeks. Mice within the same treatment group were co-housed, regardless of genotype. Baseline *in vivo* intestinal permeability was performed as described earlier. Mice were allowed to recover for 2 weeks. 5% w/v Dextran sulfate sodium salt (~36,000-50,000 MW, colitis-grade, MP Biomedicals purchased from VWR #IC16011090) was administered in drinking water ad libitum for 5 days, followed by 3 days of water. Post-DSS *in vivo* intestinal permeability was peformed on the day of sacrifice (Figure 2.1).

2.14.2 *Citrobacter rodentium* Infection

Frozen stock of *C. rodentium* was resuspended in 1X PBS, plated on LB+streptomycin and MacConkey agar plates, and incubated overnight at 37°C. A single colony was selected and placed in LB broth overnight. Mice were treated with streptomycin (50 mg/µL) 24 hours prior to infection. The next day 200 µL of *C. rodentium* were orally gavaged into anesthetized mice. Serial dilutions of the stock *C. rodentium* were plated on LB-streptomycin and MacConkey agar plates overnight at 37°C. Single colonies were counted the next day

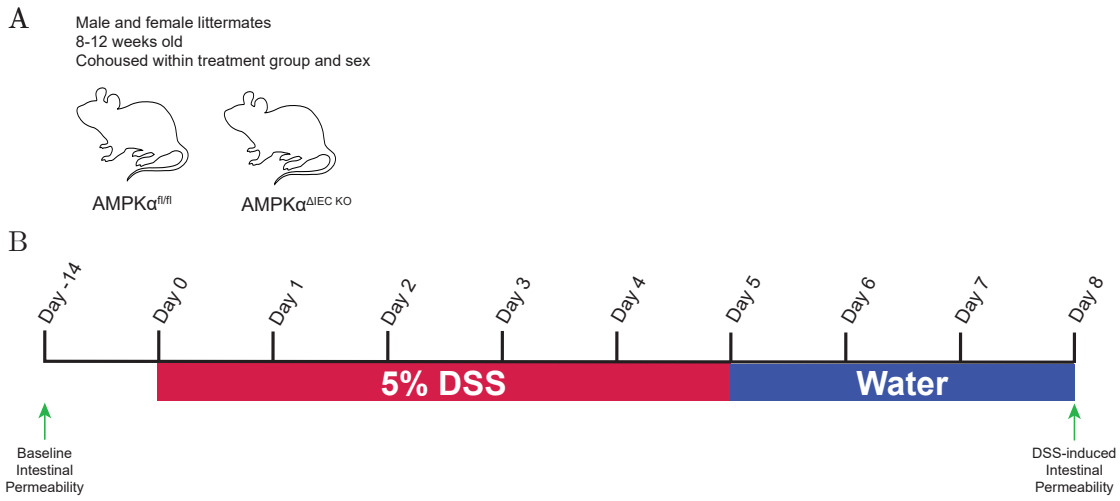

Figure 2.1: Dextran Sulfate Sodium Administration

A) Adult (8-12 weeks old) AMPK$\alpha^{fl/fl}$ and AMPK$\alpha^{\Delta IEC\ KO}$ mice were utilized. Mice from both sexes were included in the study and cohoused by sex and treatment group in conventional housing. B) Baseline intestinal permeability was measured two weeks prior to Dextran Sulfate Sodium (DSS) treatment. DSS was administered at 5% in drinking water ad libitum for 5 days, followed by 3 days of water. Mice were sacrificed at Day 8 or when >25% of body weight was lost. DSS-induced permeability was measured on the day of sacrifice.

to determine the number of colony forming-units used for infection. Body weight was measured every day and feces were collected every other day to determine fecal bacterial burden. Infected mice were sacrificed either at day 10 post-infection or after *C. rodentium* clearance (approximately 21 days post-infection).

2.14.3 Disease Activity Index

Disease activity index (2.3) was utilized to measure disease severity daily as previously described [5]. Stool was classified as loose (score of 2) if liquid present when placed on a paper towel, and watery diarrhea (score of 4) if liquid excretions were observed with no pellets or shape. Presence of blood in feces was determined used Beckman-Coulter™ Hemoccult™ Fecal Occult Blood Slide Test System (Fisher Sci. #SK-60151) according

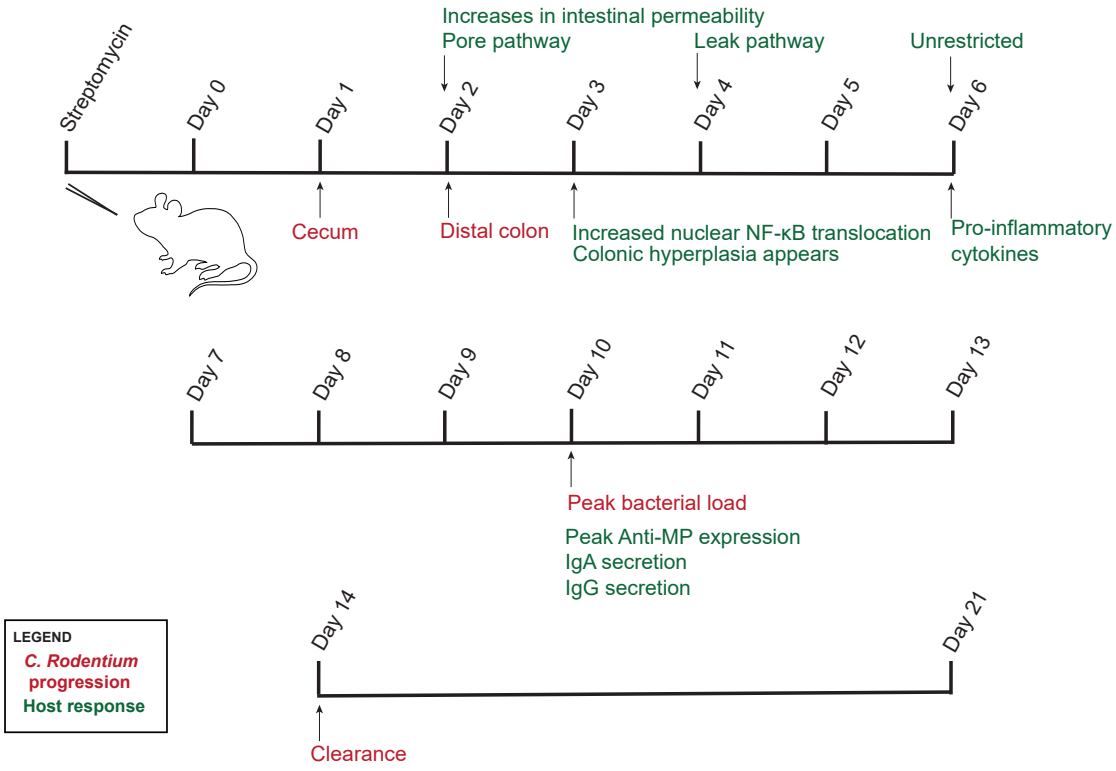

Figure 2.2: *Citrobacter rodentium* Infection

Timeline of *Citrobacter rodentium* infection with known progression of the bacteria and host responses after infection. *C. rodentium* colonization progression is depicted in red and host responses are displayed in green. Mice were oral gavaged with streptomycin 24 hours before infection. *C. rodentium* was administered by oral gavage, and is expected to colonize the distal colon by Day 2 post-infection. Intestinal permeability is increased by Day 2 (transepithelial electrical resistance) and by Day 4 macromolecular permeability is increased. Inflammatory responses are initiated by Day 3 with Nuclear Factor-kappa B activation and translocation. Peak bacterial load occurs around Day 10 post-infection and coincides with adaptive immune responses. In healthy wild-type mice, the infection is cleared by Day 14 post-infection.

to manufacturer's instructions. Presence of blood in stool was classifed as slight bleeding (score of 2) if no blood observed by the naked eye with a positive Hemoccult™ test and gross bleeding (score of 4) if blood was observed by the naked eye with a positive Hemoccult™ test.

Table 2.3 Disease Activity Index

Score	% Body Weight Loss	Stool Consistency	Presence of Blood in Stool
0	None	None	None
1	1-5%		
2	6-10%	Loose	Slight Bleeding
3	10-15%		
4	>15%	Watery Diarrhea	Gross Bleeding

2.15 Gene Expression Analysis

2.15.1 Sample preparation

Invitrogen TRIzol™ Reagent (Thermo Fisher Sci. #15596026) was added to flash frozen tissue and tissues were homogenized by sonication (40% amplitude in short intervals until complete homogenization of the tissue) or bead beating at 4°C for 30-60 seconds. RNA was isolated according to the manufacturer's instructions and isolated RNA was resuspended in RNase-free water. RNA concentration and 280/260 nm ratio was measured using a NanoDrop 2000c spectrophotometer. Reverse transcription was performed using 1 μg RNA and 5X qScript™ cDNA SuperMix (Quanta BioScience #95048) in 20 μL reactions. Resulting cDNA was diluted 1:10 and stored at 4°C.

2.15.2 Polymerase chain reactions

PCR reactions were prepared using GoTaq® Green Master Mix (Promega #M712B) according to the manufacturer's instructions. Primer sequences and cycle information is listed in the Appendix. Following cycling, reactions were loaded onto a 1-2% agarose gel containing ethidium bromide and run until adequate separation was achieved. Gels were imaged using a GelDoc system and densitometry was performed using ImageJ.

2.16 Histological Analysis

2.16.1 Tissue preparation, blocking and slides

Isolated tissues from mice were immediately placed in 1.7 mL tubes containing 0.5 mL of 4% paraformaldehyde (PFA) on ice. Tubes were transferred to 4°C and incubated overnight. 4% PFA was aspirated and discarded in an appropriate waste container. Tissues were washed three times with 1 mL of 1X PBS, aspirating and discarding after each wash. After the final wash, tissues were stored in 70% ethanol at 4°C. To paraffinze, tissues were placed in plastic cassettes labeled in pencil or with a solvent resistant marker. Plastic cassettes were placed in a paraffin embedder and embedded overnight. The next day, tissues were blocked in paraffin using a TissueTek and stored at room temperature or 4°C. Tissues were cut into 4 µm sections using a Leica microtome and placed in a warm water bath for mounting on positively charged glass slides. Slides were dried and stored at room temperature.

2.16.2 Hematoxylin and eosin staining

Paraffin sections were baked at 60°C for 1 hour followed by the following incubations: two washes in Citrisolv for 5 minutes each, one wash in Citrisolv for 1 minute, one wash in 100% Ethanol for 3 minutes, one wash in 95% Ethanol for 3 minutes, one wash in 70% Ethanol for 1 minute, two washes in ddH_2O for 2 minutes each, incubated in Hematoxylin for 1 minute, one wash in ddH_2O for 2 minutes, incubated in Eosin for 1 minute, one wash in ddH_2O for 2 minutes, one wash in 70% Ethanol for 1 minute, one wash in 95% Ethanol for 3 minutes, one wash in 100% Ethanol for 3 minutes, and two washes in Citrisolv for 5 minutes each. Slides were mounted with coverslips using Permount™ Mounting Medium (Fisher Sci.) and

Table. 2.4 Histological Analysis of Chemically-Induced Experimental Colitis

Score 1: Inflammatory Cell Infiltrate	Score Value	Score 2: Epithelial Changes and Mucosal Architecture	Score Value
No infiltration	0	No epithelial changes	0
Mild, limited to mucosa	1	Focal adhesions present	1
Moderate, present in mucosa and submucosa	2	Erosions and focal adhesions present	2
Marked transmural infiltration	3	Extended erosions with or without granulation and/or pseudopolyps	3
Total Score of Severity based on Histological Feature (Score 1 + Score 2):			0-6

allowed to dry overnight before imaging. Reagents included Citrisolv Clearing Agent (Decon Laboratories Inc.), Hematoxylin, Modified Harris Formulation, Mercury free Nuclear Stain (Ricca Chemicals), Eosin Y Solution, alcoholic (Sigma-Aldrich).

2.16.3 Imaging and Colitis Scoring

Hematoxylin and eosin-stained slides were imaged on an upright Leica. Colitis scoring was performed as described previously using the rubric in Table 2.4 [6].

2.17 TUNEL Staining

Staining was performed using the ApopTag® Fluorescein *In Situ* Apoptosis Detection Kit (Millipore #S7110) according to the manufacturer instructions. Briefly, 4 μm paraffin sections were baked at 60°C for 1 hour followed by the following incubations at room temperature: two washes in Xylene for 5 minutes each, two washes in 100% Ethanol for 5 minutes, one wash in 95% Ethanol for 3 minutes, one wash in 70% Ethanol for 3 minutes, and incubated in 1X PBS for 5 minutes. Tissues were then pre-treated with Proteinase K

(20µg/mL) for 15 minutes and washed twice with 1X PBS for 2 minutes each. Equilibration buffer was applied for at least 10 seconds followed by incubation with TdT enzyme for 1 hour at 37°C in a humidified chamber. The reaction was terminated by incubation in Stop/Wash buffer for 10 minutes at room temperature followed by washing three times with 1X PBS for 1 minute. The following steps were performed while avoiding exposure to light. Anti-digoxigenin conjugate was applied and incubated for 30 minutes at room temperature in a humidified chamber. Slides were washed with four times with 1X PBS for 2 minutes each. Slides were mounted with coverslips using ProLong™ Gold Antifade Mountant with DAPI (Invitrogen™) and stored in the dark at -20°C.

2.18 Data Acquisition and Analysis

Microscope slides for immunofluorescence, histology, and TUNEL staining were imaged using an upright Leica DM5500B microscope modular system paired with Leica CTR5500 electrical box, Leica EL6000 compact light source, and DFC365 FX and DFC450 C cameras. Image analysis was conducted using NIH ImageJ. For NKCC1 expression, at least 3 complete crypts per section were chosen as regions of interest (ROI) and green fluorescence channel intensity was measured. For TUNEL staining, cells were selected using thresholding and the number of stained cells in the green channel was measured and normalized to the number of stained cells in the blue channel. Statistical analysis was conducted in GraphPad Prism 8. Data with two experimental groups was analyzed by two-tailed t-tests. Data over time was analyzed by linear regression. Data with >3 experimental groups was analyzed by one-

way ANOVA. Grouped data was analyzed by two-way ANOVA using Tukey's post-test. Statistical significance was determined by $\alpha = 0.05$. Power analyses were performed in R.

3 | AMPK Inhibits Electrogenic Ion Secretion During Oxidative Stress in the Intestinal Epithelium

3.1 Introduction

3.1.1 Electrogenic Ion Transport in Intestinal Homeostasis

The intestinal epithelium is a site of continuous electrolyte flux that aids in absorption and maintenance of the intestinal barrier. In particular, apical chloride transport drives fluid secretion that hydrates the mucus layer, facilitates diffusion of digestive enzymes and metabolites, and protects the epithelium from the mechanical stress of passage of luminal contents [1–3]. Impaired chloride (Cl^-) secretion, such as that present in Cystic Fibrosis patients, results in intestinal obstruction and malabsorption [4, 5]. Vectorial movement of electrolytes is due to the polarized nature of intestinal epithelial cells, in which expression of transporters and channels is restricted to apical or basolateral membranes due to adherens

and tight junctions [6]. Apical chloride secretion is driven by the concentration gradients of Na^+ and K^+ generated by the Na^+/K^+ ATPase at the basolateral membrane (Figure 3.1). The $Na^+/K^+/2Cl^-$ co-transporter 1 (NKCC1) is a basolateral transmembrane protein that facilitates the electrogenic influx of Na^+, K^+ and 2 Cl^- ions driven by the Na^+/K^+-ATPase. Na^+ and K^+ are recycled to the lamina propria through the combined actions of basolateral K^+ channels and the Na^+/K^+-ATPase resulting in a net accumulation of Cl^- ions in the cell. Low intracellular sodium concentration allows NKCC1 to accumulate chloride in secretory epithelial cells above the concentration predicted from electrochemical equilibrium. Under increasing intracellular concentrations of cyclic adenosine monophosphate (cAMP) or calcium (Ca^{2+}), the apical Cystic Fibrosis Transmembrane Conductance Regulator (CFTR) or calcium-activated chloride channels (CaCCs), respectively, open to allow large movement of chloride into the luminal space [7–9]. Both mechanisms of chloride secretion can be replicated experimentally using the secretagogues Forskolin and Carbachol for cAMP- and calcium-dependent secretion, respectively. Chloride secretion is regulated by transporter activity, expression, and localization. For example, increased intracellular Ca^{2+} and cAMP activate basolateral K^+ channels leading to futher increases in apical chloride secretion [10]. In addition, NKCC1 has emerged as a regulator of chloride secretion as its activity, and therefore the availability of chloride, is a rate-limiting step in this process.

NKCC1 expression in secretory epithelia is 10-30 times higher than other cells, and it is more highly expressed in colon than small intestine [11]. Consistent with spatial organization of secretory and absorptive epithelial cells, its highest expression levels are observed in intestinal crypts and diminish towards the villus tip/surface epithelium [11, 12].

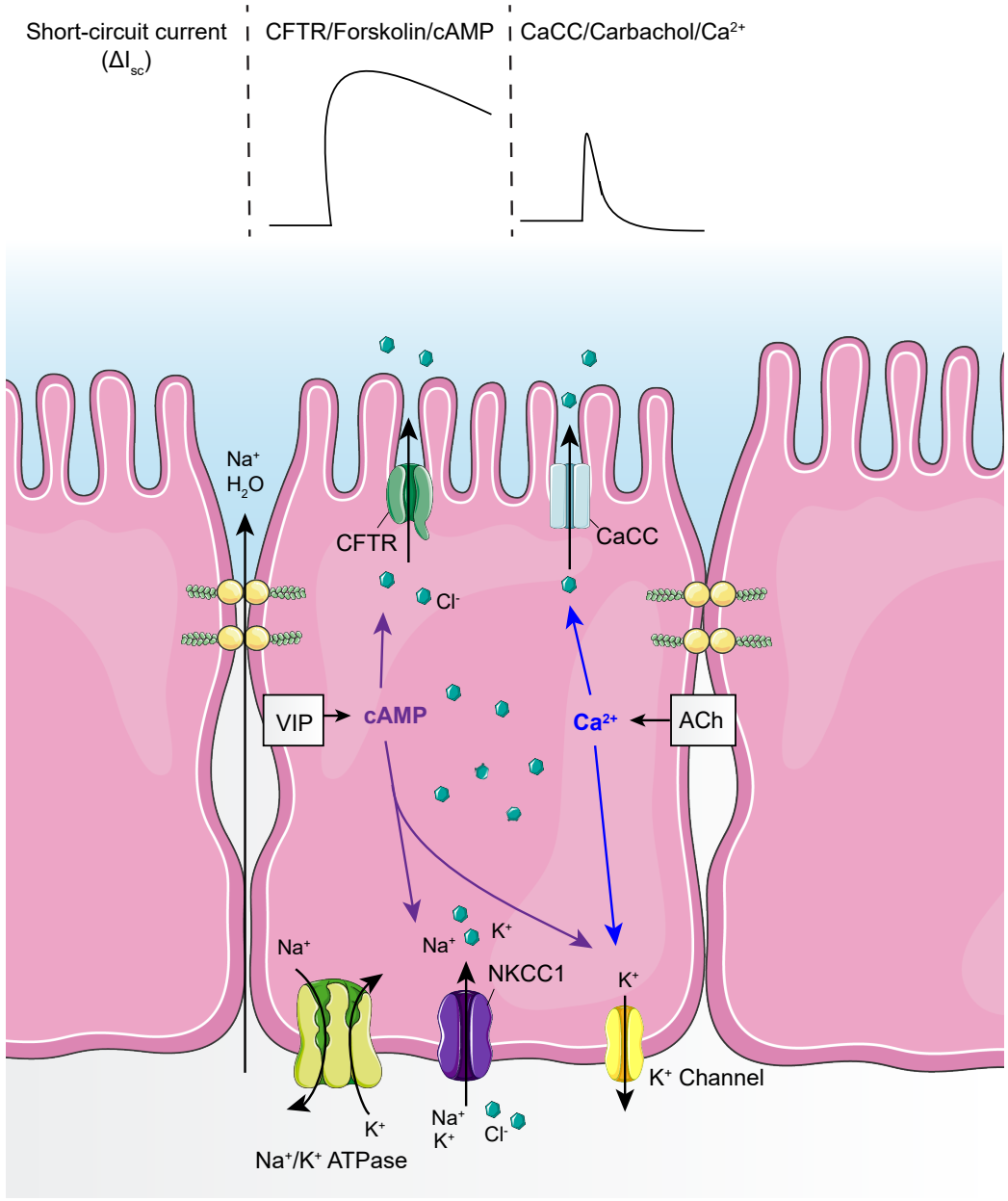

Figure 3.1: Mechanisms of Chloride Secretion in Intestinal Epithelial Cells

At the basolateral membrane, the Na^+/K^+ ATPase establishes a concentration gradient that pulls intracellular Na^+ to the lamina propria. Basolateral K^+ channels recycle K^+ to the lamina propria. Together, these drive electrogenic secondary active transport of Cl^- into the cell by the $Na^+/K^+/2Cl^-$ cotransporter 1 (NKCC1). Stimuli that increase cyclic AMP by adenylate cyclase, such as vasopressin, activate the apical Cystic Fibrosis Transmembrane Conductance Regulator (CFTR) via Protein Kinase A (PKA) phosphorylation to allow large, sustained secretion of Cl^- into the lumen. Acetylcholine increases intracellular Ca^{2+} that opens Calcium-activated Chloride Channels (CaCCs) leading to fast, transient secretion of Cl^-. Sodium and water follow chloride paracellularly, resulting in net electrogenic fluid secretion.

NKCC1 is regulated by a number of mechanisms including posttranslational modifications and endocytosis. Previous work has demonstrated induction of apical chloride secretion by cAMP increases NKCC1 activity due to phosphorylation by STE20-related proline-alanine-rich kinase (SPAK) and oxidative stress response kinase (OSR1) at Threonines 206 and 211 [13–21]. In addition, NKCC1 phosphorylation is induced by decreases in intracellular calcium [22, 23]. Following stimulation of electrogenic ion secretion, altered surface expression of NKCC1 has been observed and suggests that NKCC1 removal from the membrane promotes termination of apical secretion [24–27]. These data indicate NKCC1 is a key mediator of electrogenic ion transport regulation.

3.1.2 Oxidative Stress in the Intestinal Epithelium

Reactive oxygen species (ROS) are free radical oxygen-containing molecules, meaning they have at least one unpaired electron in the outer orbital. These species react with other molecules through oxidation and/or reduction reactions to regain their thermodynamic and electrogenic stability. They are produced from endogenous pathways in epithelial cells such as the mitochondrial electron transport chain, xanthine oxidoreductase activity, and the arachidonic acid and NADPH-dependent oxidase pathways in myeloid leukocytes. While these mediators are important for certain functions, such as the bacteria-killing respiratory burst, they can also be harmful to proteins within the cell and as a result must be reduced very quickly by antioxidants such as glutathione. This is maintained by an inherent balance of reduction-oxidation (redox) signalling in healthy tissue. Increased reactive oxygen species or decreased antioxidant activity in a tissue can result in oxidative stress [28].

Reactive oxygen species earn their name by participating in reactions with nucleic acid, fatty acids and lipids, amino acids and proteins [29]. The hydroxyl radical can react with all four DNA bases as well as damage the deoxyribose backbone, promoting mutagenesis, carcinogenesis and aging. These free radicals can also denature various proteins leading to loss of function. For example, pyruvate dehydrogenase inactivation by ROS causes loss of substrates for aerobic respiration, an important mechanism of antioxidation. Modification of structural proteins can lead to destruction of cell architecture and the basement membrane. In the intestinal epithelium, oxidative stress can also regulate immune pathways such as NF-$\varkappa$B and nuclear factor erythroid 2-related factor 2 (NRF2) which modulate gene expression to suppress local tissue damage [29, 30].

During intestinal inflammation, recruitment of neutrophils and other leukocytes contributes to the level of reactive oxygen species in the mucosa [31–33]. In states of chronic inflammation, such as Inflammatory Bowel Disease (IBD), the mucosa has a much higher capacity of free radical production compared to healthy patients leading to oxidative stress [34–37]. This was further indicated by increased levels of oxidized proteins in IBD patients and increased nucleic acid oxidation in inflamed biopsies compared to uninvolved regions and healthy controls [38]. In addition, anti-inflammatory therapies for IBD have been shown to reduce oxidative stress in the mucosa and antioxidants have been demonstrated to reduce experimental colitis [39–43]. Dysregulated ion transport is a feature of intestinal inflammation and repression of ion transport alone has been shown to promote dysbiosis. Previous evidence has demonstrated oxidative stress can also dampen intestinal ion transport [44–50]. For example Interleukin-10 (IL-10) transgenic knockout mice that develop spontaneous colitis have impaired Forskolin-stimulated chloride flux [51]. Furthermore, the importance

of fluid dynamics is underscored by mouse models of Cystic Fibrosis. A number of these mouse models display significant gastrointestinal manifestations of disease such as goblet cell hyperplasia and mucus accumulation, eosionophilic infiltrates in intestinal crypts, and intestinal blockage and rupture [52–57]. While these mice did not survive past weaning, replacement of their drinking water with an electrolyte solution increased their survival, indicating fluid dynamics contibuted to this effect [52, 53]. These results suggest a critical role of fluid secretion in intestinal homeostasis. Finally, hydrogen peroxide (H_2O_2) has been shown to decrease cAMP-dependent chloride secretion in T_{84} cell monolayers [51].

3.1.3 Known Roles of AMPK in Oxidative Stress and Ion Transport

It has been well established than AMPK can be activated under oxidative stress conditions in various cell types [58–60]. In addition, some evidence has suggested AMPK activation in the intestine inhibits chloride secretion. For example, IL-10 knockout mice with decreased Forskolin responsiveness exhibited increased AMPK activation [51]. In addition, *Vibrio cholerae* infected ileal loops treated with Metformin, a biguanide non-specific activator of AMPK, displayed decreased weight/length ratio and AMPK activation by 5-aminoindazole-4-carboxamie ribonucleotide (AICAR) treatment in wild-type mice inhibited cAMP-stimulated chloride secretion [51, 61]. In agreement with these data, AMPK inhibition by Compound C in wild-type mice and IL-10-deficient mice increased the Forskolin response, which was not observed in AMPKα1 knockout mice [51, 61]. Finally, Walker et al. demonstrated increased AMPK phosphorylation and activity was required for an inhibition of Forskolin-activated chloride flux following 1 mM H_2O_2 treatment in T_{84} intestinal epithelial cell monolayers. These data support a role of AMPK as a mediator of cAMP-dependent

ion secretion inhibition during oxidative stress. However, whether AMPK can also inhibit calcium-dependent chloride secretion remains elusive. Published work from our group has observed oxidative stress also causes inhibition of Carbachol-stimulated electrogenic ion transport [48]. In addition, Carbachol treatment in parotid acinar cells has been shown to activate AMPK through increased Na^+/K^+-ATPase turnover and decreased intracellular ATP [62]. We therefore sought to elucidate the molecular mechanisms of AMPK regulation of ion transport during oxidative stress.

3.2 Experimental Results

3.2.1 Effect of Hydrogen Peroxide on Intestinal Electrogenic Ion Transport and Resistance

I first sought to confirm the effect of oxidative stress on the intestinal barrier in mouse colon. Using an Ussing chamber system, I observed that oxidative stress had no effect on transepithelial electrical resistance in mouse proximal colon (Figure 3.2). This was consistent with previous observations from our lab [48].

I next tested the effect of oxidative stress on electrogenic ion transport in mouse colon using increasing concentrations of hydrogen peroxide administered for 30 minutes prior to stimulation. We observed that 5 mM of hydrogen peroxide resulted in a significant decrease (79% reduction, $p = 0.002$) of Ca^{2+}-dependent ion transport as induced by Carbachol (Figure 3.3, n=7). We did not observe any change in cAMP-dependent ion transport, nor did transepithelial electrical resistance over time differ among treaments.

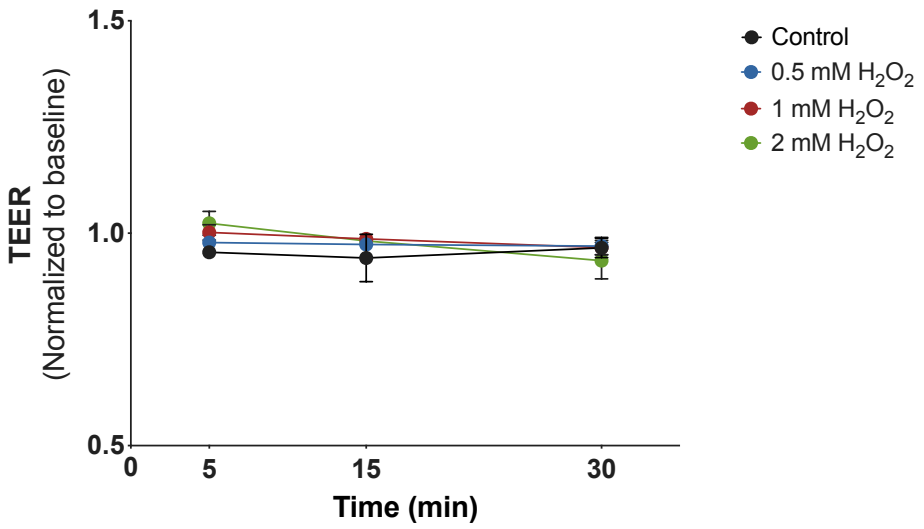

Figure 3.2: Transepithelial Electrical Resistance is Not Affected by Acute Hydrogen Peroxide

Wild-type mouse proximal colon mounted in Ussing chambers with Kreb's Ringer's Buffer was treated with 0.5 mM, 1 mM, or 2 mM H_2O_2 and transepithelial electrical resistance (TEER) was measured at 5, 15, and 30 minutes after treatment. All treatments displayed similar TEER at each time point. Values are presented as Means ± S.D. n=3.

3.2.2 Hydrogen Peroxide Activates AMPK to Repress Ion Transport

To determine if AMPK was activated by oxidative stress in our system, two intestinal epithelial cell lines were treated with 500 µM of hydrogen peroxide for 2-30 minutes. T_{84} cells resemble colonocytes while HT-29.cl19a cells are similar to enterocytes of the small intestine. Consistent with previous reports, we observed a significant increase of AMPK Threonine-172 phosphorylation at 5 and 15 minutes post-treatment. This increase was to a larger degree than our AICAR-treated positive control (Figure 3.4).

Our prior study demonstrated hydrogen peroxide inhibited calcium-dependent chloride secretion in polarized T_{84} colonic cell monolayers and AMPK has been shown

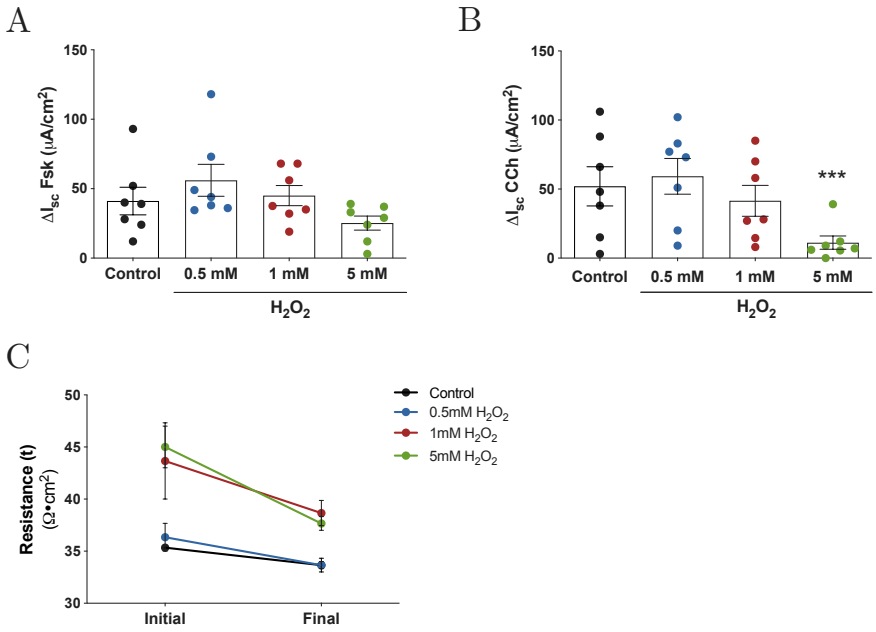

Figure 3.3: Hydrogen Peroxide Inhibits Calcium-Dependent Electrogenic Ion Transport in Mouse Colon

Wild-type mouse proximal colon mounted in Ussing chambers with Kreb's Ringer's Buffer was treated with 0 (Control), 0.5 mM, 1 mM, or 5 mM H_2O_2 for 30 minutes. A) Bilateral Forskolin (20 µM) treatment induced similar electrogenic ion transport responses for all treatment groups. B) Basolateral Carbachol treatment (300 µM) induced similar electrogenic ion transport responses in Control, 0.5 mM and 1 mM H_2O_2 treated tissues, as indicated by the change in short-circuit current (ΔIsc). 5 mM H_2O_2 significantly decreased electrogenic ion transport in response to Carbachol. C) Transepithelial electrical resistance did not differ significantly between all treatment groups for the duration of the experiment. Values are presented as Means ± S.D. *Asterisks* represent significant differences compared to control. n=7. ***p< 0.0001

extensively to repress ion secretion. We next wished to determine if AMPK mediated the inhibition of chloride secretion induced by hydrogen peroxide. To determine this, T_{84} and HT-29.cl19a intestinal epithelial cell monolayers were pre-treated with the AMPK inhibitor Compound C (1-100 µM) for 30 minutes in Ussing chambers, followed by hydrogen peroxide (500 µM) for 30 minutes. Carbachol (100 µM) was administered basolaterally to stimulate calcium-dependent chloride secretion. We observed a significant decrease in short-circuit

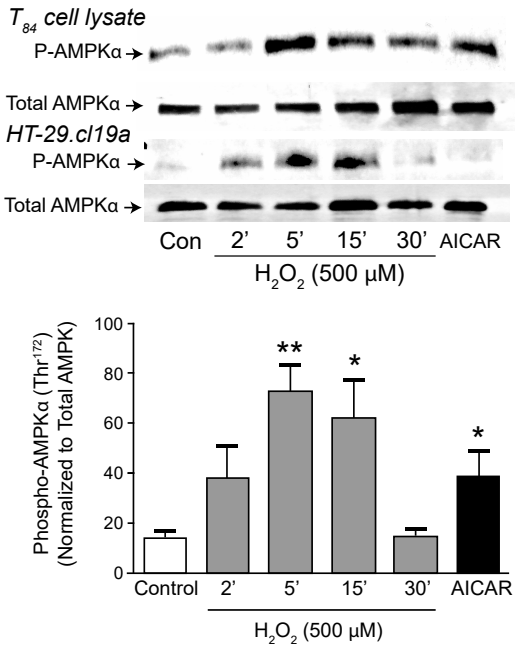

Figure 3.4: Hydrogen Peroxide Activates AMPK in Immortalized Human Intestinal Epithelial Cells

T_{84} and HT-29.cl19a intestinal epithelial cells were treated with H_2O_2 (500 µM) basolaterally for the indicated time points or AICAR as a positive control for AMPK activation. At 5 and 15 minutes post-treatment, AMPK phosphorylation was significantly increased compared to Control in both cell types. Quantification is displayed in B. Results are presented as Means ± S.E. *Asterisks* represent significant differences from Control. n=4. *$p<0.05$, **$p<0.01$

current (ΔI_{sc}) in H_2O_2-treated cells that was completely reveresed in cells pre-treated with 50 µM of Compound C (Figure 3.5).

Since our previous work has observed hydrogen peroxide induces a moderate but sustained increase in intracellular calcium, we hypothesized that activated Ca^{2+}/Calmodulin-dependent Protein Kinase Kinase β (CaMKKβ) was responsible for AMPK activation. To test this, polarized T_{84} cell monolayers were treated with 500 µM of hydrogen peroxide for 5, 15, or 30 minutes with or without pre-treatment with the CaMKKβ inhibitor STO-609 (10

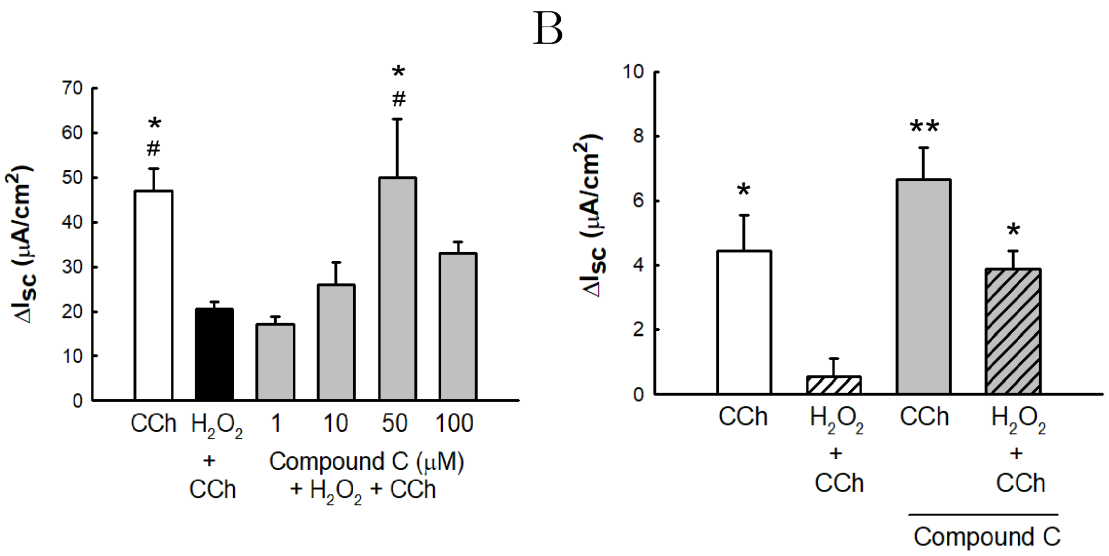

Figure 3.5: Hydrogen Peroxide Inhibits Carbachol-Induced Ion Transport in an AMPK-Dependent Manner

Polarized T_{84} and HT-29.cl19a intestinal epithelial cell monolayers were mounted in Ussing chambers containing Kreb's Ringer's Buffer. A) T_{84} cells were untreated or pre-treated with increasing concentrations of the AMPK inhibitor Compound C bilaterally for 30 minutes followed by 500 µM H_2O_2 basolaterally for 30 minutes. Chloride secretion was stimulated with 100 µM Carbachol (CCh) administered basolaterally. 50 µM of Compound C prevented H_2O_2 inhibition of chloride secretion. B) HT-29.cl19a cells were untreated or pre-treated with 50 µM of Compound C for 30 minutes. After pre-treatment, 500 µM H_2O_2 was administered basolaterally for 30 minutes and Carbachol was added to stimulate ion transport. Compound C pre-treatment restored the ion transport response to Carbachol during H_2O_2 exposure. Values are presented as Means ± S.E. *Asterisks* represent significant differences from H_2O_2 + CCh. n=3. *$p<0.05$, **$p<0.01$, # $p<0.05$ vs. Compound C (1 µM) in Figure 3.5A.

µM, bilaterally). We observed a slight decrease in AMPK Threonine-172 phosphorylation, however this was not statistically significant (Figure 3.6).

3.2.3 AMPK Inhibition of Calcium-Dependent Ion Transport is NKCC1-Dependent

As NKCC1 is rate-limiting in ion secretion, we determined if AMPK and NKCC1 interact directly during oxidative stress using co-immunoprecipitation. T_{84} colonic cells were treated

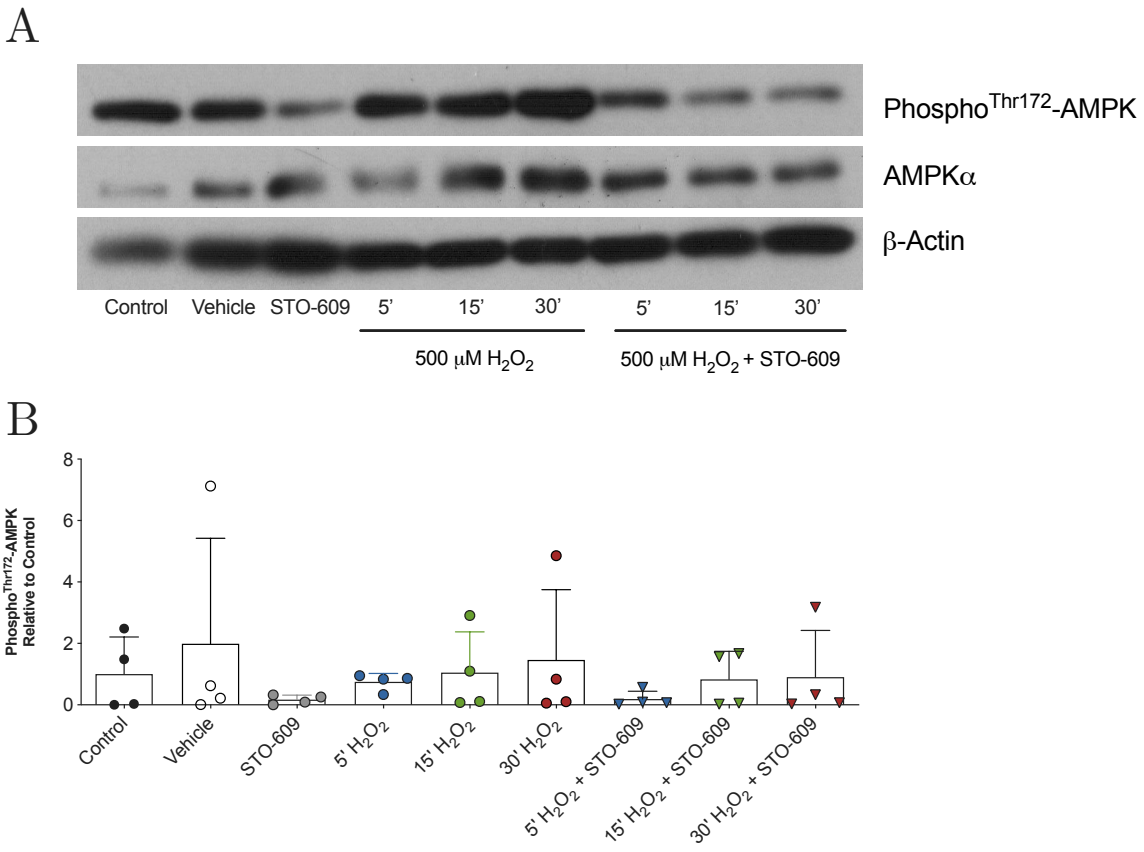

Figure 3.6: Ca^{2+}/Calmodulin-dependent Protein Kinase Kinase-β is not required for H_2O_2-Induced AMPK Activation

Polarized T_{84} cells were treated with H_2O_2 (500 μM) basolaterally for the indicated time points with or without 30 minute pre-treatment with STO-609 (10 μM) resuspended in DMSO. Vehicle treated cells were treated bilaterally with DMSO for 30 minutes. STO-609 pre-treatment slightly decreased AMPK Threonine-172 phosphorylation, although this did not reach statistical significance. Results are presented as Means ± S.D. for levels of fold-change over control of Phospho-AMPK normalized to Total AMPK. n=4.

with hydrogen peroxide as before and NKCC1 or AMPK was immunoprecipitated from whole cell lysates, followed by western blot to probe for the reciprocal protein. We confirmed AMPK and NKCC1 are physically associated and observed a significant increase in NKCC1-AMPK association during oxidative stress (Figure 3.7).

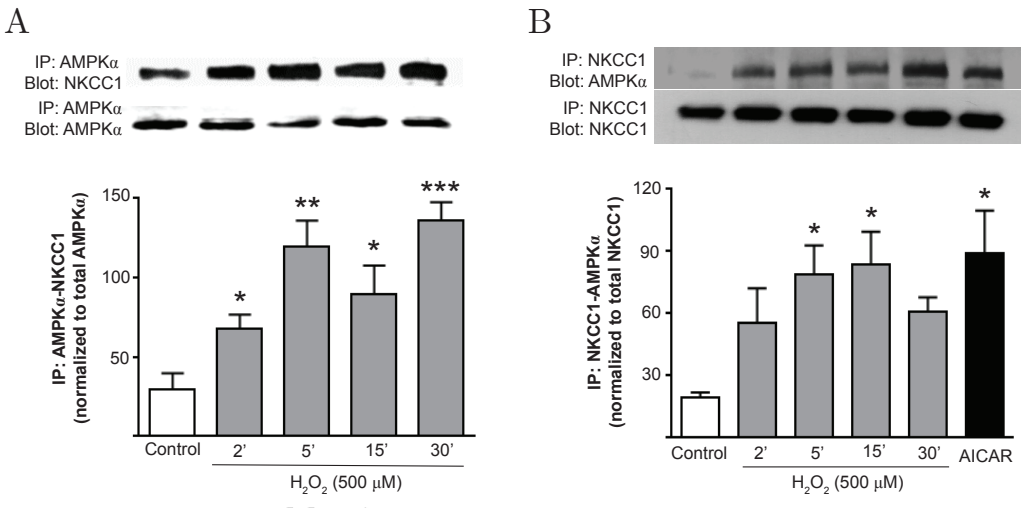

Figure 3.7: Oxidative Stress Induces Direct Interaction of AMPK and NKCC1

Polarized T_{84} cell monolayers were treated with H_2O_2 (500 µM) basolaterally for 2-30 minutes. AICAR (2.5 mM for 30 minutes) treatment was included as a positive control for AMPK activation. AMPKα (A) or NKCC1 (N-16 antibody) (B) was immunoprecipitated from cell lysates and pull-down samples were probed for NKCC1 (T4 antibody) (A) and/or AMPKα (B) by western blot. H_2O_2 treatment significantly increased AMPK and NKCC1 binding. Results are presented as Means ± S.E. for levels of pull-down normalized to total levels of the primary immunoprecipitate. n=4. *Asterisks* represent significant differences from control cells. *$p<0.05$, **$p<0.01$, ***$p<0.001$

Previous work has demonstrated cycling of NKCC1 from the membrane following stimulation of electrogenic ion secretion [24, 26, 27]. As AMPK interaction with NKCC1 is induced by hydrogen peroxide and is associated with reduced ion transport, I hypothesized this could be due to membrane removal of NKCC1. In order to determine if oxidative stress induces internalization of membrane-bound NKCC1, I performed a cell surface-biotinylation assay. Polarized T_{84} cell monolayers pre-treated with Compound C followed by hydrogen peroxide treatment were washed and the basolateral membranes were incubated with Sulfo-NHS-SS-biotin that binds proteins without permeating the cell membrane due to a its negative charge. Biotinylated proteins were isolated from whole cell lysates using streptavidin agarose beads and eluted by reducing agent in loading buffer. I observed an increase

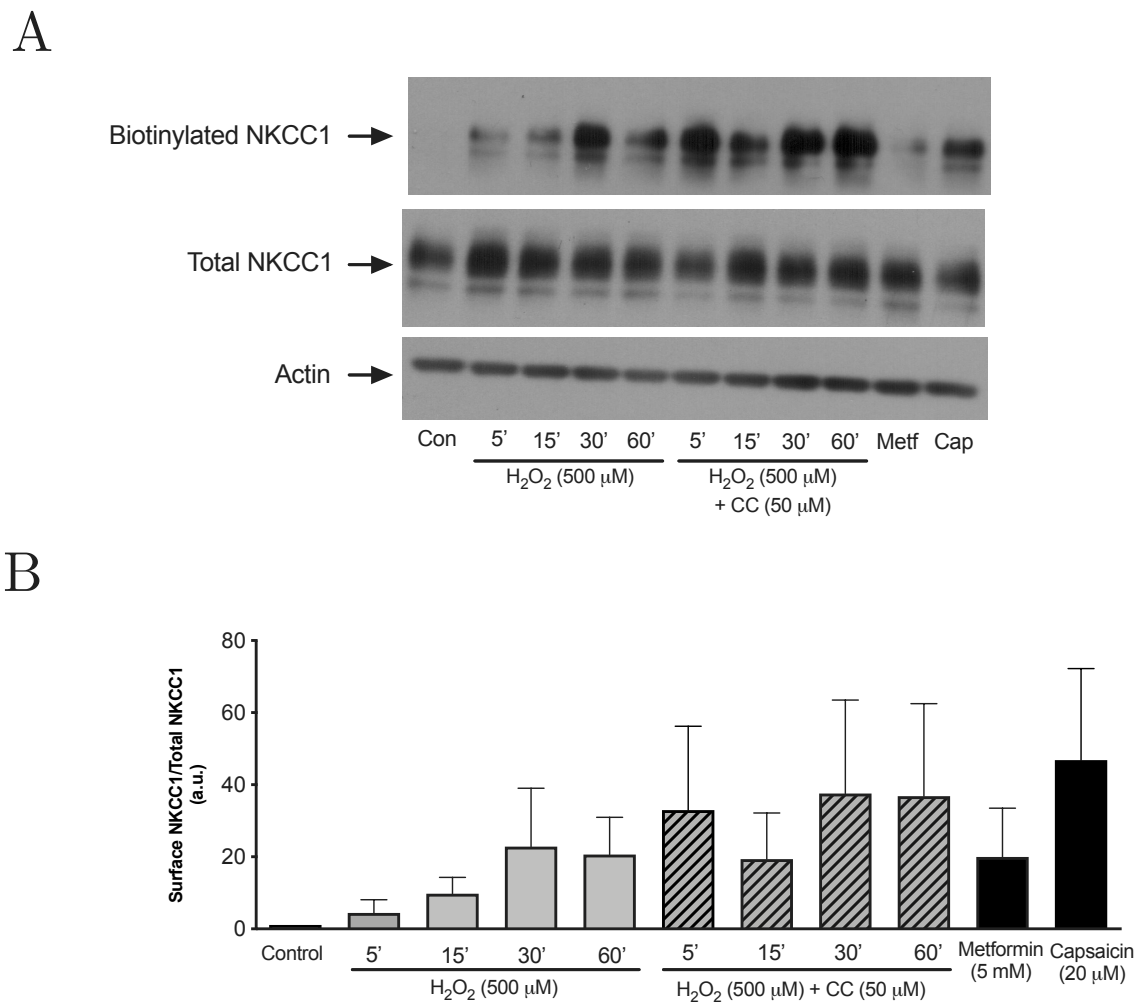

Figure 3.8: Cell Surface Expression of NKCC1 is Unaffected by AMPK Activation During Oxidative Stress

Polarized T_{84} cell monolayers were untreated or pre-treated with Compound C (50 µM) bilaterally for 30 minutes prior to treatment with H_2O_2 for 5, 15, 30, or 60 minutes. Metformin (5 mM) and Capsaicin (20 µM) were included as positive controls for AMPK activation and the biotinylation assay, respectively. Basolateral surface proteins were biotinylated and pulled down. Cell lysates were probed for NKCC1 expression in pull-down and whole cell lysates. Hydrogen peroxide slightly increased cell surface expression of NKCC1, although this was not statistically significant. Pre-treatment with Compound C slightly increased cell-surface expression. There was no significant change in biotinylated NKCC1 with AMPK activation. Results are presented as Means ± S.D. for levels of pull-down normalized to total levels of NKCC1. n=3.

in cell surface expresson of NKCC1 in hydrogen peroxide-treated cells, although this was not statistically significant (Figure 3.8). In addition, AMPK inhibition by Compound C

did not significantly alter NKCC1 membrane expression although we did observe a modest increase. Therefore, while AMPK is associated with NKCC1 during oxidative stress, it does not appear to regulate its membrane expression.

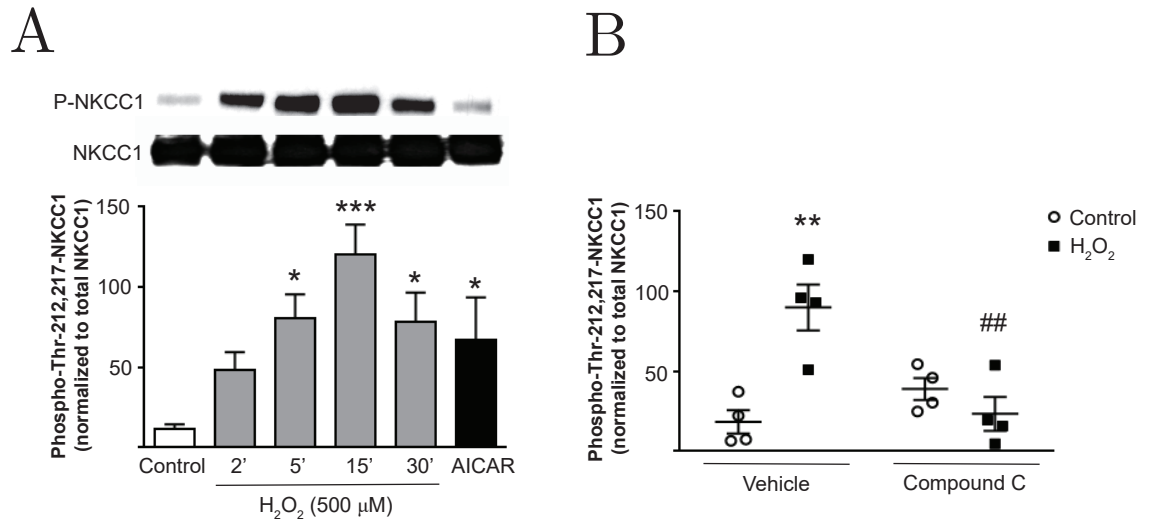

Figure 3.9: Hydrogen Peroxide Increases NKCC1 Phosphorylation via AMPK

A) Polarized T_{84} cell monolayers were treated with H_2O_2 (500 µM) basolaterally for 2-30 minutes or AICAR (2.5 mM) bilaterally for 30 minutes. H_2O_2 significantly increased NKCC1 phosphorylation after 5 minutes and AMPK activation by AICAR also resulted in an increase of NKCC1 phosphorylation. B) Polarized T_{84} monolayers were pre-incubated with Compound C (50 µM) bilaterally for 30 minutes followed by H_2O_2 treatment. Compound C prevented NKCC1 phosphorylation during H_2O_2 treatment. Results are presented as Means ± S.E. for Phospho-Thr212/217-NKCC1 normalized to total levels of NKCC1. n=4. *$p<0.05$, **$p<0.01$, ***$p<0.001$ compared to Control, Vehicle control, and Compound C alone. ## $p<0.01$ compared to Vehicle H_2O_2.

Since AMPK does not affect NKCC1 membrane localization, we hypothesized that AMPK could be regulating NKCC1 by altering its phosphorylation status. Polarized T_{84} monolayers were exposed to hydrogen peroxide as before for 2-30 minutes or the AMPK activator AICAR (2.5 mM) bilaterally for 30 minutes. We then determined phosphorylation of Threonine-212 and -217, which are known to be associated with NKCC1 activation [63]. Surprisingly, oxidative stress and AMPK activation by AICAR significantly increased

NKCC1 phosphorylation at Threonine-212/217 (Figure 3.9A). In addition, T_{84} monolayers pre-treated with Compound C (50 µM) bilaterally for 30 minutes were resistant to NKCC1 phosphorylation induced by oxidative stress compared to vehicle control cells (Figure 3.9B). We also measured oxidative stress-induced NKCC1 phosphorylation in *ex vivo* human colon biopsies obtained from uninflamed regions of patients with no active inflammatory intestinal disease. We observed a pronounced increase in NKCC1 phosphorylation that was associated with AMPK activation in hydrogen peroxide-treated explants compared to controls (Figure 3.10).

Based on our data demonstrating AMPK activation increased phosphorylation of NKCC1 at residues associated with activation, we next confirmed if NKCC1 activity was increased in an AMPK-dependent manner. Polarized T_{84} monolayers were treated with Compound C prior to hydrogen peroxide exposure (500 µM, basolaterally) for 30 minutes. Monolayers were then transferred to Ussing chambers and calcium-dependent ion transport was stimulated by basolateral Carbachol treatment (100 µM) for 1 minute to initiate physiological activation of NKCC1. Monolayers were then incubated in Kreb's Ringer's buffer containing $^{86}Rb^{+}$ in the basolateral chamber for 3 minutes. $^{86}Rb^{+}$ was used as a marker for K^{+} influx mediated by NKCC1 as it is similar in charge. Monolayers were washed and lysed, and $^{86}Rb^{+}$ content was measured by a scintillation counter. Colonic epithelial cells under oxidative stress displayed a significant decrease in $^{86}Rb^{+}$ influx indicating repression of NKCC1 activity (Figure 3.11). We determined AMPK was necessary for this effect as cells pre-treated with Compound C did not have decreased $^{86}Rb^{+}$ influx.

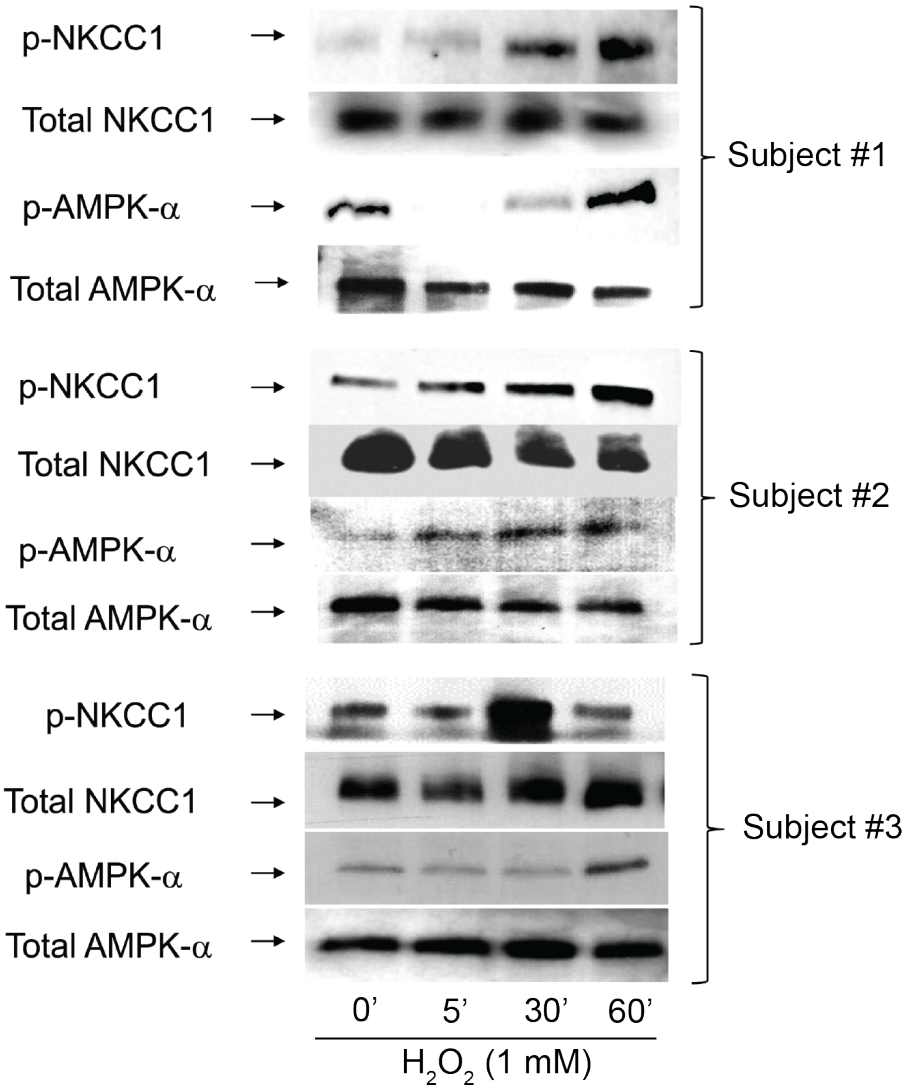

Figure 3.10: Oxidative Stress Increases NKCC1 and AMPK Phosphorylation in Human Colon Biopsies

Ex vivo human colon biopsies from non-inflamed control subjects without any active inflammatory intestinal disease were incubated with H_2O_2 (1 mM) for 30 minutes. Increased NKCC1 phosphorylation with H_2O_2 treatment was associated with increased AMPK phosphorylation. n=3.

Thus far we have shown that oxidative stress-induced activation of AMPK mediates inhibition of NKCC1 activity while NKCC1 phosphorylation at Threonine-212 and -217 was increased. I next hypothesized if AMPK could directly phosphorylate NKCC1 at

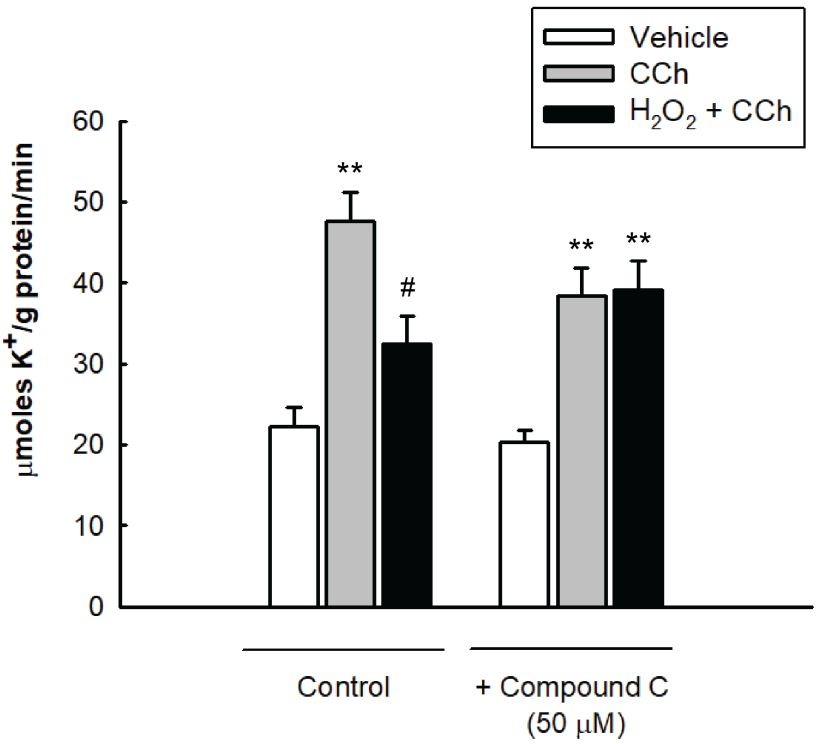

Figure 3.11: Oxidative Stress Stimulates NKCC1 Activity through AMPK

Polarized T_{84} cell monolayers were untreated or pre-incubated in Compound C (50 µM) bilaterally for 30 minutes then treated with H_2O_2 (500 µM) basolaterally for 30 minutes. Cells were transferred to Ussing chambers containing Ringer's buffer in the apical chamber and Ringer's buffer or Ringer's buffer + Carbachol (100 µM) in the basolateral chamber for 1 minute. Monolayers were then transferred to a basolateral $^{86}Rb^+$-containing buffer for 3 minutes. Compound C treatment prevented the H_2O_2-induced reduction of NKCC1 activity after Carbachol stimulation. Data are expressed as Means ± S.E. rate of K^+ uptake (µMoles K^+/gram protein/minute). n=4. *Asterisks* represent significant differences from Control cells and # represent significant differences from Carbachol-treated cells. **$p<0.01$, # $p<0.05$

a different site. I determined that the primary sequence flanking Serine-1084 resembled the AMPK consensus sequence where basic-hydrophobic-basic reside motif was located -4 of the proposed Serine and a hydrophobic residue followed at +4 [64]. Serine-1084 is located in the cytoplasmic tail, where it could contribute to cotransporter regulation. To confirm if AMPK phosphorylates NKCC1 directly at this site I performed *in vitro* kinase assays using the wild-type NKCC1 sequence and a mutant sequence with a Serine-1084 to Alanine-1084

substitution. I did not observe significant phosphorylation of Serine-1084 compared to both the mutant sequence and SAMS peptide, a known AMPK phosphorylation substrate included as a positive control (Figure 3.12).

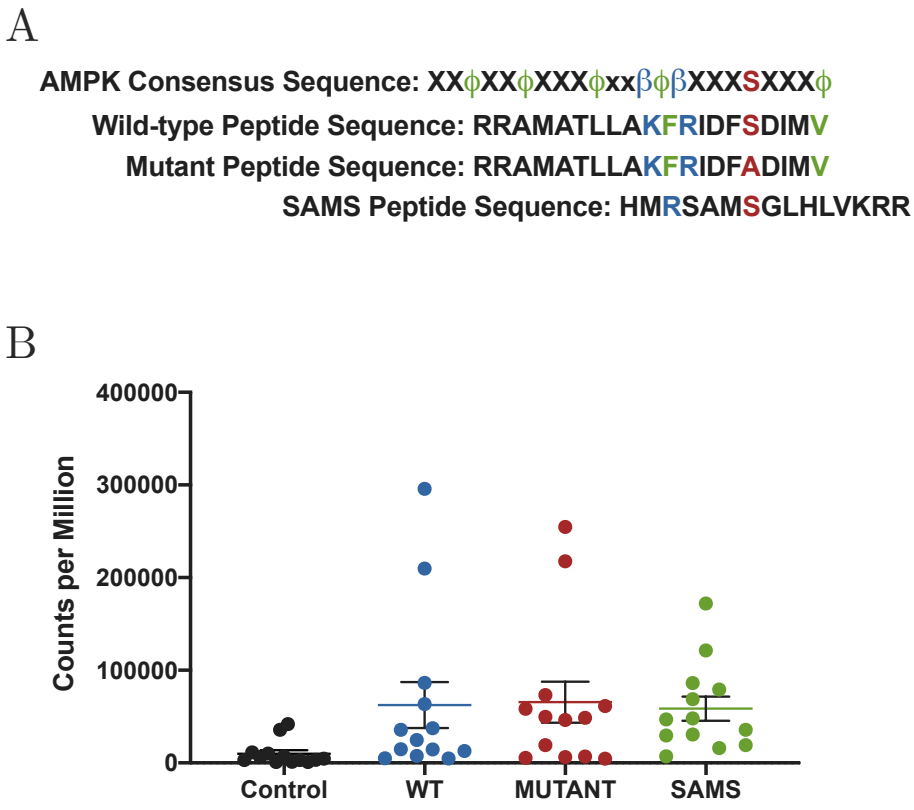

Figure 3.12: AMPK Does Not Phosphorylate NKCC1 at Serine-1084

A) AMPK consensus sequence and NKCC1 peptide sequences flanking Serine-1084. The mutant peptide contains Alanine for Serine-1084. B) Recombinant AMPK protein was added to reactions containing ^{32}P-ATP and peptides with Ser-1084 (Wild-type), Ala-1084 (Mutant) or SAMS peptide as a positive control. All peptide-containing reactions displayed similar levels of ionizing radiation and therefore I could not definitively conclude AMPK phosphorylates Serine-1084. Results are depicted as Means ± S.E. n=13.

3.2.4 H_2O_2-Induced Inhibition of Ion Transport in AMPKα2 Knockout Mice

Finally, I sought to confirm AMPK as a mediator of oxidative stress-induced repression of calcium-dependent ion secretion using a whole-body deletion of the AMPKα2 catalytic subunit transgenic mouse model. Proximal colons were excised, serosa was stripped, and tissue was mounted in Ussing chambers with Kreb's Ringer's buffer. Tissues were exposed to hydrogen peroxide for 30 minutes followed by stimulation of electrogenic ion secretion by the secretagogues Forskolin (20 µM) and Carbachol (300 µM). Consistent with previous results, we observed a significant decrease in calcium-dependent ion secretion with hydrogen peroxide. However, this effect was intact in AMPKα2 knockout mice (Figure 3.13). We did not observe an oxidative stress-dependent alteration in cAMP-dependent ion transport, although AMPKα2 knockout mice did have an increased response in both conditions.

3.3 Discussion

Regulation of epithelial transport is an intricate and multi-faceted physiological process that requires careful orchestration of acute vs. chronic and transient vs. sustained events. Immune cells such as macrophages and neutrophils in the lamina propria secrete reactive oxygen species acutely following sensing of bacterial components. This results in short-term regulation of electrolyte transport. In this context, we investigated whether the cellular energy sensor AMP-activated Protein Kinase (AMPK), itself capable of acute and/or sustained regulation of many metabolic events, was involved in the H_2O_2-mediated regulation

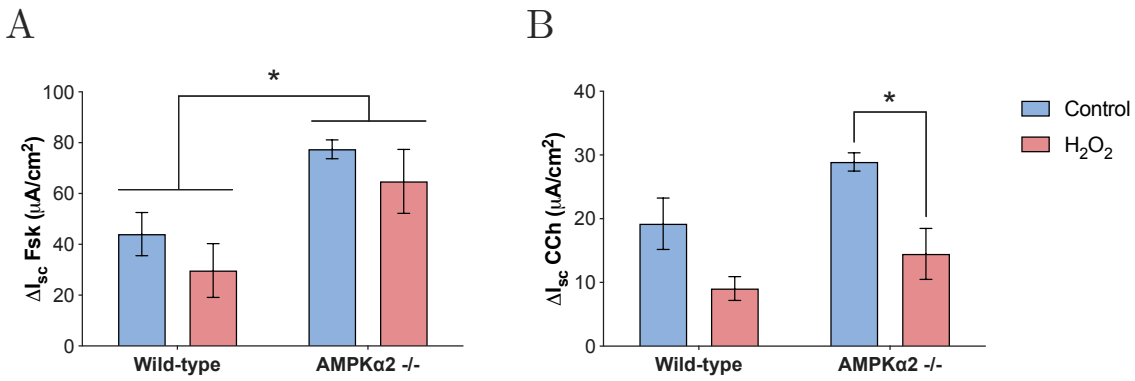

Figure 3.13: AMPKα2 Knockout Mice Have Repressed Ca^{2+}-Stimulated Ion Transport in Oxidative Stress

Proximal colons from male AMPKα2 KO and wild-type mice were stripped of serosa and mounted in Ussing chambers. H_2O_2 (1mM, bilaterally) was added and tissue was incubated for 30 minutes. Electrogenic ion transport was initiated using Forskolin (20 µM) (A) followed by Carbachol (300 µM) (B). AMPKα2 deletion had no appreciable effect on inhibition of Ca^{2+}-dependent ion secretion by H_2O_2 however, these mice did exhibit increased cAMP-dependent ion secretion compared to wild-type mice. Results depicted as mean ± S.E. n=3-5. *p<0.05, **p<0.01

of calcium-dependent ion transport. This study determined oxidative stress in the intestinal epithelium activates AMPK and leads to suppression of calcium-stimulated electrogenic ion secretion through AMPK regulation of NKCC1 activity (Figure 3.14).

3.3.1 Regulation of Ion Transport in the Intestinal Epithelium during Oxidative Stress

Oxidative stress has previously been shown to alter intestinal ion transport [65, 66]. The first study of the effect of oxidative stress on intestinal ion flux demonstrated that a high concentration of hydrogen peroxide (5.5 mM) administered to either the apical or basolateral compartment or bilaterally, resulted in equivalent responses in short-circuit current without agonist treatment [65]. However, these large changes in short-circuit current may have been

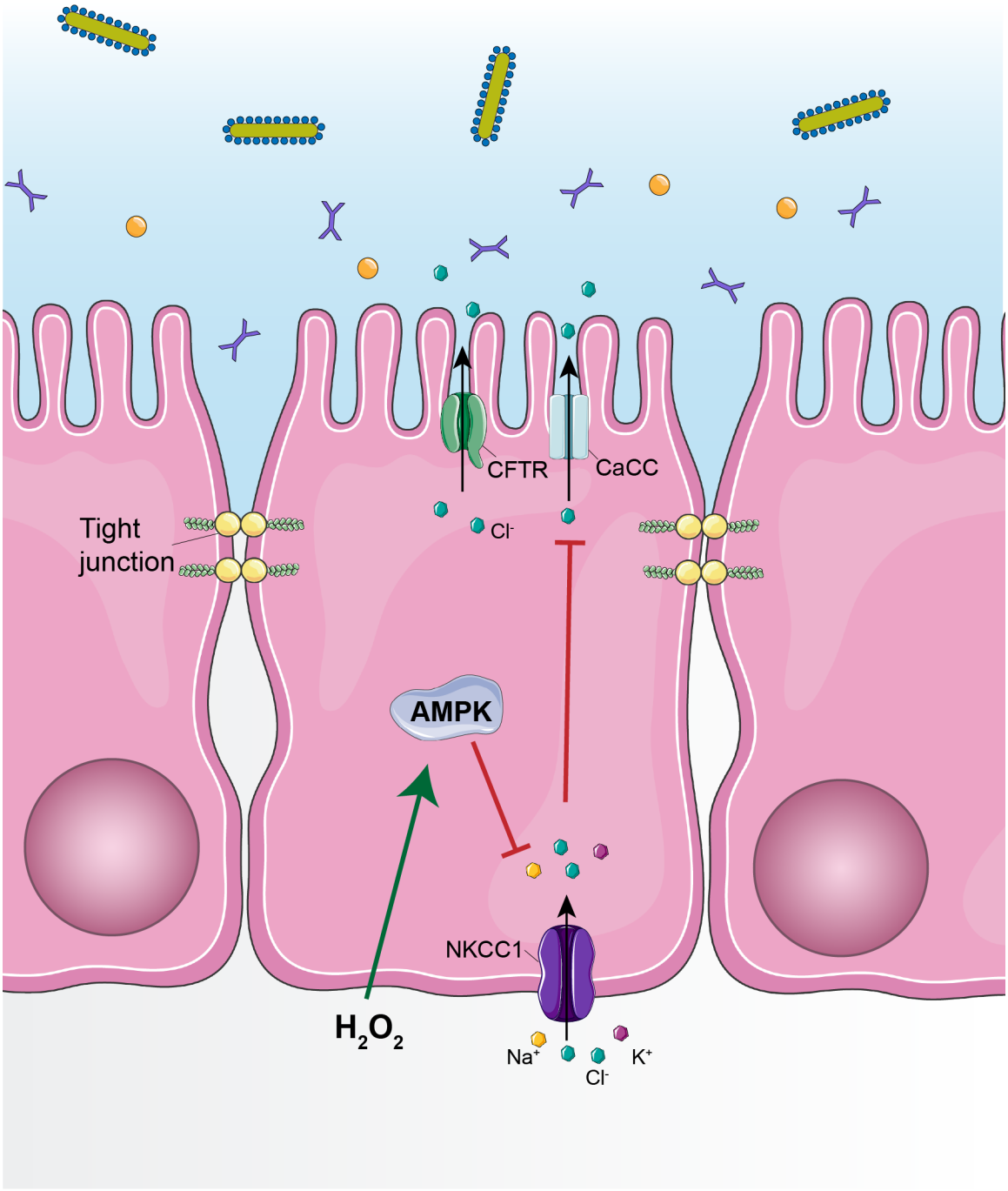

Figure 3.14: AMPK Mediates Inhibition of Ca^{2+}-Stimulated Electrogenic Ion Transport during Oxidative Stress

Oxidative stress in the form of hydrogen peroxide activates AMPK in intestinal epithelial cells. AMPK activation results in inhibition of NKCC1 activity and calcium-activated electrogenic ion transport.

due to the large quantity of hydrogen peroxide used in the study. For our experiments, hydrogen peroxide was administered basolaterally to mimic reactive oxygen species release by immune cells in the lamina propria. As in previous studies, under these conditions we observed that initial addition of hydrogen peroxide stimulated a small and transient increase in short-circuit current (data not shown) [48, 66]. We observed inhibition of Ca^{2+}-dependent ion transport in immortalized human intestinal epithelial cells, wild-type mouse intestinal epithelium, and human colon biopsies. This was not accompanied by an impairment in intestinal permeablity, consistent with previous results [48]. In addition, our findings confirmed earlier work that hydrogen peroxide treatment could repress calcium-dependent ion secretion, however we did not observe any change in cyclic AMP-dependent ion transport [48]. This is in contrast to previous studies that identified decreased cAMP-dependent ion transport responses [51, 65, 66]. However these studies differed from ours in the concentration and administration location of hydrogen peroxide. Nguyen et al. utilized a much higher dose of hydrogen peroxide (5.5 mM) and while Duvall et al. treated cells with the same concentration of hydrogen peroxide (500 µM), treatments were administered bilaterally rather than basolaterally. Increases in short-circuit current were previously characterized to be due largely to apical chloride secretion, although changes in other transporters that contribute to overall apical chloride secretion have been previously observed [47, 65, 66]. Our findings that NKCC1 activity is repressed leading to net inhibition of calcium-dependent electrogenic ion transport are consistent with these data. These observations suggest oxidative stress has a concentration-dependent effect on intestinal ion transport.

3.3.2 AMPK Activation by Oxidative Stress

Concurrently, oxidative stress in intestinal epithelial cells activated AMPK independently of CaMKKβ. Earlier work from our lab demonstrated hydrogen peroxide led to a moderate but sustained increase in intracellular calcium [48]. Thus, we initially hypothesized H_2O_2-induced AMPK activation would be mediated by CaMKKβ which is activated by increases in intracellular calcium. However, I did not observe a significant reduction in AMPK phosphorylation in colonic epithelial cells treated with a CaMKKβ inhibitor. Other kinases that can activate AMPK include Liver Kinase B1 (LKB1) and Transforming Growth Factor β-Activated Kinase 1 (TAK1). LKB1 activation of AMPK is downstream of increases in intracellular AMP and ADP (and decreases in intracellular ATP). Our lab previously observed H_2O_2 decreases intracellular ATP in T_{84} colonic cells and others have determined AMPK activation by H_2O_2 is AMP/ADP-dependent [67, 68]. In addition, previous work has demonstrated H_2O_2 activation of AMPK is through LKB1 and not CaMKKβ in hepatoma cells [69]. These findings suggest AMPK activation is likely due to LKB1 and allosteric promotion of phosphorylation. Furthermore, earlier work demonstrated a number of signaling pathways are activated by hydrogen peroxide in intestinal epithelial cells, including Src, p38 MAPK, PI3K, Pyk2, and ERK1/2 signaling [48]. AMPK and PI3K/Akt are known to play antagonistic roles and Akt is known to phosphorylate AMPK at Serine residues within the ST loop that discourage its activation by Threonine-172 phosphorylation. ERK1/2 is also capable of phosphorylating AMPK at Serine-485 [70]. This suggests a complex network of signaling is activated by hydrogen peroxide that can regulate AMPK, although the discrete steps remain unknown. Apart from AMPK phosphorylation, previous work has demon-

strated that hydrogen peroxide may activate AMPK through oxidation of the α catalytic subunit [71]. The authors observed oxidation and S-glutathionylation of cysteine residues in the C-terminal domain were present in HEK293 cells and mouse lung with oxidative stress and was associated with increased AMPK activity. Together these data support our conclusion that oxidative stress activates AMPK and may do so through a number of mechanisms that converge on the α catalytic subunit.

3.3.3 Regulation of NKCC1 by AMPK

In addition to AMPK activation, we determined hydrogen peroxide induced association of AMPK with the basolateral cotransporter NKCC1. While NKCC1 activity can be regulated by membrane removal and recycling, we determined AMPK association with NKCC1 did not result in alteration of its cell surface expression. We did observe that AMPK activation increased NKCC1 phosphorylation at Threonine-212 and -217. These posttranslational modifications are typically associated with increased activation of NKCC1 [63]. Paradoxically, AMPK activation was necessary for repression of NKCC1 activity. We hypothesized AMPK could directly phosphorylate NKCC1 at Serine-1084 within the cytoplasmic tail of NKCC1 whose sequence conforms to the AMPK consensus sequence. However, kinase assays determined AMPK did not directly phosphorylate NKCC1 at Serine-1084. Fraser et al. demonstrated AMPK phosphorylates Serine-77 of NKCC1 in kidney cell lines leading to its inhibition [72]. Thus, phosphorylation of Serine-77 by AMPK during oxidative stress could lead to repression of NKCC1 activity. In addition, while Fraser et al. observed reduced Threonine-212/217 phosphorylation with AMPK activation, we believe that activation of

other signaling pathways may explain why Threonine-212/217 phosphorylation increased during oxidative stress in our experiments.

3.3.4 Oxidative Stress-Induced Inhibition of Ion Transport in AMPKα2 Knockout Mice

To confirm these findings in an *in vivo* model, we utilized an AMPKα2 whole-body knockout mouse. Importantly, these mice still retain AMPKα1 expression and activity. AMPKα2 knockout mice were not protected from oxidative stress-induced changes in ion transport, however these mice did exhibit increased capacity for cAMP-dependent ion secretion that was maintained with hydrogen peroxide treatment. Therefore it appears that oxidative stress regulates only calcium-dependent electrogenic ion transport and not cAMP-dependent ion secretion. In addition, these data suggest AMPKα2 mediates basal inhibition of chloride secretion at least partially, but that AMPKα1 may be responsible for hydrogen peroxide-induced inhibition of calcium-dependent electrogenic ion secretion. This is also consistent with previous data showing AMPKα1 can phosphorylate NKCC1 [72].

Together these data add to our previous understanding of how oxidative stress can affect intestinal epithelial ion transport. Oxidative stress appears to act in a context-dependent manner with different outcomes based on concentration and localization of exposure. Our study has demonstrated that in a model mimicking immune cell-secreted hydrogen peroxide, there is a net inhibition of calcium-dependent ion secretion without effect on cAMP-dependent ion movement and transepithelial electrical resistance. This inhibition is AMPK-dependent, where AMPK associates and inhibits NKCC1 activity leading to reduced ion transport. This is not due to removal of NKCC1 from the membrane but rather

appears to be modulated by NKCC1 phosphorylation. AMPK activation was not due to the increase in intrallcellular calcium, but may result from decreased intracellular ATP and/or oxidation of AMPK itself. This work further clarifies the control of ion transport in the context of cellular stress, which may occur physiologically during fasting and inflammation.

4 | Alteration of Homeostatic Intestinal Epithelial Functions by Loss of AMPKα Expression

4.1 Introduction

The intestinal epithelium is a critical component of the gastrointestinal tract. The epithelium serves to facilitate digestion through nutrient absorption and fluid secretion, and maintain tolerogenic immunity by precise regulation of its permeability. In addition, the leaky gut hypothesis of Inflammatory Bowel Disease pathogenesis suggests that increased intestinal permeability preceding clinical symptoms increases susceptibility of the intestine to develop chronic inflammation. Therefore, it is critical to understand how barrier function develops and is maintained during health and disease. Intestinal permeability in a healthy gut is largely determined by expression of tight junction proteins and their regulation. There are three distinct pathways of permeability that vary by molecule size and regulation. The pore pathway allows passage of ions and other small molecules through

the Tight Junction Complex. The leak pathway allows passage of larger molecules through regulation of Occludin and myosin light chain (MLC) phosphorylation. Finally, the unrestricted pathway allows unregulated movement of molecules due to epithelial cell death. In addition to regulation of permeability, another critical function of the intestinal epithelial cells is modulation of fluid secretion and reabsorption. The basic processes of fluid dynamics and their alteration during disease is reviewed in Chapters 1.2.2 and 3.1.1.

4.1.1 The Tight Junction Complex in Intestinal Epithelial Cells

The Tight Junction Complex is a critical protein structure at the apical membrane that tightly regulates paracellular passage of electrolytes and other small molecules across the epithelial monolayer. The tight junction complex is composed of transmembrane proteins such as claudins and TJ-associated Marvel Proteins or TAMPs (Occludin, Tricellulin/MARVELD2, MARVELD3). The intracellular domains of these proteins interact with a network of proteins termed the cytosolic junctional plaque. These plaque proteins include the Zonula occludens family and cytoskeletal proteins such as F-actin and microtubules. Claudin proteins form the basis of a tight junction 'pore' where their extracellular loop domains form a β-sheet fold that interact with claudins on neighboring cells as well as adjacent claudins within the same cell, forming characteristic intramembrane strands. Specific charged residues on these domains confers the specificity of permeable ions. In addition, expression of certain claudins within a tight junction can vary and is thought to determine tissue-specific permeability characteristics. TAMPs have been demonstrated to preferentially localize to particular membrane junctions. For example, Occludin is enriched at bicellular junctions while tricellulin is increased at intersections of three cells. Occludins

also have extracellular loop domains that interact with those on adjacent cell membranes. Zonula occludens proteins act as scaffolds by binding transmembrane junction proteins and F-actin intracellularly to connect the tight junction complex and the cytoskeleton. Tight junction assembly occurs through a multistep process and has largely been studied experimentally through the use of calcium-switch assays. Cells cultured in a low calcium media exhibit little junction formation, which can then be induced by addition of calcium. These studies revealed cell-cell contact initiates formation of immature junctions composed of E-cadherin and nectin at the basolateral membrane. Zonula occludens-1 (ZO-1) and α-catenin bind these primordial junctions allowing communication of adherens and tight junction components. This is followed by increased recruitment of tight junction proteins that activate RhoA and CDC42 to induce junction maturation where tight and adherens junctions become distinct and increase interaction with the cytoskeleton. Activation of myosin promotes columnar cell morphology and polar activation of CDC42 initiates cell polarization. Together these junctions give intestinal epithelial cells their polarized character and form the basis of the intestinal barrier.

4.1.2 Regulation of Permeability in the Intestinal Epithelium

As described earlier, intestinal permeability is a function of both pore (tight junction-mediated) and leak (MLC-mediated) pathways. Pore pathway permeability can be altered by claudin proteins as each claudin has distinct properties that allow passage of distinct molecules. In addition, claudin expression varies along the intestine further conferring regional functional differences in the intestine. Claudin-2 is widely studied as it is a pore-forming claudin, meaning it exerts charge-selectivity to the tight junction. Claudin-2 is

expressed highly in deep crypts and allows passage of small cations and water. Claudin-15 is also a cation-selective pore-forming claudin that is highly expressed in the small intestine and decreases distally. Conversely, Claudins 1 and 4 are barrier-forming claudins, in that they do not confer charge selectivity and further increase transepithelial electrical permeability where tight junctions are already present [1]. In accordance with these classifications, increased expression of pore-forming claudins and/or decreased expression of barrier-forming claudins is associated with decreased transepithelial electrical resistance. Increased leak pathway permeability occurs during physiopathological conditions and is due to the regulation of Occludin and the cytoskeleton by Myosin light-chain II kinase (MLCK). Studies have demonstrated Tumor Necrosis Factor-α (TNF-α) activates MLCK leading to its promotion of occludin endocytosis from the plasma membrane. In addition, MLCK-dependent contraction of the peri-junction acto-myosin ring and peri-junction microfilament aggreation induces membrane retraction and opening of large spaces between cells. In addition to TNF-α, other cytokines such as IL-1β can also regulate MLCK through increased gene and protein expression.

4.1.3 AMPK in the Intestinal Epithelium

While a number of studies have suggested important roles for AMPK in the intestinal epithelium, much of these data have relied on use of pharmacological agents and single catalytic isoform knockout mouse models. While useful, these methodologies have their limitations. As described earlier, pharmacological activators and inhibitors of AMPK are non-specific and have been demonstrated to have AMPK-independent effects [2–7]. These restrict the ability to draw conclusions that AMPK is necessary and required for a number

of observed effects. In addition, the use of single catalytic isoform knockout animals complicates observations since expression and/or activity of the remaining catalytic isoform can increase to compensate for the loss in expression [8, 9]. As such, researchers have turned to tissue-specific models where it is possible to excise both catalytic isoform genes in order to more robustly test the effects of AMPK in physiology and pathophysiology. I have obtained an intestinal epithelial-specific knockout mouse model that lacks expression and activity of both AMPK catalytic isoforms. In this study, I have characterized this mouse model to observe if AMPK deletion resulted in any defect of epithelial organization and turnover, barrier function, and intestinal functions such as ion transport.

4.2 Experimental Results

4.2.1 AMPK Subunit Expression in the Murine GI Tract

Intestinal epithelial-specific AMPK knockout mice (hereafter referred to as AMPK$\alpha^{\Delta \text{IEC KO}}$ mice) were generated by crossing AMPK$\alpha^{\text{fl/fl}}$ mice with Villin-Cre transgenic mice. Villin-Cre mice express Cre recombinase under the Villin-1 promoter, a protein expressed at brush border membranes. AMPK$\alpha^{\text{fl/fl}}$ mice have LoxP sites flanking the *Prkaa1* and the *Prkaa2* genes, that encode AMPKα1 and AMPKα2 respectively. Resulting progeny are either AMPK$\alpha^{\text{fl/fl}}$ mice or AMPK$\alpha^{\Delta \text{IEC KO}}$ mice where Cre recombinase is expressed and results in excision of *Prkaa1* and *Prkaa2* (Figure 4.1).

I first sought to confirm complete deletion of AMPKα expression and activity in AMPK$\alpha^{\Delta \text{IEC KO}}$ mice. Intestinal epithelial cells were isolated from segments of the large intestine (cecum, proximal colon, and distal colon) of AMPK$\alpha^{\text{fl/fl}}$ and AMPK$\alpha^{\Delta \text{IEC KO}}$ mice

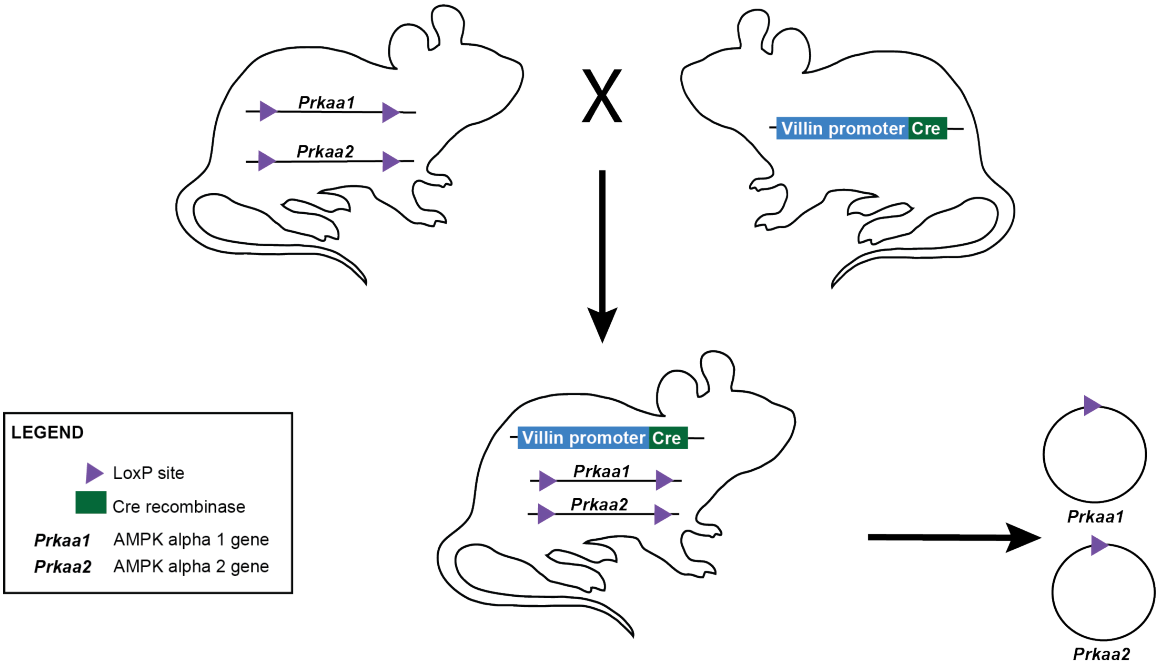

Figure 4.1: Breeding Scheme to Generate AMPKα$^{\Delta \text{IEC KO}}$ mice

AMPKα$^{\Delta \text{IEC KO}}$ mice were generated using a tissue-specific Cre-lox system. Villin-Cre mice express Cre recombinase under the Villin promoter, a brush border protein expressed in the intestinal epithelium. These mice were crossed with AMPKα$^{\text{fl/fl}}$ mice that have LoxP sites flanking the genes encoding AMPKα1 (*Prkaa1*) and AMPKα2 (*Prkaa2*). These sites are recognized by Cre recombinase dimers that will tetramerize and cleave the DNA, facilitating excision of intervening sequence. Thus, deletion of both *Prkaa1* and *Prkaa2* is accomplished only in cells expressing Villin protein, namely the intestinal epithelium.

using an EDTA-based method (described in Ch.2.12) and run on western blot to determine epression levels of AMPKα1, AMPKα2, and AMPKβ subunits isoforms. AMPKα1/2 expression was absent in AMPKα$^{\Delta \text{IEC KO}}$ mice, confirming epithelial-specific knockout (Figure 4.2). In addition, AMPK activity measured by phosphorylation of the target substrate Acetyl-CoA Carboxylase (ACC) was also absent from AMPKα$^{\Delta \text{IEC KO}}$ mice confirming the validity of this mouse model.

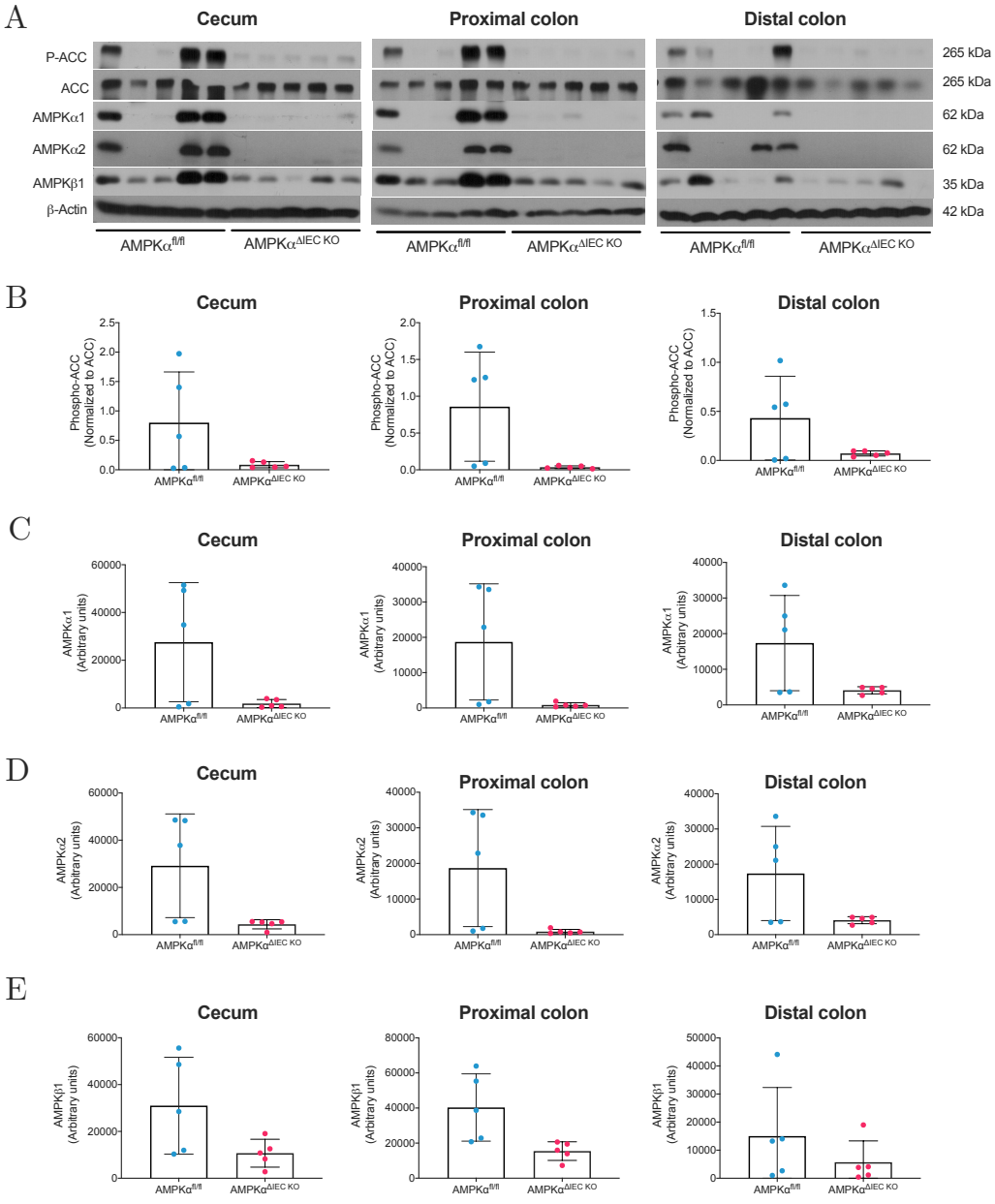

Figure 4.2: AMPK Activity and Subunit Expression in AMPKα$^{\Delta IEC\ KO}$ Mice

Isolated intestinal epithelial cells of the large intestine from AMPKα$^{fl/fl}$ and AMPKα$^{\Delta IEC\ KO}$ mice were assessed for AMPK subunit isoform and substrate expression. A) Blots of Phospho-Acetyl-CoA Carboxylase (P-ACC), Total Acetyl-CoA Carboxylase (ACC), AMPKα1, AMPKα2, and AMPKβ1 from large intestine segments of AMPKα$^{fl/fl}$ and AMPKα$^{\Delta IEC\ KO}$ mice. B) Quantification of Phospho-ACC blots in A. Phosphorylation of ACC was decreased in AMPKα$^{\Delta IEC\ KO}$ mice and AMPKα$^{fl/fl}$ mice with decreased AMPKα expression. C,D) Quantification of AMPKα1 and AMPKα2 expression. Expression of both isoforms varied in AMPKα$^{fl/fl}$ mice and was lost in AMPKα$^{\Delta IEC\ KO}$ mice as expected. E) Quantification of AMPKβ1 expression. AMPKβ1 levels correlated with expression of AMPKα, although was not absent in AMPKα$^{\Delta IEC\ KO}$ mice. Values exhibited as Means ± S.D. n=5

I observed expression of AMPKβ1 was present in the large intestine of both AMPKα$^{fl/fl}$ and AMPKα$^{\Delta IEC\ KO}$ mice, however expression was decreased in AMPKα$^{\Delta IEC\ KO}$ mice (Figure 4.2). I was not able to detect AMPKβ2, suggesting AMPKβ1 may be the predominant AMPKβ isoform in intestinal epithelial cells. AMPKα expression varied in AMPKα$^{fl/fl}$ mice where some animals expressed very high levels and others expressed very low levels. This was consistent throughout segments of the large intestine and among the two catalytic isoforms. In addition, AMPKβ1 expression was increased in animals with higher levels of AMPKα expression suggesting AMPKα may promote AMPKβ1 expression and/or stability.

4.2.2 The Role of AMPK in Intestinal Structure and Barrier Function

I next sought to determine if loss of AMPK activity in the intestinal epithelium would lead to altered intestinal structure due to potential involvement of AMPK in epithelial turnover. Intestine was excised from AMPKα$^{fl/fl}$ and AMPKα$^{\Delta IEC\ KO}$ mice, fixed and sectioned for histomorphological analysis. I did not observe any change in villus length in the small intestine or crypt depth in the small and large intestines (Figure 4.3). In addition, structural or inflammatory abnormalities such as crypt bifurcation, cryptitis, etc. were not observed. These data indicate loss of AMPK activity alone does not have an appreciable impact on epithelial structure.

Despite no obvious effect of AMPK on intestinal epithelial histomorphology, I hypothesized that alterations in intestinal barrier function might exist. To determine this, tissue from the large intestine of adult mice was stripped of the serosa and mounted in

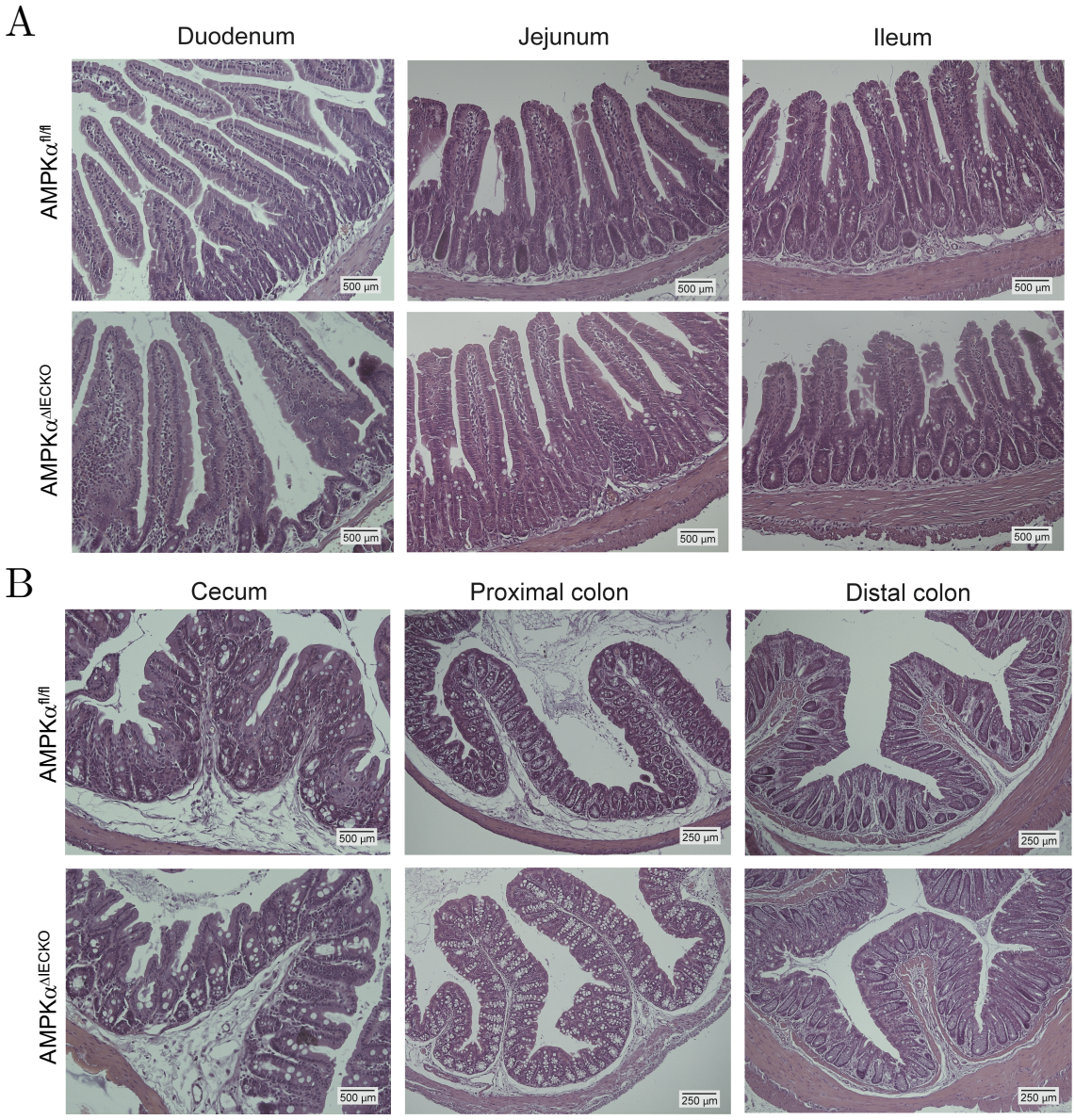

Figure 4.3: AMPKα$^{\Delta \text{IEC KO}}$ Mice have Normal Epithelial Structure and Tissue Morphology

Intestine from AMPKα$^{\text{fl/fl}}$ and AMPKα$^{\Delta \text{IEC KO}}$ mice was dissected, fixed and subjected to hematoxylin and eosin staining. A) Small intestine segments have similar villus length and crypt depth in AMPKα$^{\text{fl/fl}}$ and AMPKα$^{\Delta \text{IEC KO}}$ mice. B) Large intestine segments have similar crypt depth in AMPKα$^{\text{fl/fl}}$ and AMPKα$^{\Delta \text{IEC KO}}$ mice.

Ussing chambers containing Kreb's Ringer's Buffer (KBR) + D-glucose. Following a brief rest period, transepithelial electrical resistance (TEER) was measured. I observed similar

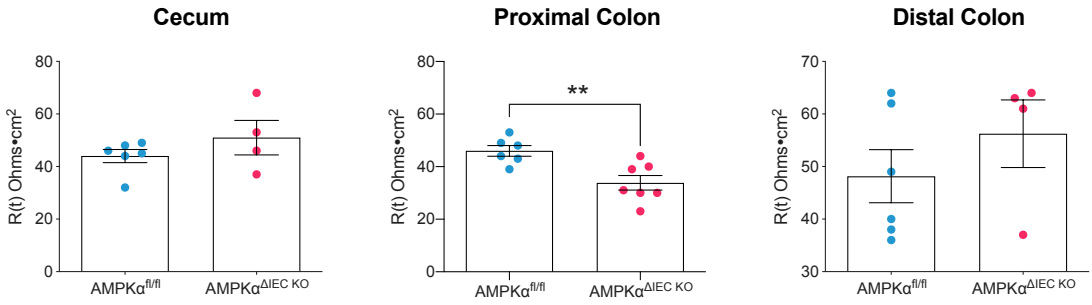

Figure 4.4: AMPKα Deficiency Decreased Resistance of the Proximal Colon

Cecum, proximal colon, and distal colon were excised and the serosal layer removed. Mucosa was mounted in Ussing chambers containing KBR and transepithelial electrical resistance was measured. AMPKα$^{\Delta \text{IEC KO}}$ mice displayed decreased resistance in the proximal colon. There was no significant change in resistance of the cecum and distal colon. Values represent Means ± S.D. *Asterisks* denote significant differences from AMPKα $^{\text{fl/fl}}$ mice. **p<0.01. n=4-7

TEER readings in the cecum and distal colon, however AMPKα$^{\Delta \text{IEC KO}}$ mouse proximal colon had significantly decreased resistance compared to AMPKα$^{\text{fl/fl}}$ mice (Figure 4.4).

To determine if AMPKα-deficiency resulted in increased macromolecular permeability, whole intestinal tissues were mounted in Ussing chambers containing Kreb's Ringer's buffer. 4 kDa fluorescein thiocyanate (FITC)-dextran was added to the apical side. The basolateral side was sampled at regular intervals to observe FITC-dextran flux over time. I determined AMPKα$^{\Delta \text{IEC KO}}$ mice had no significant difference in 4 kDa FITC-dextran permeability compared to AMPKα $^{\text{fl/fl}}$ mice (Figure 4.5).

Tight Junction Protein Expression Since I observed a significant decrease in resistance in the AMPKα$^{\Delta \text{IEC KO}}$ mouse proximal colon, I hypothesized that this could be due to altered expression of tight junction proteins. Intestinal epithelial cells were isolated from AMPKα$^{\text{fl/fl}}$ and AMPKα$^{\Delta \text{IEC KO}}$ mice and protein content was analyzed by western blot.

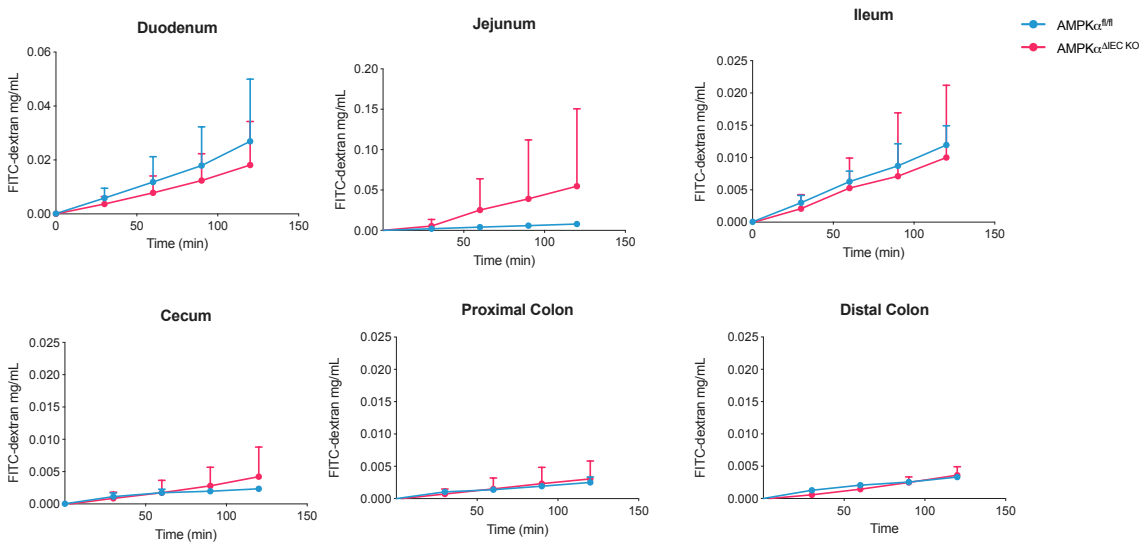

Figure 4.5: AMPKα$^{\Delta \text{IEC KO}}$ Mice Do Not Have Altered Macromolecular Intestinal Permeability

Intestine was excised and mounted in Ussing chambers containing Kreb's Ringer's buffer. 4 kDa FITC-dextran (FD4) was added to the apical side. The basolateral side was sampled every 30 minutes and 4 kDa FITC-dextran concentration was quantifed using a standard curve. Absence of epithelial AMPKα did not affect FD4 permeability in intestinal segments compared to AMPKα$^{\text{fl/fl}}$ mice. Values presented as Means ± S.D. n=2-5

I did not observe a significant change in E-cadherin and Zonula Occludens-1 expression (Figure 4.6). In addition, expression of Occludin was also unaltered in intestinal epithelial cells from the proximal colon of AMPKα$^{\Delta \text{IEC KO}}$ mice (Figure 4.7).

However, as claudin proteins can specify the permeability characteristics of tight junctions, I next wanted to determine if claudin expression was altered by loss of AMPK activity. Claudin-2 and Claudin-15 are known as pore-forming claudins whose increased expression can decrease transepithelial electrical resistance. I observed no significant change in expression of the pore-forming Claudins 2 and 15 (Figure 4.8). However, I did determine that Claudin-4 expression was significantly decreased in the distal colon and to a similar

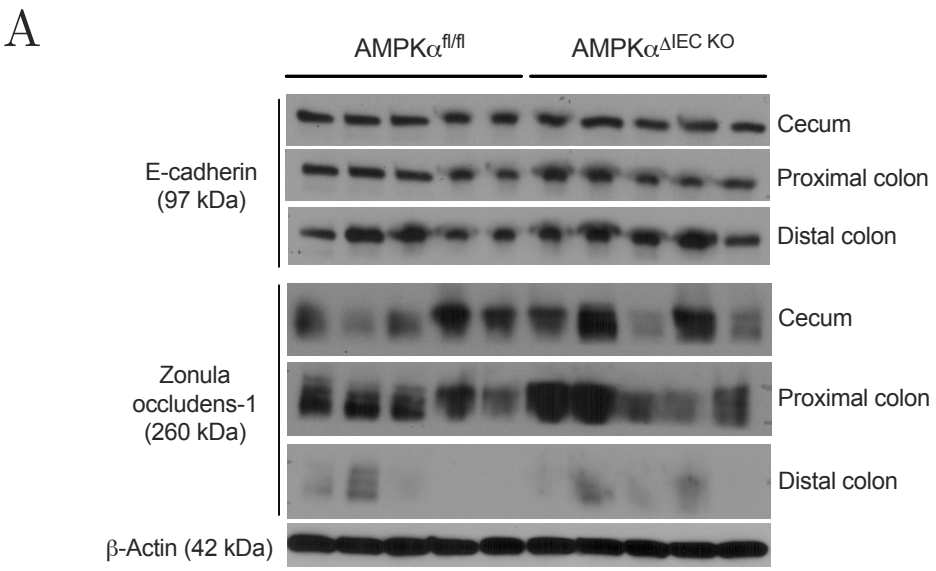

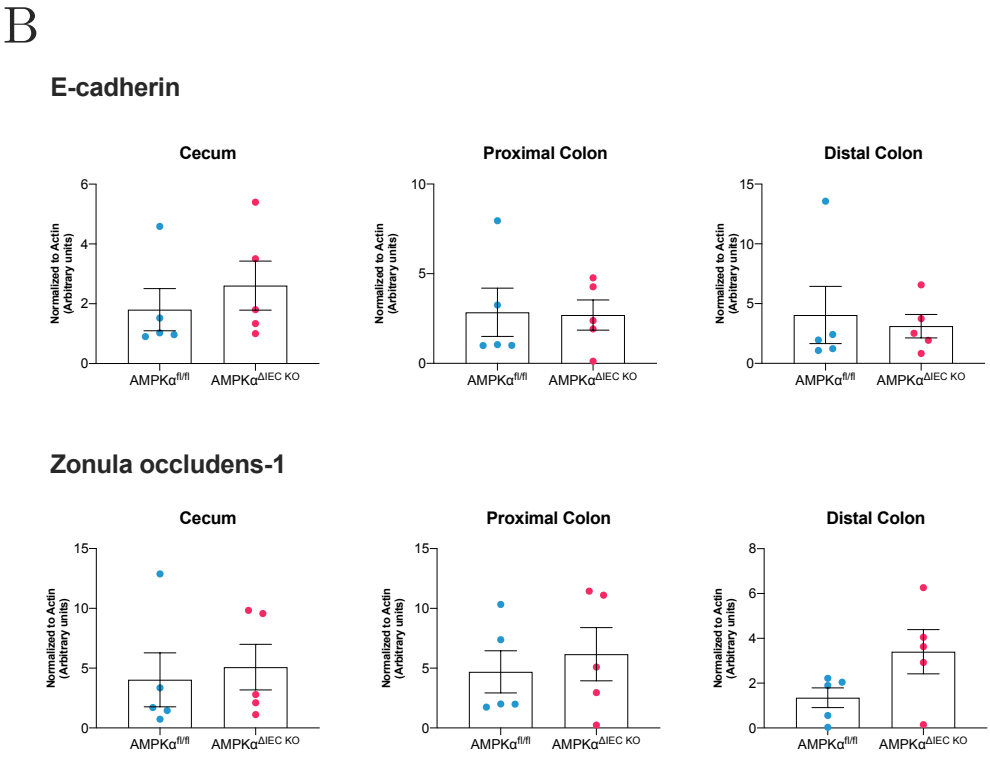

Figure 4.6: E-cadherin and ZO-1 are Expressed at Similar Levels in AMPKα$^{fl/fl}$ and AMPKα$^{\Delta IEC\ KO}$ Mice

Isolated intestinal epithelial cells from AMPKα$^{\Delta IEC\ KO}$ and AMPKα$^{fl/fl}$ mice were lysed and prepared for western blot. A) Blots of E-cadherin and ZO-1 expression in the large intestine from AMPKα$^{\Delta IEC\ KO}$ and AMPKα$^{fl/fl}$ mice normalized to loading control (β-Actin). B) Quantification of blots in A. Values are representative of Means ± S.D. n=5

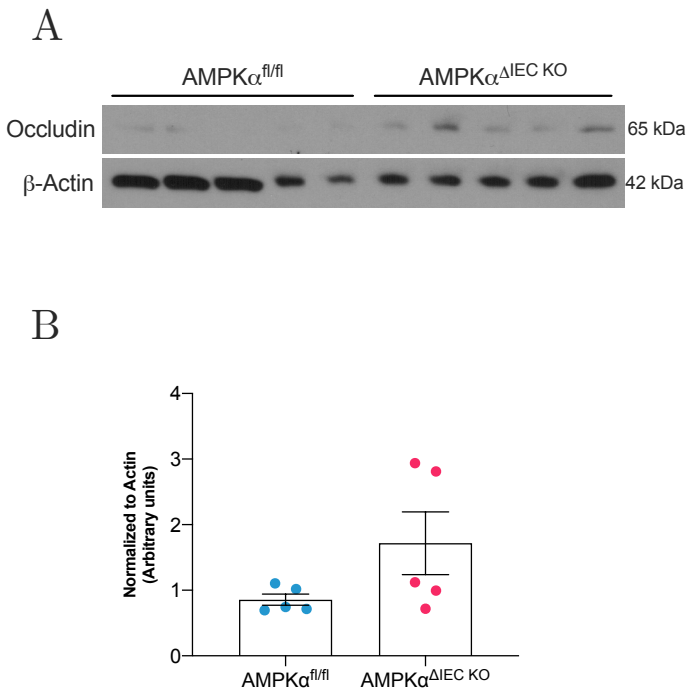

Figure 4.7: Occludin Expression is Similar in AMPKα$^{fl/fl}$ and AMPKα$^{\Delta IEC\ KO}$ Mice

Intestinal epithelial cells isolated from AMPKα$^{fl/fl}$ and AMPKα$^{\Delta IEC\ KO}$ mouse proximal colon were lysed and subjected to western blot. A) Blots of Occludin and β-Actin from AMPKα$^{fl/fl}$ and AMPKα$^{\Delta IEC\ KO}$ mice. B) Quantification of blots in A normalized to loading control (β-Actin). Values are expressed as Means ± S.D. n=5

degree in the proximal colon (not statistically significant) (Figure 4.9). Claudin-4 is a barrier forming claudin whose expression correlates with changes in transepithelial electrical resistance. Thus, these findings are consistent with the observed decrease in resistance in AMPKα $^{\Delta IEC\ KO}$ mouse colon.

4.2.3 Ion Transport Regulation

Electrogenic Ion Transport Responses As described earlier, AMPK is known as a modulator of apical chloride channels. We and others have previously shown AMPK can

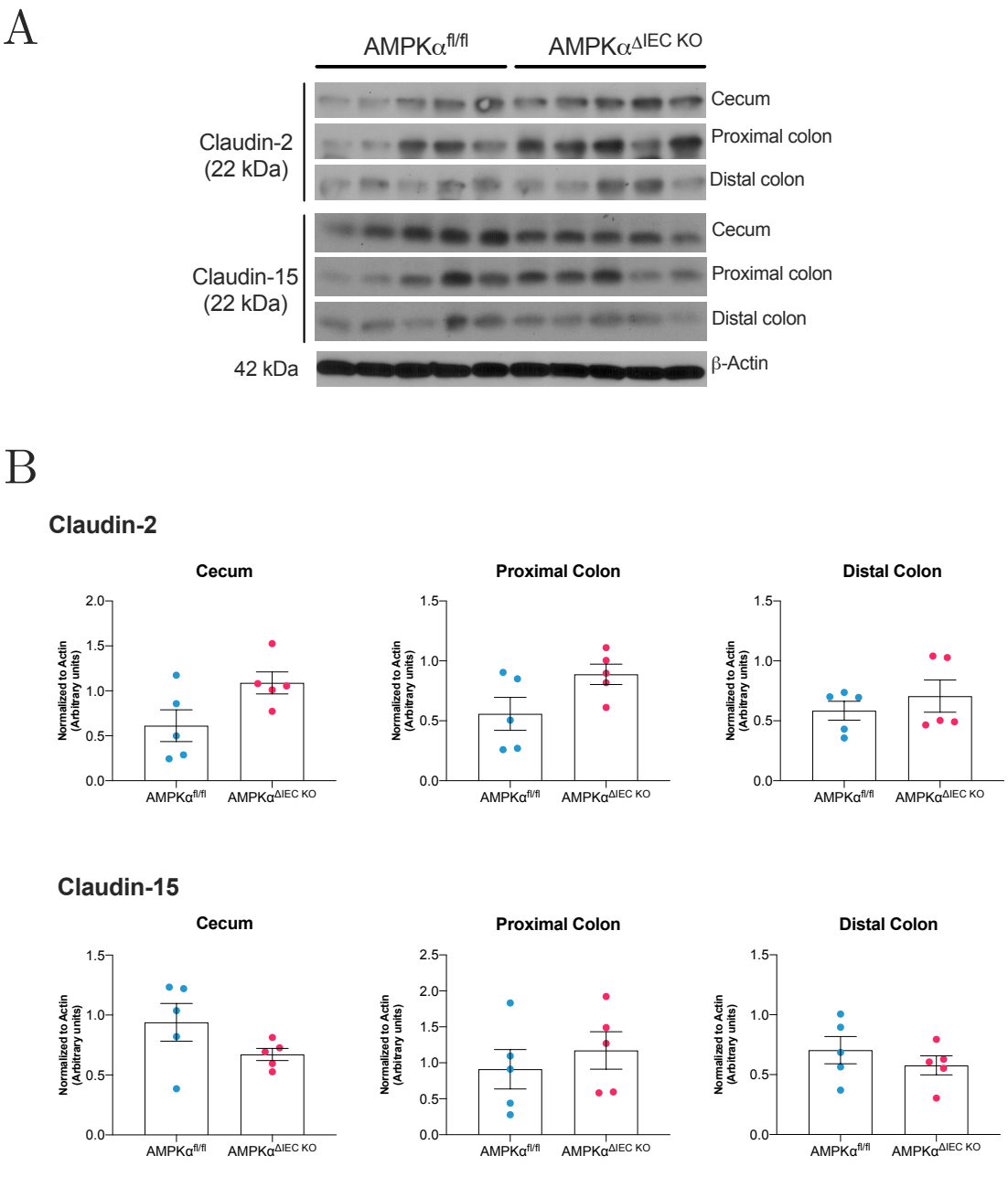

Figure 4.8: Expression of Pore-Forming Claudins 2 and 15 is Not Dependent on AMPK

Intestinal epithelial cells isolated from AMPKα$^{fl/fl}$ and AMPKα$^{\Delta IEC\ KO}$ mouse large intestine were lysed and subjected to western blot. A) Blots of Claudin-2 and Claudin-15 in AMPKα$^{fl/fl}$ and AMPKα$^{\Delta IEC\ KO}$ mice. B) Quantification of blots in A normalized to loading control (β-Actin). Values are expressed as Means ± S.D. n=5

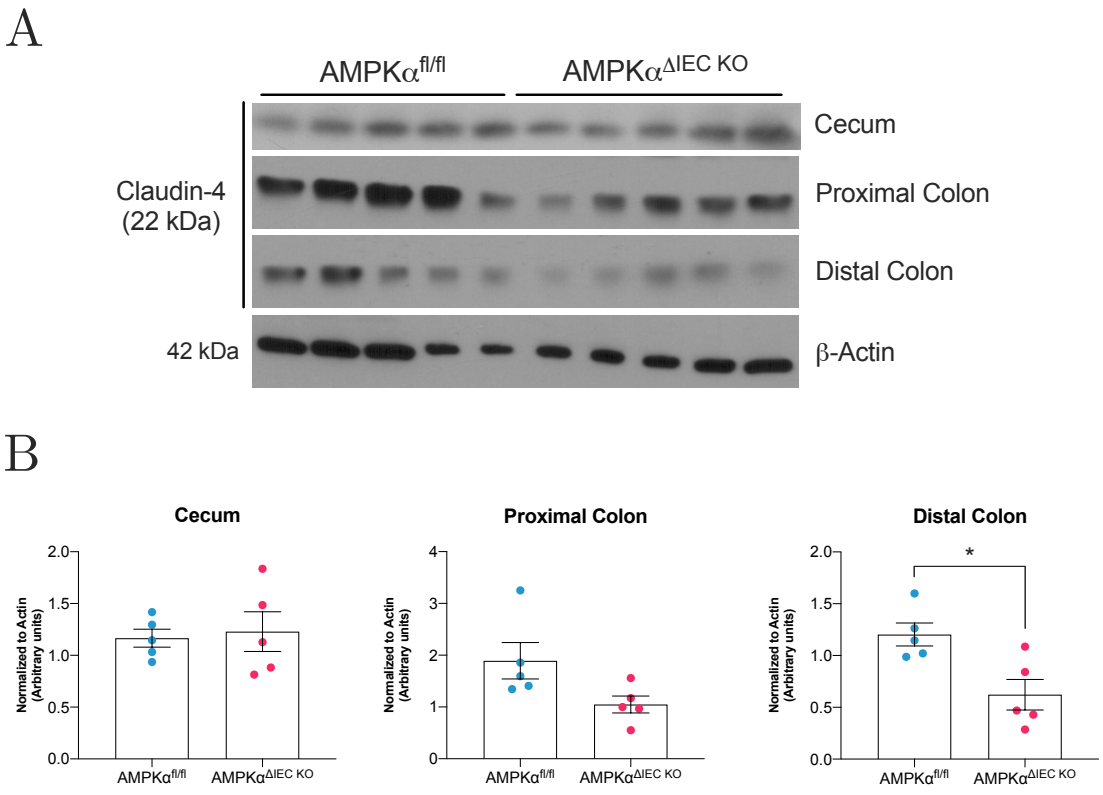

Figure 4.9: Claudin-4 Expression is Significantly Decreased in AMPKα$^{\Delta \text{IEC KO}}$ Mouse Colon

Isolated intestinal epithelial cells of large intestinal segments from AMPKα$^{fl/fl}$ and AMPKα$^{\Delta \text{IEC KO}}$ mice were lysed and subjected to western blot. A) Blots of Claudin-4 expression from cecum, proximal colon, and distal colon of AMPKα$^{fl/fl}$ and AMPKα$^{\Delta \text{IEC KO}}$ mice. B) Quantification of blots in A normalized to loading control (β-Actin). Values presented as Means ± S.D. *Asterisks* indicate significant differences from AMPKα$^{fl/fl}$ mice. *p<0.05. n=5

inhibit Ca^{2+}- and cAMP-dependent electrogenic ion transport. Thus, I hypothesized loss of AMPK would increase electrogenic ion secretion consistent with previous data. Segments from the large intestine of AMPKα$^{fl/fl}$ and AMPKα$^{\Delta \text{IEC KO}}$ mice were excised and the serosal layer was removed. The mucosa was mounted in Ussing chambers containing Kreb's Ringer's buffer and stimulated with Forskolin (20 µM) to initiate a cAMP-dependent response and Carbachol (300 µM) to trigger a Ca^{2+}-dependent response. I did not observe a significant difference in cAMP-initiated ion transport in segments of the large intestine (Figure 4.10).

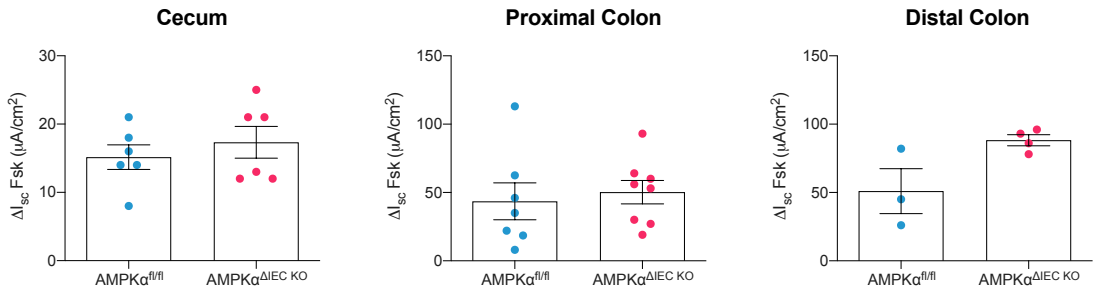

Figure 4.10: Forskolin-Induced Responses are Unaffected by AMPKα Deficiency

Large intestine from AMPKα$^{fl/fl}$ and AMPKα$^{\Delta IEC\ KO}$ mice was excised and stripped of the serosa. The mucosa was mounted in Ussing chambers with Kreb's Ringer's buffer. After 20 minutes, cAMP-dependent electrogenic ion secretion was initiated by bilateral addition of Forskolin (Fsk; 20 μM). Change in short-circuit current (ΔIsc μA/cm^2) was similar among both genotypes in all large intestinal segments. Values are expressed as Means ± S.D. n=3-8

However, I did observe a significant increase in Ca^{2+}-dependent ion transport in the cecum of AMPKα$^{\Delta IEC\ KO}$ mice compared to AMPKα$^{fl/fl}$ mice (Figure 4.11). These data agree with previous work from our lab demonstrating AMPK can inhibit Ca^{2+}-dependent electrogenic ion secretion during oxidative stress.

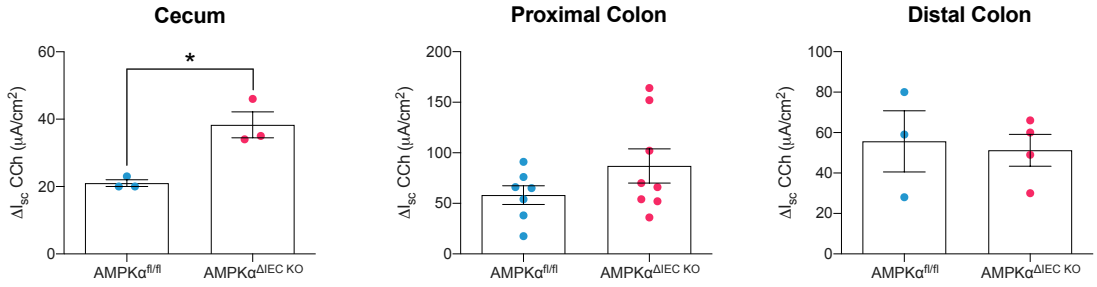

Figure 4.11: AMPK Inhibits Ca^{2+}-Dependent Ion Transport at Basal Conditions in Mouse Cecum

Large intestine from AMPKα$^{fl/fl}$ and AMPKα$^{\Delta IEC\ KO}$ mice was excised and stripped of the serosa. The tissue was mounted in Ussing chambers with Kreb's Ringer's buffer. After 20 minutes, Carbachol (CCh; 300 μM) was added to the basolateral chamber. Change in short-circuit current (ΔIsc μA/cm^2) was increased in cecum lacking epithelial expression of AMPKα. Responses in the colon were similar between genotypes. Values are displayed as Means ± S.D. *Asterisks* denote significant differences from AMPKα$^{fl/fl}$ mice. *p<0.05. n=3-8

Ion Transporter Expression We and others have previously demonstrated that AMPK inhibition of NKCC1 can lead to repression of Ca^{2+}-dependent electrogenic ion secretion [10]. I hypothesized that NKCC1 expression was suppressed by AMPK activity. To test this, I measured NKCC1 expression in the large intestine from AMPK$\alpha^{fl/fl}$ and AMPK$\alpha^{\Delta IEC\ KO}$ mice by immunofluorescence. I determined that AMPK$\alpha^{\Delta IEC\ KO}$ mice had increased NKCC1 expression at the basolateral membrane in the cecum and distal colon (Figure 4.12). These results are consistent with previous reports and suggest AMPK inhibition of electrogenic ion secretion is at least partially mediated by NKCC1.

4.3 Discussion

In this study I utilized a tissue-specific knockout mouse model where expression and activity of the AMP-activated protein kinase (AMPK) α catalytic subunit was absent in the intestinal epithelium. These data confirm a number of previous studies that suggested AMPK can regulate tight junction complexes and electrolyte transport in the mouse intestinal epithelium. I observed that loss of AMPK activity decreased transepithelial electrical resistance in the colon and this was associated with decreased Claudin-4 protein expression (Figure 4.13). Importantly, macromolecular permeability was unaltered in intestinal epithelial-specific AMPKα knockout mice. In addition, I confirmed that AMPK is a basal inhibitor of calcium-dependent electrogenic ion transport and that regulation of NKCC1 expression may play a role in this mechanism.

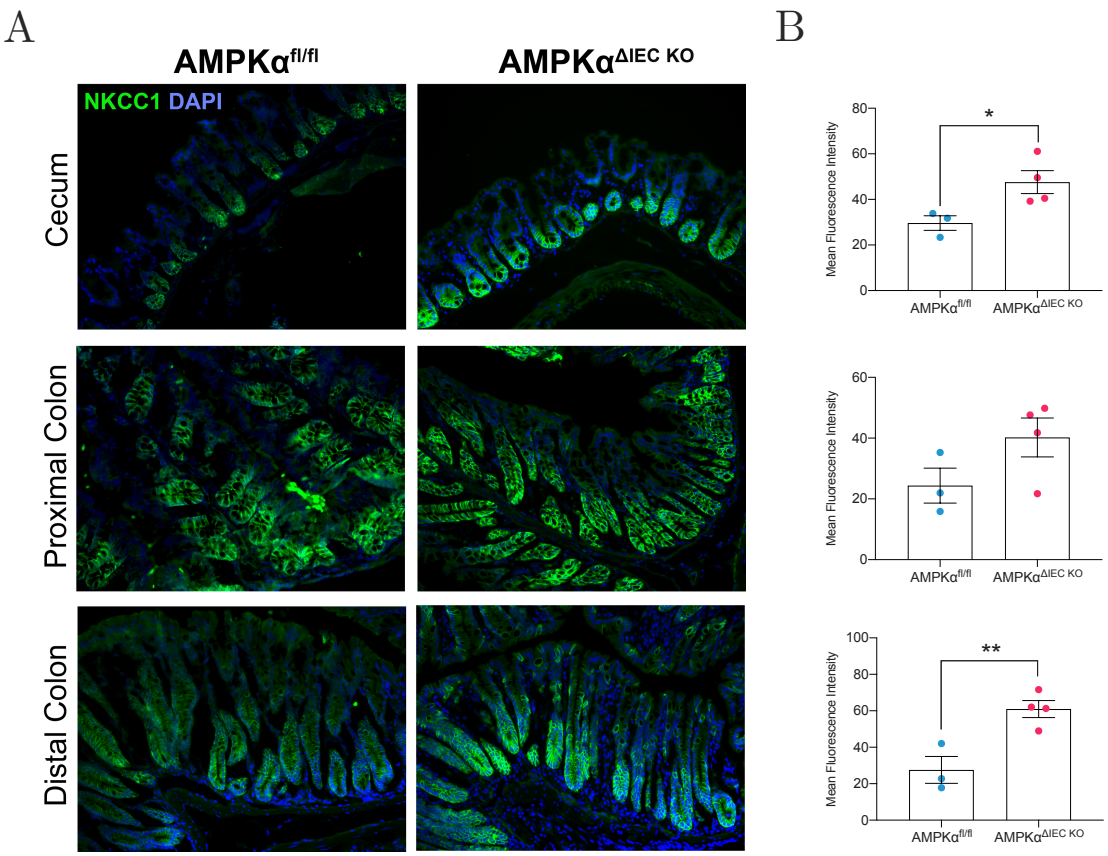

Figure 4.12: AMPK Inhibits NKCC1 Expression in Mouse Large Intestine

Large intestine from AMPKα$^{fl/fl}$ and AMPKα$^{\Delta IEC\ KO}$ mice was excised, fixed, and blocked for cryosectioning. 5 µm sections were subjected to immunofluorescence. Mean fluorescence intensity was quantified using NIH ImageJ with at least three crypt-defined regions of interest per section. NKCC1 expression was significantly increased in the cecum and distal colon from AMPKα$^{\Delta IEC\ KO}$ mice. Values are shown as Means ± S.D. *Asterisks* indicate significant differences from AMPKα$^{fl/fl}$ mice. *p<0.05, **p<0.01. n=3-4

4.3.1 AMPK Subunit Expression in Intestinal Epithelial Cells

Much work has implied AMPK plays an important role in the intestinal epithelium [11–15]. However, until now the expression of AMPK subunit isoforms and AMPK activity in intestinal epithelial cells has not been characterized. Here, I determined both α catalytic subunits of AMPK are expressed in the large intestine. In addition, I observed AMPKβ1

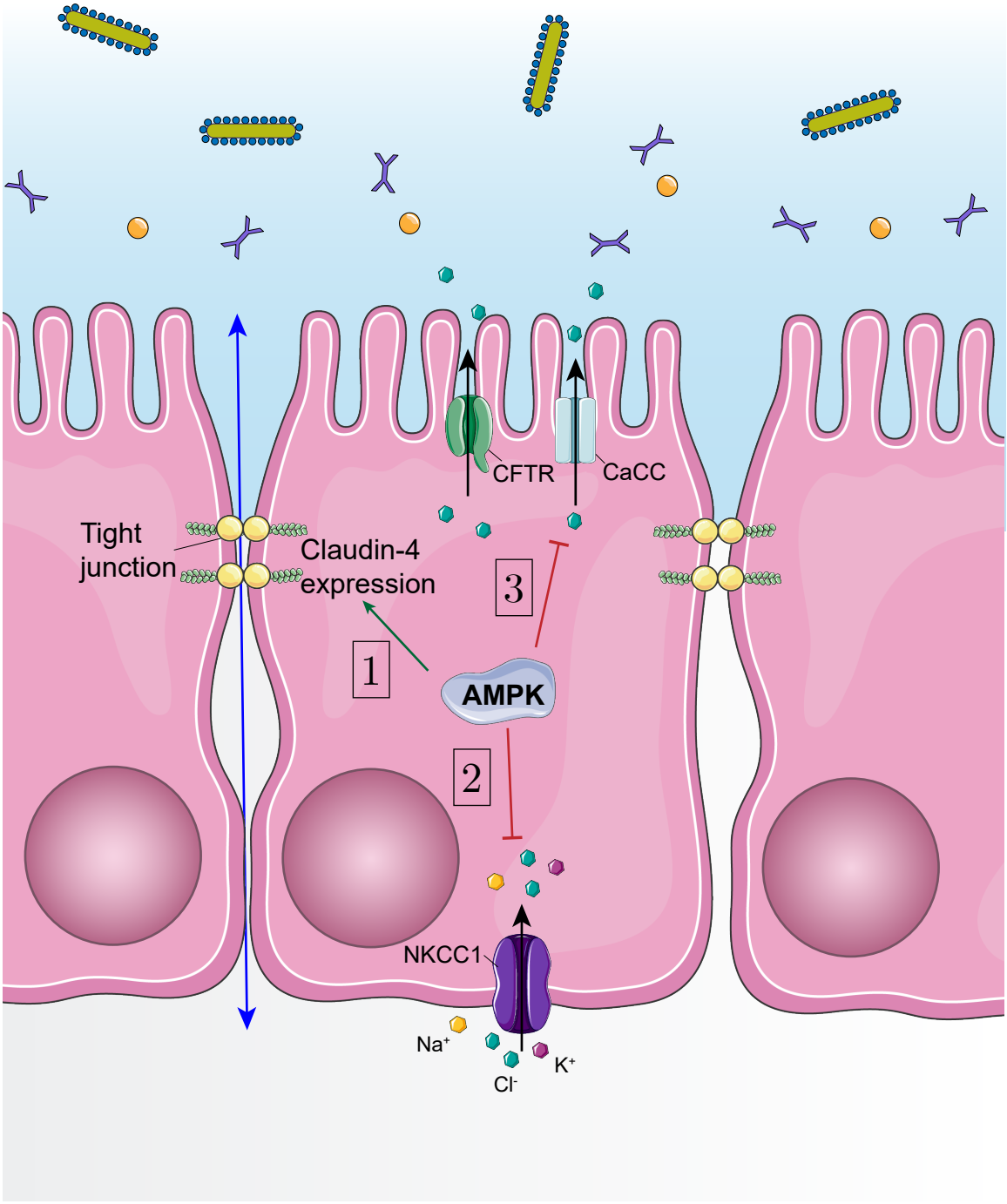

Figure 4.13: AMPK Regulates Intestinal Barrier Function and Ion Transport

AMP-activated protein kinase (AMPK) promotes intestinal barrier function through regulation of tight junctions. 1) AMPK maintains expression of the barrier-forming Claudin-4 protein to maintain transepithelial electrical resistance and therefore tight junction complexes. 2) AMPK is a basal repressor of the $Na^+/K^+/2Cl^-$ cotransporter 1 (NKCC1). NKCC1 is a basolateral cotransporter responsible for increasing intracellular Cl^- concentration. 3) AMPK suppression of NKCC1 is associated with decreased calcium-dependent electrogenic ion secretion.

expression and was not able to detect AMPKβ2 expression, perhaps suggesting AMPKβ1 may be the predominant scaffolding subunit expressed in intestinal epithelial cells. To confirm this, additional experiments with additional AMPKβ2 antibodies should be performed to ensure this effect is not an artefact of the AMPKβ antibody I used in this study. Curiously, the levels of AMPKβ1 expression correlated with AMPKα expression in AMPKα$^{fl/fl}$ mice. These data may suggest that expression of AMPK subunits is needed to promote its stabilization and/or protein expression, however further studies are needed to confirm this hypothesis. Finally, expression of the AMPK γ subunit isoforms in the intestinal epithelium remains to be elucidated.

4.3.2 Intestinal Epithelial Turnover and Differentiation

Following confirmation that I successfully bred AMPKα$^{\Delta IEC\ KO}$ mice that lacked expression of AMPKα and AMPK activity in intestinal epithelial cells, I next determined if this led to changes in epithelial structure and morphology. AMPK is known to regulate cell proliferation and death although these effects can vary. In canonical signaling, AMPK restricts cell growth in order to preserve cellular energy [16]. Similarly, AMPK has been shown to regulate cell differentiation through its demands on cellular energy [17, 18]. Proliferation and turnover is highly regulated in the intestinal epithelium to ensure proper differentiation of the epithelial cells and fast but controlled turnover. Increased proliferation is observed as increased crypt depth and villus length while differentiation is observed as decreased crypt depth and villus height. I confirmed that AMPKα-deficiency did not result in altered crypt depth or villus length in AMPKα$^{\Delta IEC\ KO}$ mouse intestine compared to AMPKα$^{fl/fl}$ mice. Previously, Sun et al. determined that intestinal epithelial deletion of the α1 cat-

alytic subunit isoform resulted in increased cell differentiation [14]. This was observed as impaired mucosal height and decreased migration of BrdU labelled cells. In addition, Caco-2 intestinal epithelial cells treated with the AMPK activator AICAR displayed increased protein expression of differentiation markers such as sucrose isomaltase, E-cadherin, and dipeptidyl peptidase-4 [14]. A number of factors could have contributed to this discrepancy. For example, mice used in the Sun et al. study retained expression of the α2 catalytic subunit, which is known to be able to shuttle from the nucleus to the cytoplasm. Potentially, deletion of the α1 catalytic isoform resulted in a compensatory increase of the α2 isoform either in expression and/or activity. This could have amplified its physiological function to modulate caudal type homeobox 2 (Cdx2), a transcription factor important for intestinal development. This is further supported by the observation that AMPK activation increased Cdx2 expression by changing its histone methylation status [14]. In mice that lack complete AMPK activity, AMPK-dependent Cdx2 regulation and therefore an increase in differentiation would be lost.

4.3.3 AMPK Regulation of Tight Junctions

AMPK was first reported to promote tight junction assembly during a calcium-switch assay in Madin-Darby Canine Kidney (MDCK) cells [19, 20]. These studies demonstrated increased LKB1-dependent activation of AMPK during calcium-switch and that AICAR treatment could promote tight junction assembly observed by membrane localization of Zonula Occludens-1 (ZO-1) at low and normal calcium concentrations compared to untreated cells. In addition, AICAR pre-treatment reduced tight junction disassembly during calcium depletion. This was confirmed as expression of kinase-dead AMPK led to impaired

tight junction assembly during calcium-switch. Further work clarified that AMPK regulation of tight junction assembly is dependent on the nectin-Afadin cell adhesion system and Afadin is a direct substrate of AMPK [21]. Nectin and Afadin function to link ZO-1 with F-actin during junction formation. In addition, AMPK phosphorylation of cingulin in Eph4a epithelial cells promoted association of tight junctions with microtubules [22]. AMPK has also been shown to regulate tight junction composition as AICAR administration was observed to result in increased claudin-4 phosphorylation, claudin-4 localization to the membrane, and interaction with occludin in an ERK1/2-dependent manner in rat submandibular gland cells [23]. Together, these data indicate AMPK promotes tight junction assembly through modulation of tight junction protein expression, localization, and association of scaffolding proteins.

Work examining the role of AMPK on tight junction assembly in the intestinal epithelium has emerged more recently. Peng et al. first showed that in Caco-2 intestinal epithelial cells, treatment with the short-chain fatty acid butyrate further increased AMPK activation during calcium switch to promote tight junction assembly [24]. Inhibition of AMPK by Compound C reversed these effects, although induced changes in ZO-1 localization were not confirmed to be AMPK-dependent. In addition, inulin permeability in Caco-2 cell monolayers was decreased by butyrate and AICAR treatment alone, and these effects were reversed with Compound C treatment. These findings were further expanded to confirm that AMPK regulates tight junction assembly through inhibition of Myosin Light Chain Kinase and decreased phosphorylation of myosin II regulatory light chain (MLC2) [25]. AMPK was previously shown to directly phosphorylate MLCK and desensitize it to calcium/calmodulin [26]. Another group found evidence that activation of the zinc-sensing

G protein-coupled receptor GPR39 increased tight junction assembly and required AMPK activation by Ca^{2+}/Calmodulin-dependent protein kinase kinase β (CaMKKβ) [27]. This work went further by confirming ZO-1 localization required CaMKKβ, suggesting it may be AMPK-dependent. These studies demonstrated AMPK promotes tight junction assembly in both calcium-dependent and -independent mechanisms.

In addition to these studies, others have suggested AMPK activation by exogenous molecules promotes barrier function and is protective in the intestinal epithelium. For example, Park et al. demonstrated theaflavins, compounds present in black tea, reduced fluorescein permeability in Caco-2 cell monolayers mounted in Ussing chambers [28]. This effect was reversed with AMPK inhibition by Compound C treatment and theaflavins were found to increase AMPK activation. The authors confirmed theaflavin treatment increased mRNA and protein expression of ZO-1, occludin, and claudin-1, although they did not confirm these observations required AMPK. My findings demonstrated epithelial AMPKα-deficiency resulted in decreased expression of Claudin-4, but that expression of ZO-1, Occludin, and Claudins 2 and 15 were unchanged. These data suggest impaired transepithelial electrical resistance in $AMPK\alpha^{\Delta IEC\ KO}$ mice is mediated at least partially by Claudin-4 protein abundance. However, I have not confirmed if ZO-1 and occludin are mislocalized in these mice as has been suggested by earlier data. Although a lack of altered Occludin expression and no increase in macromolecular permeability suggests Occludin function is maintained in these mice. As previous work has utilized calcium-switch assays to observe the effect of AMPK on tight junction assembly, I believe the AMPK-dependent effects on tight junctions in healthy mice would be minimal. For example, to observe AMPK inhibition of MLCK and therefore MLCK-mediated intestinal permeability

would require an inflammatory context. Therefore, the evidence supports the hypothesis that AMPK promotes barrier function through regulation of tight junction assembly and maintenance of mature tight junctions.

4.3.4 AMPK Regulation of Epithelial Ion Transport

Previous publications have suggested AMPK functions as a basal inhibitor of cAMP-dependent chloride secretion and during oxidative stress and hypoxia [29–34]. Further, AMPK activation by an inflammatory milieu and agonists restricted pathological activity of the Cystic Fibrosis Transmembrane Conductance Regulator (CFTR) [35, 36]. Despite these findings, I did not observe increased cAMP-dependent (CFTR-mediated) electrogenic ion secretion. This observation is consistent with Kongsuphol et al., who did not observe increased colonic Forskolin-stimulated ion transport in AMPKα1 knockout mice compared to wild-type mice [37]. In contrast, the authors did observe increased cAMP-dependent ion secretion with Compound C treatment in wild-type mice but this had no effect in AMPKα1 knockout mice. This could be due to the relative nonspecificity of Compound C as an AMPK inhibitor [6, 7]. Inhibition of CFTR occurs by binding of AMPK to the C-terminus and phosphorylation of Serine residues within the R domain, resulting in increased channel opening probability [29, 38, 39]. These sites are also phosphorylated by Protein Kinase A (PKA) and Protein Kinase C (PKC). Another study by Kongsuphol et al. determined that the order of phosphorylation events is critical and complex [39]. These data suggested early phosphorylation of Serine-785 suppressed subsequent Serine phosphorylation in the R domain [39, 40]. Therefore, together these data suggest intact phosphorylation of Serine-

785 by another kinase could explain why loss of AMPK activity did not result in increased cAMP-dependent ion transport.

In contrast to CFTR-mediated ion secretion, I did observe a significant increase in Ca^{2+}-dependent ion transport in the cecum of AMPK$\alpha^{\Delta IEC\ KO}$ mice. In addition, expression of NKCC1 was significantly increased in the cecum and distal colon of AMPK$\alpha^{\Delta IEC\ KO}$ mice. Our laboratory and others previously demonstrated AMPK can inhibit NKCC1 through modulation of its activity and potentially through phosphorylation [41]. Electrogenic ion transport responses are a summation of a number of channels and transporters such as Ca^{2+}-activated chloride channels, K^+ channels, and Na^+ channels such as the Epithelial Na^+ Channel (ENaC) in the distal colon. Previous groups have confirmed AMPK can also inhibit ENaC in addition to NKCC1 [42, 43]. Thus, it is possible NKCC1 inhibition is only a partial component of the overall effect. Further studies would be needed to fully characterize the composition of AMPK-mediated inhibition of electrogenic ion secretion.

In this study I characterized the effect resulting from loss of AMPKα expression and activity specifically in intestinal epithelial cells. I observed normal epithelial structure indicating intact cell proliferation and turnover. However, transepithelial electrical resistance was impaired in the proximal colon and this was correlated with reduced expression of Claudin-4 in the colon. In addition, I observed a significant increase in calcium-dependent ion secretion in the cecum and increased NKCC1 expression in the large intestine. Although the extent to which these effects could be relevant clinically is unknown, these data indicate that AMPK does indeed regulate barrier function in the intestinal epithelium as well as ion transport processes.

5 | Effect of Epithelial AMPKα Deletion on Experimental Colitis

"[...] once you eliminate the impossible, whatever remains, not matter how improbable, must be the truth [...]" - Sherlock Holmes in *The Sign of the Four* by Sir Arthur Conan Doyle

5.1 Introduction

A number of published studies have described administration of pharmacological activators of AMPK in various models of colitis is protective against intestinal inflammation [1–6]. In agreement with these studies, untreated colitic mice were found to have decreased phosphorylation of AMPK in intestinal tissue, although one study using 1% Dextran sodium sulfate (DSS) in mice observed an increase in AMPK activation during colitis [7]. However, these models are associative at best as many AMPK activators including Metformin, exert AMPK-independent effects [8–10]. Further, the effect of AMPK activation on innate immune functions in intestinal epithelial cells and whether its activity in these cells is sufficient to protect from colitis is unknown. I sought to clarify the role of AMPK in inflammatory

signaling using AMPKα intestinal epithelial specific knockout mice and experimental models of colitis: Dextran Sulfate Sodium and *Citrobacter rodentium* to model epithelial injury and pathogenic bacterial infection, respectively.

Dextran Sulfate Sodium (DSS) is a heparin-like polysaccharide consisting of three sulfate groups conjugated to each molecule of glucose. Administration of DSS in drinking water in mice leads to development of colitis whose macroscopic symptoms in mice manifest as progressive loss of body weight, diarrhea, rectal bleeding, piloerection and hunching [11]. While DSS is most commonly used as an acute colitis model and therefore cannot be interpreted as an exact model of such a complicated and longitudinal disease as ulcerative colitis, this model does share some features of Ulcerative Colitis (UC) such as mucosal inflammation and erosions observed in histological sections with the greatest severity in the distal colon. Development of DSS-induced colitis in mice is dependent on the presence of gut microbiota, as germ-free and antibiotic-treated animals develop little or no disease [12]. In addition, DSS-induced colitis is independent of adaptive immune functions as *Rag1* knockout and severe-combined immunodeficiency (SCID) (which lack mature T and B cells) mice have similar severity of colitis as wild-type littermates [13]. However, innate immunity is important for induction of colitis as *MyD88* knockout mice which lack a critical signaling mediator of innate immune toll-like receptors, do not develop colitis. The mechanism(s) of action of DSS is unknown, however as it is a large, negatively charged molecule it is unable to passively permeate cell membranes and recent evidence has demonstrated DSS crosses cell membranes by binding medium-chain fatty acids and forming nano-lipocomplexes thought to induce epithelial injury [14]. Epithelial damage from DSS leads to apoptosis and recruitment of neutrophils and macrophages, resulting in increased pro-inflammatory cytokine

and chemokine production such as IL-1β, IL-6, TNF-α and CCL2. Previous studies have demonstrated AMPK activation during colitis suppresses cytokine production and AMPK has previously been shown to inhibit CCL2 expression. Therefore, I expect to observe altered production of inflammatory mediators like CCL2 as has been observed previously.

In addition to the DSS injury model of colitis, I also tested how animals would compare in a pathogenic infection model of colitis. *Citrobacter rodentium* is a mouse attaching and effacing (A/E) pathogen which causes transmissible murine crypt hyperplasia (TMCH). *C.rodentium* infection of colonic epithelia is facilitated by a Type 3 secretion system similar to that of the human pathogens, Enteropathogenic *E. Coli* (EPEC) and Enterohemorrhagic *E. Coli* (EHEC). EPEC and EHEC are unable to efficiently colonize the mouse intestine, thus *C. rodentium* has been utilized as a mouse model to study these human enteric pathogens. The Type 3 secretion system and effector proteins are encoded within a LEE (locus of enterocyte effacement) pathogenicity island. One such effector protein is an EPEC homologue of the mitochondrial associated protein (Map) which targets mitochondria. Overexpression of Map leads to mitochondrial membrane instability during EPEC infection and progressive loss of mitochondrial membrane potential [15, 16]. Bacterial Map causes mitochondrial damage observed as disrupted matrix, swelling, and formation of cytoplasmic inclusion bodies in mouse colon [15, 16]. In addition, decreased expression of the mitochondrial protein succinate dehydrogenase at the crypt surface of infected colonic enterocytes requires Map expression. *C. rodentium* strains with a Map deletion have decreased ability to colonize mice and induced a less severe decrease of TEER in Caco-2 cells [16–18]. As AMPK is widely known to promote mitochondrial biogenesis and function, I hypothesized that AMPKα-deficiency in intestinal epithelial cells would increase

mouse susceptibility to *C. rodentium* infection. Much of the work surrounding AMPK has demonstrated it has a context-dependency that I hope to elucidate using these two colitis models.

5.2 Experimental Results

5.2.1 AMPK Expression is Not Required for Intestinal Permeability in Conventional-Housed Mice

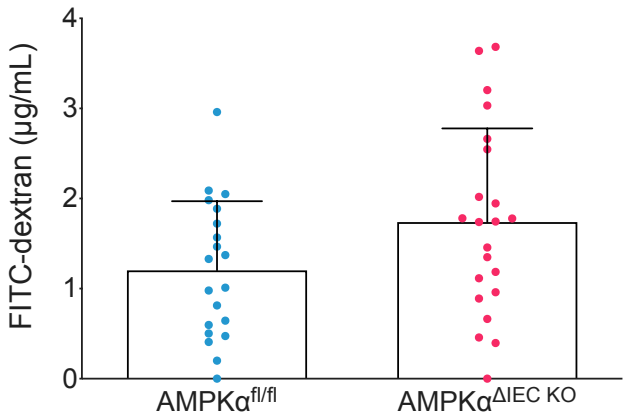

Figure 5.1: Loss of AMPK Does Not Alter Intestinal Permeability in Conventionally-Housed Mice

Mice were oral gavaged with 4 kDa Fluorescein thiocyanate (FITC)-dextran based on body weight. After 4 hours, blood was collected and serum levels of 4 kDa FITC-dextran were determined using a standard curve. Both mouse genotypes exhibited similar levels of intestinal permeability. Values are expressed as Means ± S.D. n=20-22.

Following acclimation to conventional housing, AMPK$\alpha^{fl/fl}$ and AMPK$\alpha^{\Delta IEC\ KO}$ mice were assessed for changes in macromolecular intestinal permeability using a 4 kDa Fluorescein thiocyanate (FITC)-dextran assay. As expected, I confirmed that there was no change in intestinal permeability due to AMPK expression and therefore determined this

was unaffected by differences in gut microbial composition arising from conventional vs. specific-pathogen-free housing (Figure 5.1).

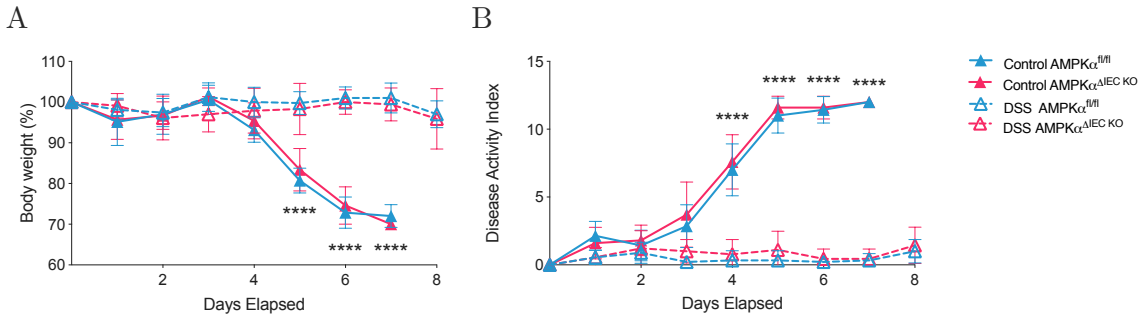

Figure 5.2: 5% DSS Induces Severe Colitis in AMPK$\alpha^{\Delta \text{IEC KO}}$ and AMPK$\alpha^{\text{fl/fl}}$ Mice

Body weight and disease activity index were measured daily as described previously (Ch.2.14.3) A) DSS-treated mice exhibited significant loss of body weight beginning at Day 5 post-treatment. Weight loss over time was similar within treatment groups. B) DSS-treated mice had significantly increased disease activity index score compared to control mice. Disease activity index score over time was similar among genotypes within treatment groups. Values are presented as Means ± S.D. *Asterisks* indicate a significant difference compared to Control mice. n=7-10. ****p<0.0001.

5.2.2 Absence of AMPK does not exacerbate DSS-induced colitis

I next sought to observe whether complete loss of AMPK activity would exacerbate DSS colitis, since previous work demonstrated knockout of the AMPKα1 subunit in intestinal epithelial cells increased body weight loss during 3% DSS colitis [19]. Mice in conventional housing were treated with 5% DSS for 5 days *ad libitum* followed by 3 days of water. I assessed body weight and presence of bloody diarrhea daily for the duration of the experiment. AMPK$\alpha^{\text{fl/fl}}$ and AMPK$\alpha^{\Delta \text{IEC KO}}$ mice treated with 5% DSS developed severe colitis as illustrated by a significant loss of initial body weight which was inversely correlated with a significant increase in disease activity index (Figure 5.2).

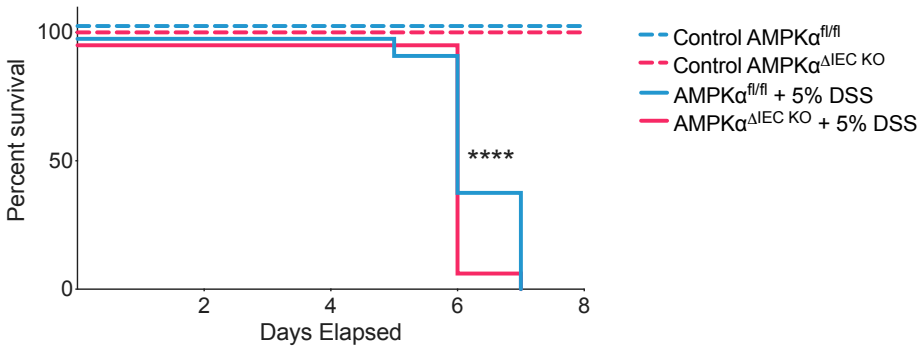

Figure 5.3: Animal Survival During 5% DSS Experimental Colitis

Administration of 5% DSS to C57BL/6 mice in conventional housing induced severe colitis that was fatal at Day 7. AMPK activity did not impact survival. Raw values are expressed. *Asterisks* indicate a significant difference compared to untreated Control mice. n=8-10. ****p<0.0001.

Due to the severity of disease, mice were euthanized at Day 7, on average, in accordance with institutional animal use committee approval (Figure 5.3). Unexpectedly, AMPK$\alpha^{\Delta IEC\ KO}$ mice did not exhibit more severe symptoms than their AMPK$\alpha^{fl/fl}$ counterparts nor did they have altered survival.

DSS colitis is known to increase intestinal permeability through direct damage to epithelial cells. I observed that macromolecular intestinal permeability was significantly increased in DSS-induced colitis as expected, although this was independent of AMPK and AMPK activity did not affect the degree of permeability (Figure 5.4).

Colon shortening is a feature of acute DSS colitis that results from tissue wasting [11]. I measured colon shortening as a function of decreases in colon weight and length in both genotypes of mice treated with DSS. I observed that colon shortening was induced by DSS treatment and that colon dimensions in colitic AMPK$\alpha^{\Delta IEC\ KO}$ mice did not differ from AMPK$\alpha^{fl/fl}$ mice (Figure 5.5).

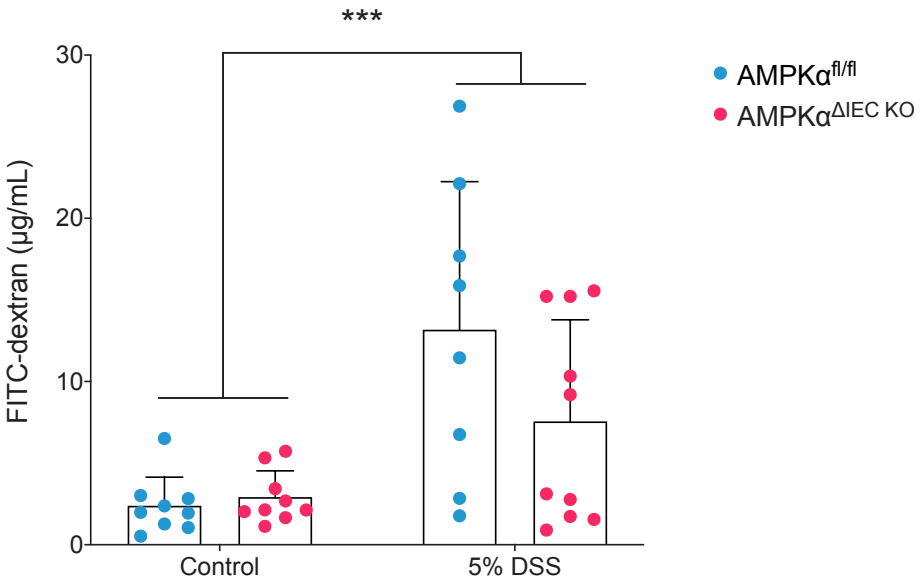

Figure 5.4: Increased Intestinal Permeability during DSS Colitis is Unaffected by AMPK Activity

Mice treated with 5% DSS exhibited significantly increased macromolecular intestinal permeabilty compared to untreated Control animals. AMPK$\alpha^{\Delta IEC\ KO}$ mice displayed similar levels of permeability as AMPK$\alpha^{fl/fl}$ mice. Intestinal permeability was determined using an *in vivo* 4 kDa FITC-dextran assay. Values are expressed as Means ± S.D. *Asterisks* indicate a significant difference compared to Control mice. n=8-10. ***p<0.001.

Histological analysis of the large intestine revealed that DSS-treated animals exhibited loss of crypt structure and erosions, thickening of the lamina propria, increased immune cell infiltration and the presence of edema in DSS-treated animals (Figure 5.6). As expected, colitis scores were highest in the distal colon. Histological features displayed during colitis were consistent in both mouse genotypes indicating AMPK activity did not alter disease.

Previous reports have demonstrated AMPK activation during intestinal inflammation is context-dependent. To confirm this in our study, whole proximal colon from untreated Control and DSS-treated AMPK$\alpha^{fl/fl}$ mice was homogenized and analyzed by western blot.

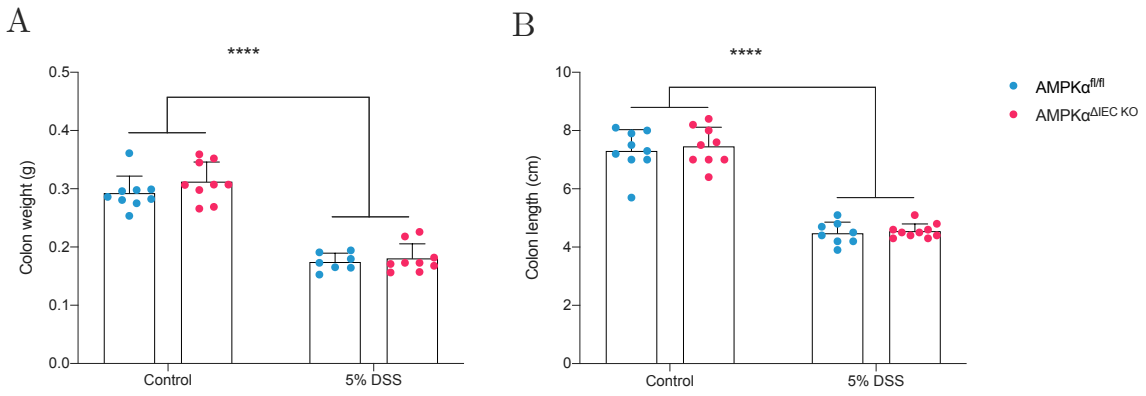

Figure 5.5: AMPK Does Not Protect Against Colon Shortening Induced by DSS

5% DSS treatment significantly decreased colon length and weight, indicative of colon shortening, compared to water only Control mice. AMPK expression had no appreciable effect on colon shortening during experimental colitis. Values are presented as Means ± S.D. *Asterisks* indicate a significant difference compared to Control mice. n=8-10. ****p<0.0001.

I determined that DSS colitis led to an increase in AMPK activation, however expression of AMPKα was overall decreased during colitis (Figure 5.7).

Due to the decreased survival of mice following 5% DSS, I next turned to a lower dose of DSS to test if effects of AMPKα-deficiency would be more pronounced in a milder form of colitis. Therefore I treated mice with 2.5% DSS which is comparable to a similar study conduced by another group where AMPK-dependent effects were observed [19]. Surprisingly, 2.5% DSS treated mice developed severe colitis much like that of 5% DSS-induced colitis (Figure 5.8). Given this similarity, further experiments were performed in 5% DSS-treated mice.

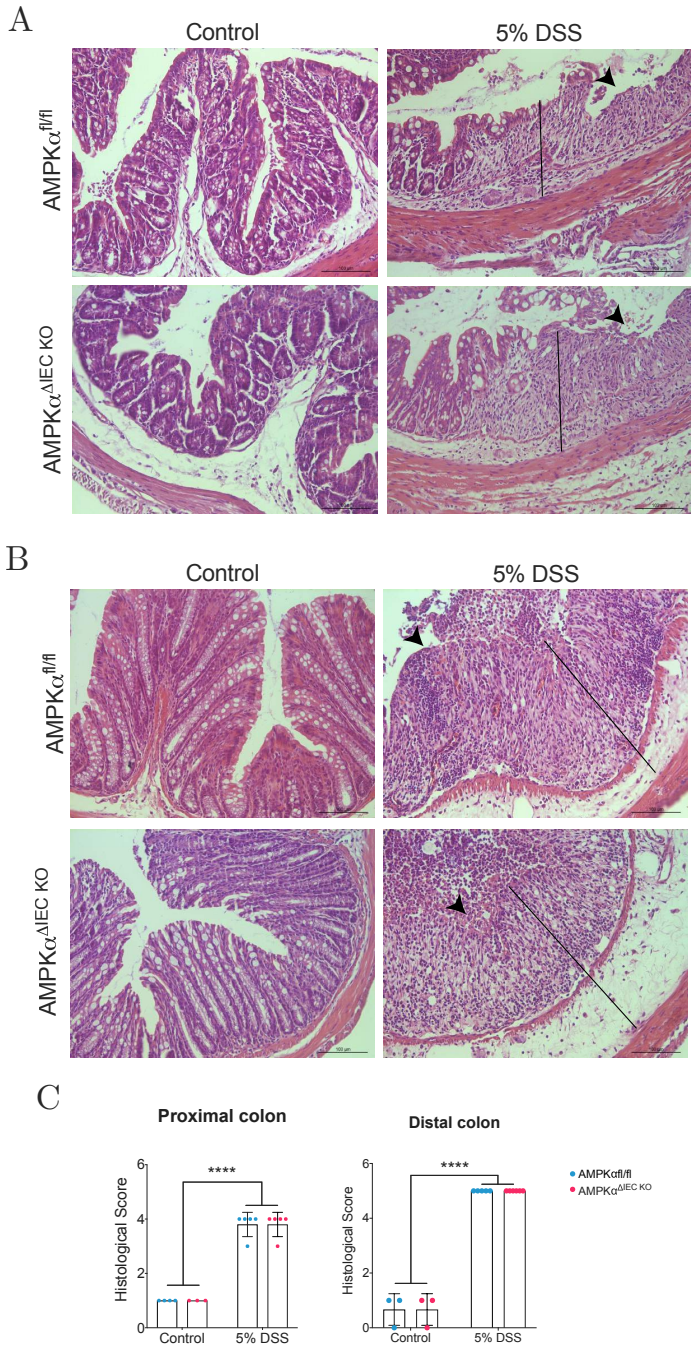

Figure 5.6: AMPKα Deletion Does Not Impact Histological Features of Experimental Colitis

Colons from Control and DSS-treated AMPKα$^{fl/fl}$ and AMPKα$^{\Delta IEC\ KO}$ mice were stained with hematoxylin and eosin and imaged. Scores were assigned based on the scoring rubric in Table 2.4. DSS treatment induced mucosal and submucosal immune cell infiltration and epithelial erosions. A) Representative images of proximal colon. B) Representative images of distal colon. C) Quantification of scores from images from proximal and distal colons. Lines indicate width of immune cell infiltration. Arrows indicate sites of erosion. Values are depicted as Means ± S.D. *Asterisks* indicate significant differences from Control mice. ****p<0.0001. n=3-6

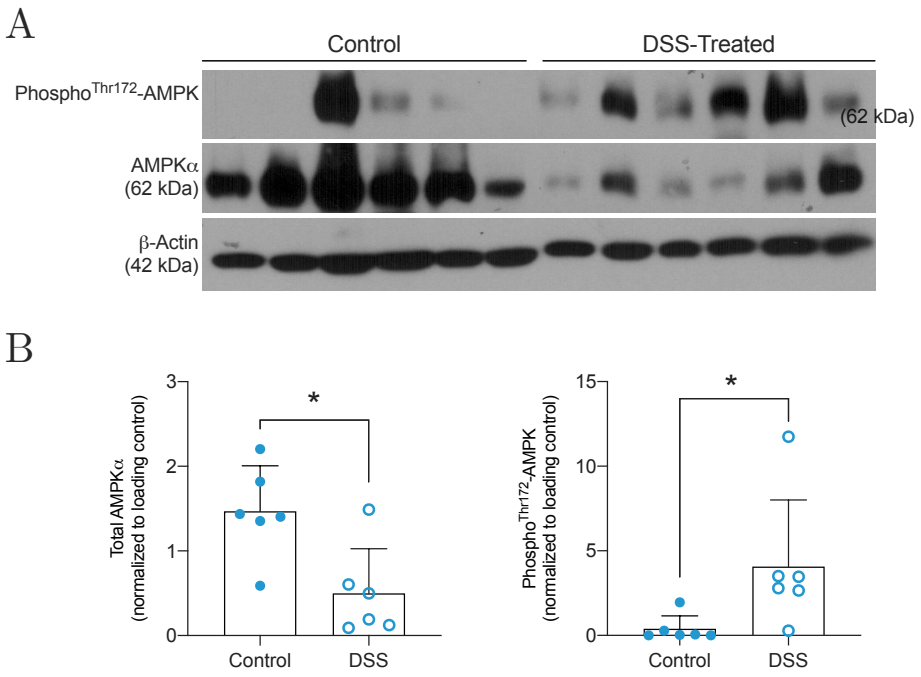

Figure 5.7: AMPK Activation and Expression during DSS Colitis

Whole proximal colon was excised and flash-frozen from untreated Control and DSS-treated AMPK$\alpha^{fl/fl}$ mice. Frozen tissues were homogenized and subjected to western blot. A) Blots of Phospho-Thr172-AMPK and Total AMPKα. B) Quantification of blots in A. AMPKα expression was significantly increased during DSS treatment, however AMPK phosphorylation was significantly decreased. Values are shown as Means ± S.D. *Asterisks* denote significant differences from control AMPK$\alpha^{fl/fl}$ mice. *$p<0.05$. n=6

5.2.3 AMPK Does Not Regulate Pro-Inflammatory Mediators During Colitis

Despite comparable changes in disease severity and intestinal permeability to DSS-induced colitis, I postulated if intestinal AMPKα-deficiency altered molecular responses during colitis such as pro-inflammatory signaling in the intestinal mucosa. AMPK has previously been shown to modulate cell stress and immune responses, usually as a repressor of pro-inflammatory gene expression such as the C-C motif chemokine ligand 2 (*Ccl2*) and inducible Nitric Oxide Synthase (*Nos2*/iNOS) [2, 20–22]. Elevated expression of iNOS in

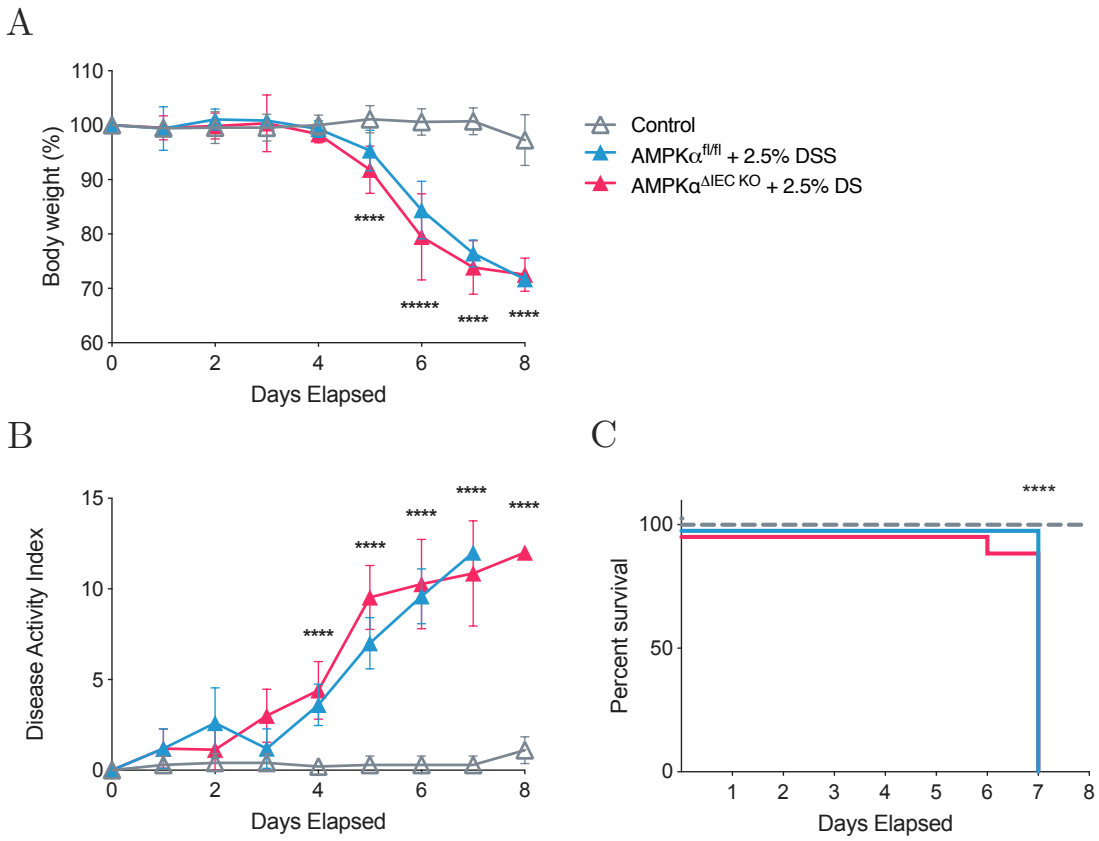

Figure 5.8: 2.5% DSS Causes Severe Colitis in C57BL/6 Mice

A) Percentage of initial body weight over time during DSS treatment. AMPKα$^{fl/fl}$ and AMPKα$^{\Delta IEC\ KO}$ mouse body weight loss during DSS treatment was similar. B) Disease activity index over time during DSS treatment. Both mouse genotypes exhibited similar disease severity with 2.5% DSS treatment. C) Survival of mice following treatment with 2.5% DSS. Mice treated with 2.5% DSS succumbed on Day 7. Mice in conventional housing were treated with 2.5% DSS in drinking water for 5 days *ad libitum* followed by 3 days of water. Values are depicted as Means ± S.D. n=5-10. *Asterisks* represent significant differences from control, untreated mice. ****p<0.0001

cells increases production of nitric oxide and CCL2 expression increases immune cell recruitment to sites of inflammation. Both of these genes are typically upregulated during colitis [2, 23]. I determined that expression of *Ccl2* and *Nos2* was unchanged in whole large intestinal tissue from Control and DSS-treated AMPKα$^{\Delta IEC\ KO}$ mice compared to

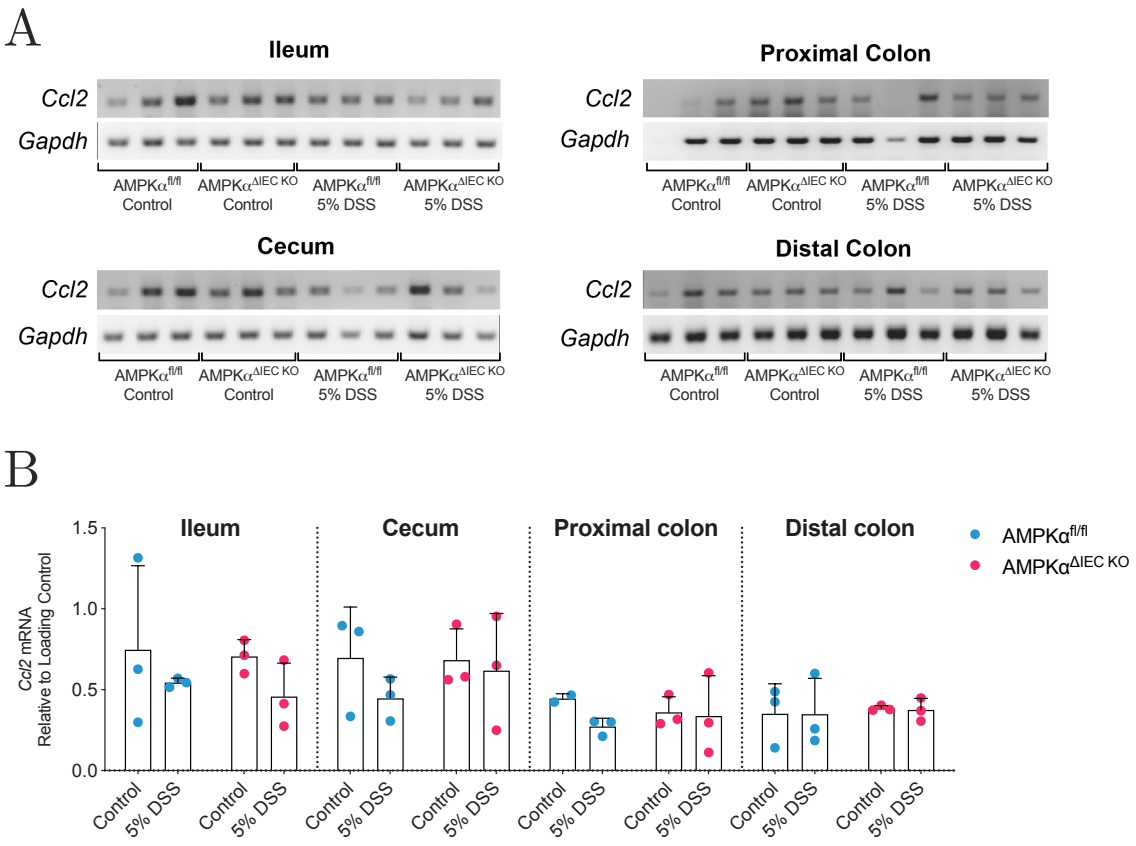

Figure 5.9: *Ccl2* Gene Expression is AMPK-Independent

Expression of *Ccl2* mRNA is unaltered by DSS treatment and AMPKα-deficiency. Whole tissue from ileum and the large intestine of untreated or DSS-treated AMPKα$^{fl/fl}$ and AMPKα$^{\Delta IEC\ KO}$ mice was analyzed for gene expression. A) Ethidium bromide agarose gels of *Ccl2* mRNA expression. B) Quantification of gels in A. Values are representative of Means ± S.D. n=3.

AMPKα$^{fl/fl}$ mice using PCR (Figure 5.9 and 5.10, respectively). Surprisingly, I did not detect an increase in *Ccl2* and *Nos2* gene expression with DSS treatment.

5.2.4 Altered Apoptotic Marker Expression in AMPKα$^{\Delta IEC\ KO}$ mice

DSS administration causes direct intestinal epithelial cell injury, leading to cell death. AMPK is known to regulate apoptosis although its effect appears to be context-dependent.

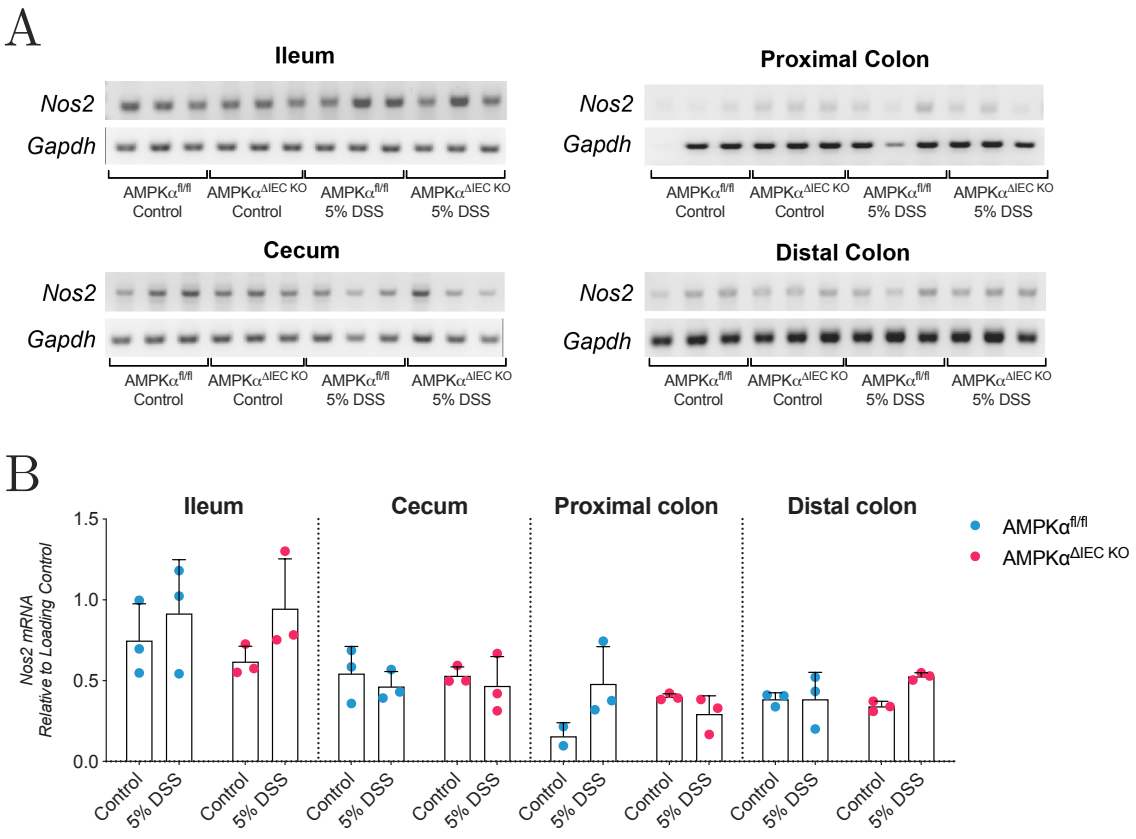

Figure 5.10: *Nos2* Gene Expression is AMPK-Independent

Expression of *Nos2* mRNA is unaltered by DSS treatment and AMPKα expression. Whole tissue from ileum and the large intestine of untreated or DSS-treated AMPKα$^{fl/fl}$ and AMPKα$^{\Delta IEC\ KO}$ mice was analyzed for gene expression. A) Ethidium bromide agarose gels of *Nos2* mRNA expression. B) Quantification of gels in A. Values are presented as Means ± S.D. n=3.

In order to determine if AMPKα$^{\Delta IEC\ KO}$ mice had increased apoptosis, I determined the protein expression of cleaved Caspase-3, Poly (ADP-ribose) Polymerase (PARP), and PARP cleavage as markers of apoptosis downstream of both the intrinsic and extrinsic pathways of apoptosis initiation. I observed that cleaved Caspase-3 was significantly decreased in the proximal colon mice treated with 5% DSS (Figure 5.11. This effect was similar in DSS-

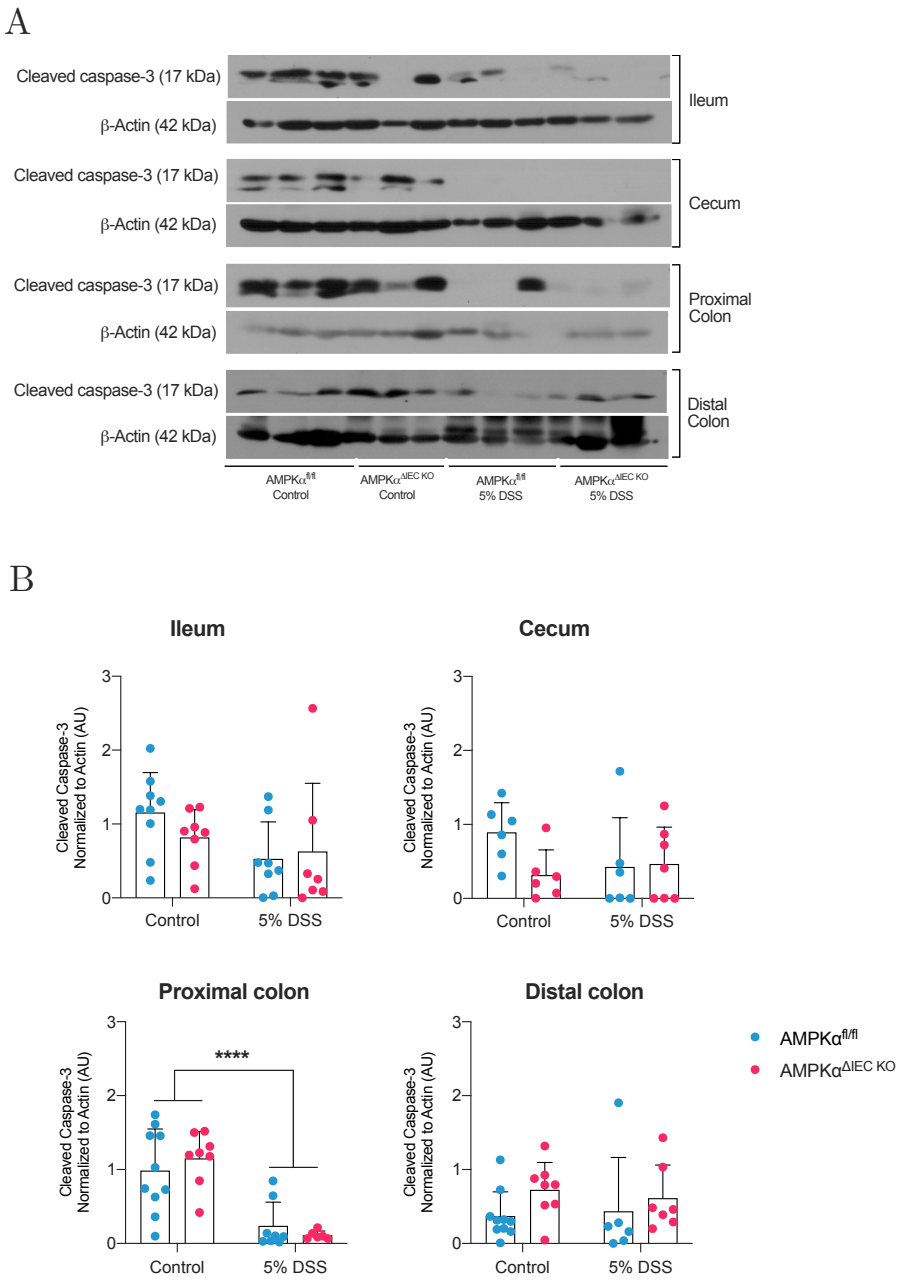

Figure 5.11: Cleaved Caspase-3 is Decreased in Colitic Murine Proximal Colon

A) Blots of Cleaved Caspase-3 Expression in whole intestinal tissue from untreated Control and DSS-treated AMPK$\alpha^{fl/fl}$ and AMPK$\alpha^{\Delta IEC\ KO}$ mice. DSS-treated proximal colon had significantly less cleaved Caspase-3 expression. AMPK activity did not affect cleaved Caspase-3 expression. B) Quantification of blots in A. Values are representative of Means ± S.D. n=6-10. *Asterisks* denote significant differences from untreated Control mice. ****$p<0.0001$.

treated AMPK$\alpha^{fl/fl}$ and AMPK$\alpha^{\Delta IEC\ KO}$ mice. In addition, untreated Control mice also had similar expression of cleaved Caspase-3.

PARP expression was unaltered by experimental colitis and similar among both genotypes of mice (Figure 5.12B). However, similar to cleaved Caspase-3, cleaved PARP was also decreased by 5% DSS in the proximal colon, irrespective of genotype (Figure 5.12C). PARP cleavage occurs downstream of cleaved Caspase-3 during apoptosis initiation. Thus decreased PARP cleavage is consistent with decreased expression of cleaved Caspase-3. These findings suggest apoptosis is suppressed in murine proximal colon during DSS-induced experimental colitis.

5.2.5 Loss of AMPK Increases Cell Death During Colitis

To further confirm my findings in apoptotic marker expression, I determined the percentage of apoptotic cells in intestinal tissue sections using a TUNEL assay that labels nuclei with cleaved DNA. In untreated mice the proportion of TUNEL+ cells was low (1-3%) and occurred at similar levels in both mouse genotypes. This is consistent with previous reports identifying only a very small percentage of intestinal epithelial cells undergo apoptosis during homeostasis. Following 5% DSS treatment, I observed decreased TUNEL-positive staining in the cecum and distal colon of AMPK$\alpha^{\Delta IEC\ KO}$ mice compared to AMPK$\alpha^{fl/fl}$ mice (Figure 5.13). These data suggest that AMPK may promote cell death during DSS-induced experimental colitis.

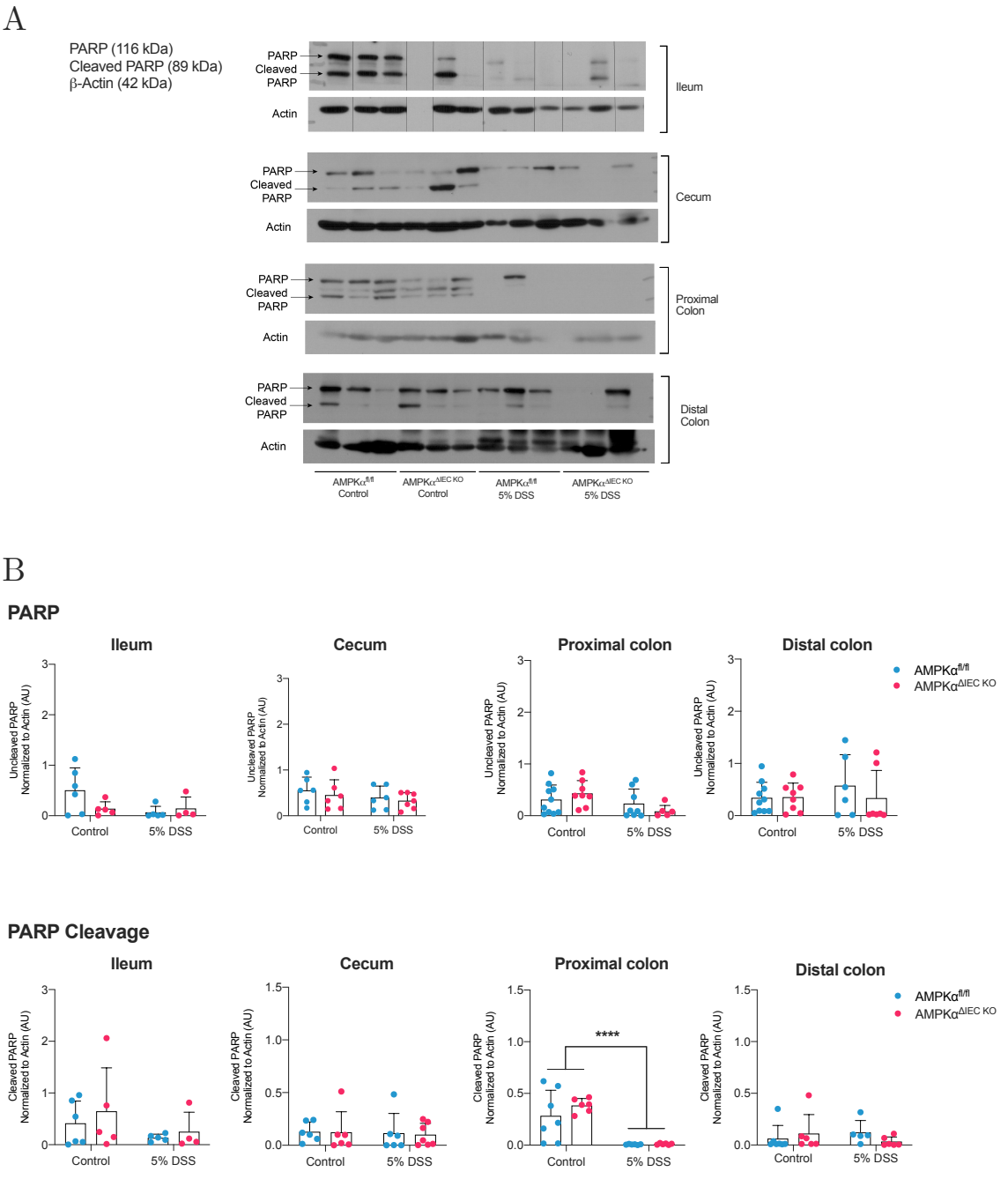

Figure 5.12: Decreased PARP Cleavage in DSS Treatment

A) Blots of PARP expression in whole intestinal tissue from untreated Control and DSS-treated AMPKα$^{fl/fl}$ and AMPKα$^{\Delta IEC\ KO}$ mice. B) Quantification of uncleaved PARP in A. C) Quantification of PARP cleavage in A. Values are expressed as Means ± S.D. n=6-10. *Asterisks* indicate significant differences from untreated mice. ****p<0.0001.

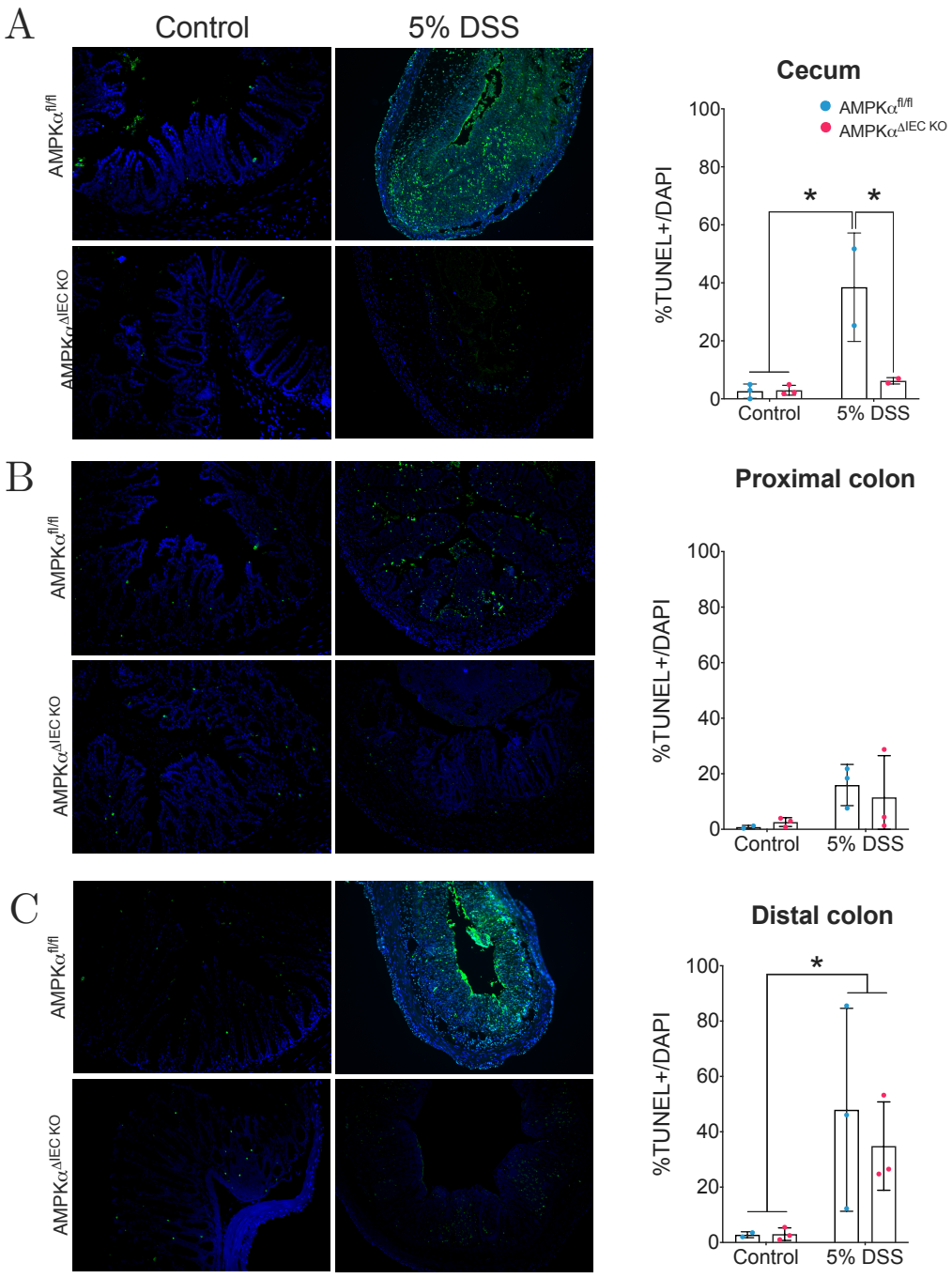

Figure 5.13: Decreased Cell Death in Cecum of DSS-Treated AMPKα$^{\Delta \text{IEC KO}}$ Mice

Large intestine from Control and DSS-treated AMPKα$^{\text{fl/fl}}$ and AMPKα$^{\Delta \text{IEC KO}}$ mice were subjected to TUNEL staining. Images were quantified using NIH ImageJ. Representative images and quantification of cecum (A), proximal colon (B), and distal colon (C). DSS treatment increased the percentage of TUNEL-positive cells of both mouse genotypes in the colon. DSS-treated AMPKα$^{\Delta \text{IEC KO}}$ mice had significantly decreased TUNEL-positive staining in cecum compared to DSS-treated AMPKα$^{\text{fl/fl}}$ mice. Control mice displayed low levels of TUNEL staining that was similar in both genotypes. Values are displayed as Means ± S.D. *Asterisks* indicate significant differences. *p<0.05. n=2-3

5.2.6 *Citrobacter rodentium* Infection in AMPKα$^{\Delta IEC\ KO}$ Mice

Chemical injury models of colitis are known for their severe effects on the intestinal epithelium such that they are not reliable models for less pronounced alterations in the intestinal barrier. To better determine if intestinal epithelial AMPKα-deficiency impacts other insults to the mucosa, I employed the *Citrobacter rodentium* infection model of colitis. In C57BL/6 mouse strains, *C. rodentium* is known to cause very mild colitis and bacterial burden peaks at day 10 post-infection [24]. Thus, to capture changes during the most severe point of disease I infected mice and monitored disease activity and fecal bacterial burden until sacrifice on Day 10 post-infection. *C. rodentium* infection did not causes significant changes in body weight although mice exhibited significant increases in fecal bacterial burden thus confirming that they were successfully infected (Figure 5.14).

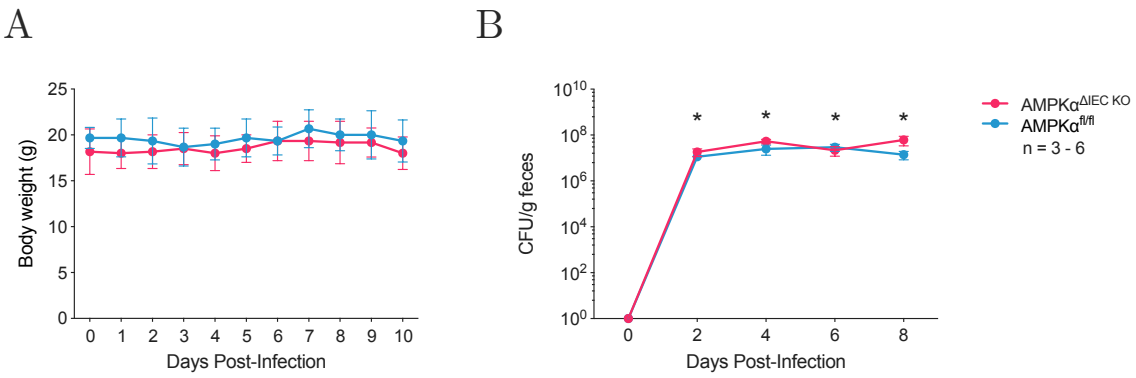

Figure 5.14: *C. rodentium* Infection Did Not Induce Body Weight Loss

AMPKα$^{fl/fl}$ and AMPKα$^{\Delta IEC\ KO}$ mice were infected with *Citrobacter rodentium* following 24 hour streptomycin treatment. Body weight was measured daily and fecal bacterial burden was determined every other day until peak of infection (Day 10). A) Percentage of initial body weight over time during *C. rodentium* infection. AMPK activity did not affect body weight maintenance during infection. B) Fecal bacterial burden of *C. rodentium* during infection. AMPKα$^{fl/fl}$ and AMPKα$^{\Delta IEC\ KO}$ mice displayed similar increases in *C. rodentium* bacterial burden. Values are representative of Means ± S.D. n=3-6.

In accordance with the absence of colitis, infected mice did not exhibit colon shortening and had similar levels of intestinal permeability at Day 10 post-infection (Figure 5.15). These data demonstrated *Citrobacter rodentium* infection did not cause colitis or induce an AMPK-dependent defect in barrier function in our mouse model.

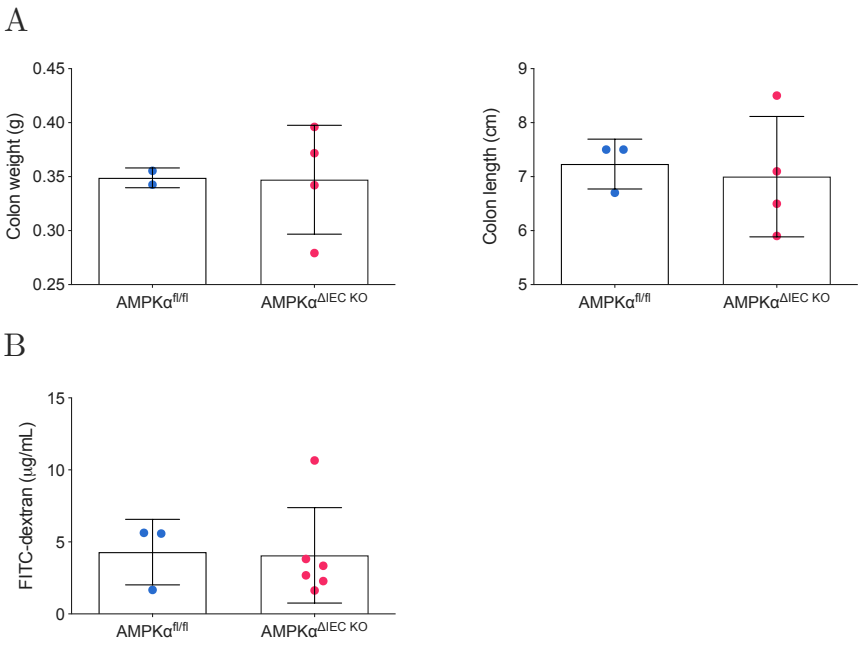

Figure 5.15: *C. rodentium* Infection Did Not Induce Colitis

At peak infection (Day 10), mice were assessed for *in vivo* intestinal permeability and colon shortening. A) Colon weight and length at Day 10 post-infection was similar in AMPKα$^{fl/fl}$ and AMPKα$^{\Delta IEC\ KO}$ mice. Significant colon shortening was not observed. B) 4 kDa FITC-dextran macromolecular permeability during *C. rodentium* infection was unimpacted by AMPK activity. Values are expressed as Means ± S.D. n=3-6.

Finally, I determined bacterial burden in the colon and extra-intestinal tissues (mesenteric lymph nodes, spleen, and liver) to determine if infection spread beyond the intestine. I observed no change in bacterial dissemination to extra-intestinal tissues at Day 10 post-infection in both mouse genotypes (Figure 5.16). This was expected in mice

lacking overt intestinal inflammation during infection. In addition, colonic colonization by *C. rodentium* was similar in AMPKα$^{fl/fl}$ and AMPKα$^{\Delta IEC\ KO}$ mice.

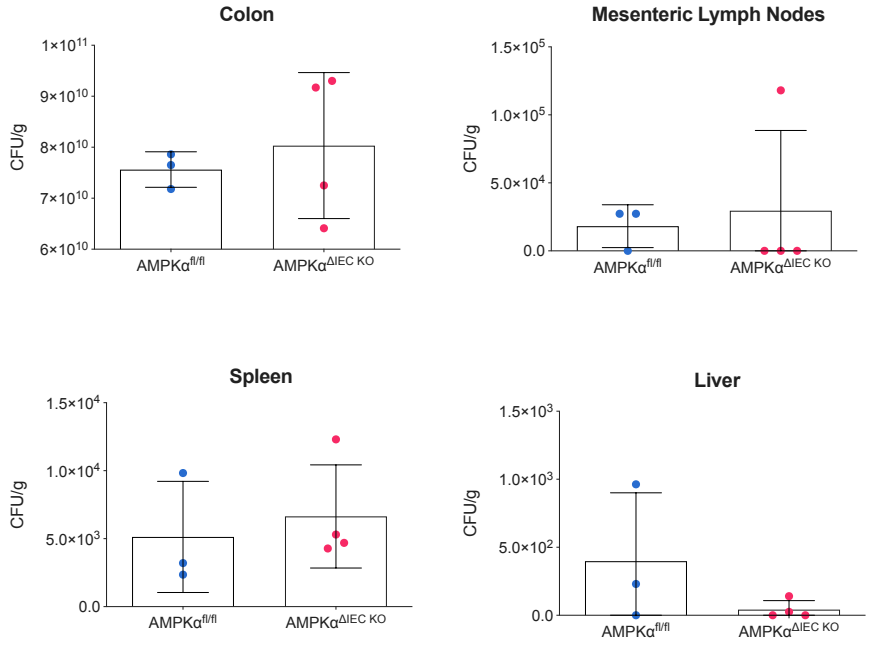

Figure 5.16: Bacterial Burden of Colonic and Extra-Intestinal Tissues at Peak of *C. rodentium* Infection

Tissue was excised from animals at Day 10 post-infection, homogenized, and diluted for plating on LB-agar. Individual colonies were counted the next day to determine bacterial burden. *C. rodentium* bacterial burden at Day 10 post-infection was similar between AMPKα$^{fl/fl}$ and AMPKα$^{\Delta IEC\ KO}$ mice. There was little colonization of extra-intestinal tissues. Values are depicted as Means ± S.D. n=3-4.

5.3 Discussion

In this study, I sought to provide further clarification of the role of AMP-Activated Protein Kinase (AMPK) in intestinal inflammation by inducing colitis in mice with intestinal epithelial-specific loss of AMPKα with the expectation that AMPKα$^{\Delta IEC\ KO}$ mice would display increased susceptibility to experimental colitis. AMPK has been demonstrated as

a mediator for both maintaining intestinal homeostasis and facilitating inflammatory signaling downstream of cytokines [25, 26]. In addition, AMPK has previously been shown to be both pro- and anti-apoptotic and this appears to be context-dependent [27]. As AMPK performs important functions during inflammation and other stress conditions, I tested if loss of AMPK would exacerbate disease in the DSS chemical injury model of colitis. Given that AMPK activity has been shown to be required for epithelial barrier formation, it was surprising that loss of this conserved kinase did not result in a barrier defect, as measured by macromolecular paracellular permeability, or loss of significant histological features indicative of altered intestinal epithelial cell differentiation and inflammation (Chapter 4). This is in contrast to previous data demonstrating loss of AMPKα1 in intestinal epithelium increases paracellular permeability [19]. Thus despite altered expression of the tight junction protein Claudin-4 described in Ch.4.2.2 and thus transepithelial electrical resistance, mice did not exhibit increased susceptibilty to DSS colitis or enteric infection.

5.3.1 AMPKα-Deficiency Did Not Result in Increased Susceptibility to Colitis

5% and 2.5% DSS induced severe colitis in conventionally-housed mice, however AMPKα expression had no impact on disease susceptibility. Previous groups have demonstrated loss of a single AMPKα catalytic isoform specifically in intestinal epithelial cells exacerbates DSS-induced acute colitis [19]. I previously observed that AMPKα2 whole-body knockout mice have increased expression of the AMPKα1 isoform in isolated IECs (data not shown) and have shown in Ch.4.2.1 that both α catalytic isoforms are expressed in intestinal epithelial

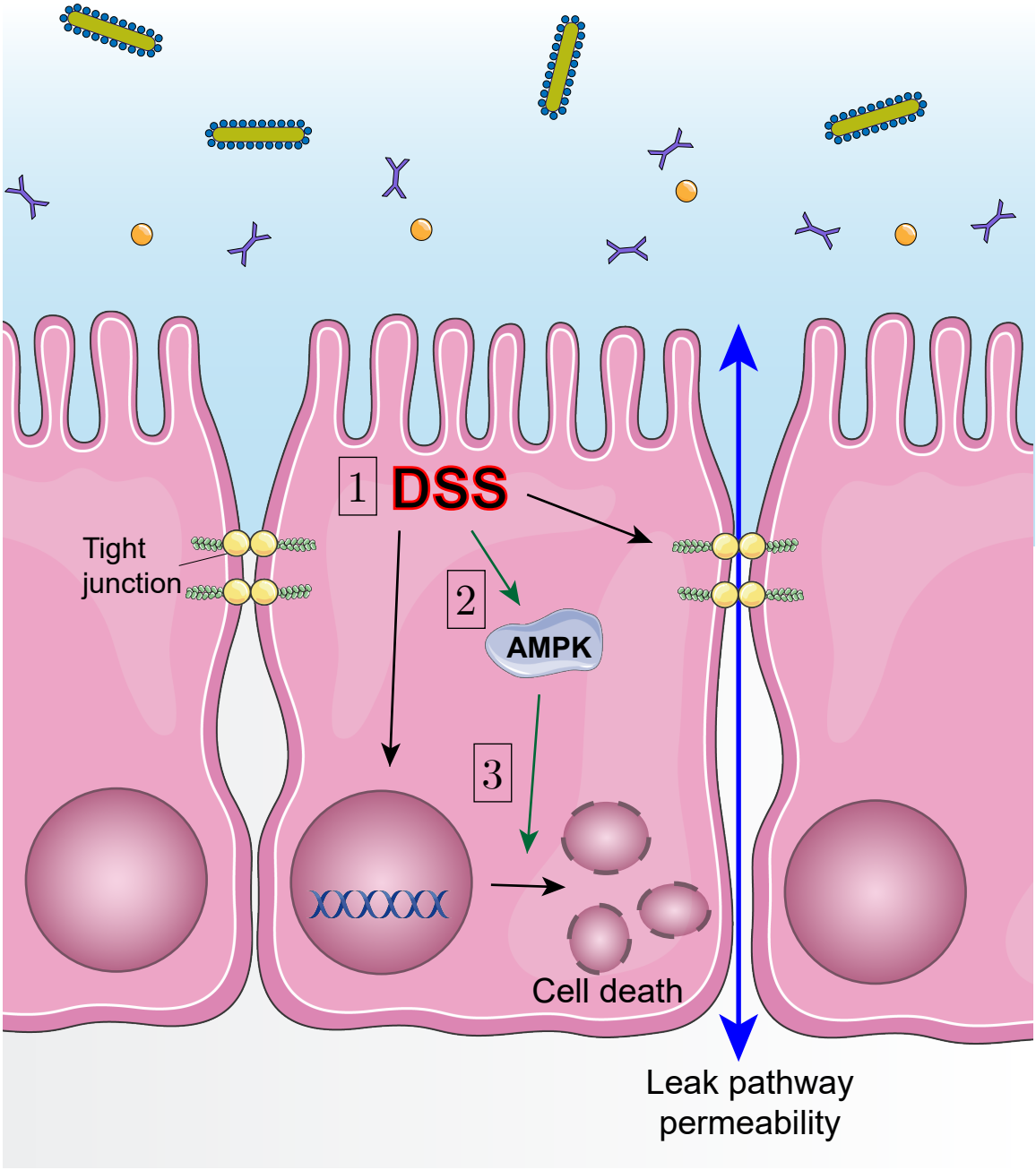

Figure 5.17: AMPK Promotes Cell Death during DSS Colitis

Dextran sodium sulfate (DSS) treatment induces colitis through epithlial cell injury. 1) Epithelial cell injury results in increased cell death and increased intestinal permeability. 2) DSS treatment increases AMPK phosphorylation and activation. 3) Activation of AMPK is associated with increased cell death during DSS colitis.

cells. Therefore, these differences may be influenced by increased compensatory expression of the AMPKα2 isoform as has been observed in other mouse models with a single catalytic isoform deletion [28]. In addition, environmental factors could also contribute to this difference as 2.5% DSS administration in our vivarium resulted in more severe disease than a similar concentration in AMPKα1 Villin-Cre mice from another institution [19]. Further, I observed DSS-induced colitis in AMPKα2 knockout mice under both specific-pathogen free and conventional housing, with conventionally housed mice exhibiting a greater degree of disease (data not shown). This is consistent with previous reports that the resident gut microbiota can affect intestinal inflammation in various mouse colitis models [11, 12, 29, 30]. Finally, I observed AMPK activation by phosphorylation was increased in colitis although expression was overall decreased. A majority of studies that have measured AMPK activation during colitis have demonstrated its phosphorylation is decreased [1, 3, 4, 31]. Only a few studies have observed increased AMPK phosphorylation [7, 32]. These data suggest regulation of AMPK activation in intestinal inflammation is likely context-dependent.

Prior evidence has shown AMPK activation by the pharmacological agonist 5-aminoimidazole-4-carboxamide ribonucleoside (AICAR) is associated with amelioration of DSS-induced colitis due to altered function of immune cells such as macrophages and T-helper cells [2]. However, the concentration of AICAR (500 mg/kg body weight) utilized in this study was extremely high to suggest a robust activation of AMPK is needed for protection. In addition, the impact of AMPK activity in immune cells may have an important influence on colitis outcomes than signaling in intestinal epithelial cells alone. This has been observed in other tissue-specific transgenic mouse models where loss of expression of an IBD candidate gene in the intestinal epithelium alone is not sufficient to cause colitis

[33]. This study also determined AMPK signaling in intestinal epithelial cells likely does not affect immune cell recruitment and function as expression of chemoattractant genes and immune cell infiltration, based on histological assessment, were equivalent in AMPK$\alpha^{fl/fl}$ and AMPK$\alpha^{\Delta IEC\ KO}$ mice challenged with DSS. Furthermore, previous evidence has demonstrated AMPK activity is critical in leukocytes including macrophages [34]. Potentially, AMPK activation in immune cells rather than intestinal epithelial cells during intestinal inflammation could result in less severe disease as has been observed in other studies using agonists for AMPK.

5.3.2 AMPK Promotes Cell Death in Colitis

Increased apoptosis has been associated with increased susceptibility to experimental colitis [35–37]. Previous studies have demonstrated AMPK can upregulate or downregulate apoptosis based on context [27]. Despite no overt change in disease severity, I did observe decreased cell death (% TUNEL-positive cells) in the cecum of DSS-treated AMPK$\alpha^{\Delta IEC\ KO}$ mice. However, expression of the apoptotic markers cleaved caspase-3 and cleaved PARP were decreased in DSS-treated mice irrespective of genotype. I did not observe alteration of apoptosis in untreated AMPK$\alpha^{fl/fl}$ and AMPK$\alpha^{\Delta IEC\ KO}$ mice. Based on these results, AMPK activation may act as a promoter of cell death during colitis. The discrepancy in TUNEL staining and apoptotic marker expression may be due to increased necroptosis which AMPK has recently been shown to repress [38–40]. Further studies would need to confirm if AMPK promotes necroptosis in intestinal inflammation. In addition, as mice were sacrificed at Day 7 I may have captured the disease as it was beginning to initiate recovery processes, resulting in repression of apoptosis initiation and inflammatory mediator expres-

sion. This includes increased intestinal epithelial cell proliferation to reepithelialize erosions. This could be determined by Ki67 (a marker of cell proliferation) staining or BrdU incorporation in newly mice, a synthetic thymidine analog which labels cells undergoing DNA replication.

5.3.3 AMPK Does Not Exacerbate Enteric Infection

To the best of my knowledge, this is a novel study describing the effect of AMPK on disease induced by the enteric pathogen *Citrobacter rodentium*. Initially I hypothesized that AMPK$\alpha^{\Delta \text{IEC KO}}$ mice would have worse disease as AMPK is known to regulate a number of cellular functions important for *Citrobacter rodentium* infection and bacterial clearance. For example, *C. rodentium* infection induces mitochrondrial dysfunction in colonocytes and cytokines such as interleukin-4 and interleukin-6 are protective [16, 41]. AMPK is known to promote mitochondrial biogenesis through direct phosphorylation of Peroxisome proliferator-activated receptor γ coactivator 1-α (PGC-1α) leading to transcriptional activation. In addition, AMPK subunit expression and activation has been shown to be repressed during *C. rodentium* infection [42]. AMPK is also known to promote autophagy by direct phosphorylation of Unc-51 like autophagy activating kinse (ULK1) which is an important component of the autophagy initiator complex. Previous work has shown that autophagy is required for *C. rodentium* clearance [43]. Despite this evidence, I observed that loss of intestinal epithelial AMPK does not increase susceptibility to infection or colitis development as measured by fecal bacterial burden and body weight change during infection. In addition, analysis of colon and extra-intestinal tissue at the peak of infection confirmed similar levels of colonization in the colon and little dissemination of the bacteria to mesenteric lymph

nodes, spleen, and liver. These data indicate that I was unable to completely assess the impact of AMPK in intestinal inflammation due to enteric infection since animals did not develop colitis. The lack of change in disease progression of AMPK$\alpha^{\Delta \text{IEC KO}}$ mice could be due in part to the background of mice used in the experiment. It has been well-documented that C57BL/6 mice have reduced sensitivity to *C. rodentium*-induced colitis and my data are consistent with these observations [24].

In conclusion, in this chapter I have demonstrated that expression of AMPKα in intestinal epithelial cells is dispensible during intestinal inflammation due to epithelial injury. I observed significant decreases in TUNEL staining in AMPK$\alpha^{\Delta \text{IEC KO}}$ mice, however this difference did not extend to other symptoms and features of colitis. Both mouse genotypes exhibited similar trends in body weight loss, increasing disease activity index scores, survival, and histological features during DSS-induced colitis.

6 | Conclusions

In this dissertation, I have confirmed the cellular energy sensor AMP-activated protein kinase (AMPK) is able to regulate functions of intestinal epithelial cells both during homeostasis and disease (Figure 6.1). I utilized both *in vitro* and *in vivo* model systems to test these hypotheses. In addition, I also used various models of intestinal inflammation to elucidate how AMPK regulation is dependent on stimulus and context. In this chapter I summarize the findings from previous chapters, describe how these inform our understanding of intestinal epithelial barrier maintenance and inflammatory signaling, and outline future directions of this work.

6.1 AMPK Expression and Function in the Homeostatic Intestinal Epithelium

In this dissertation I described a novel tissue-specific AMPK knockout mouse model that lacked expression and activity of both α catalytic subunit isoforms in the intestinal epithelium. I observed that intestinal epithelial cells express both α isoforms at similar levels, although expression can vary between animals. However, these cells express only the β1

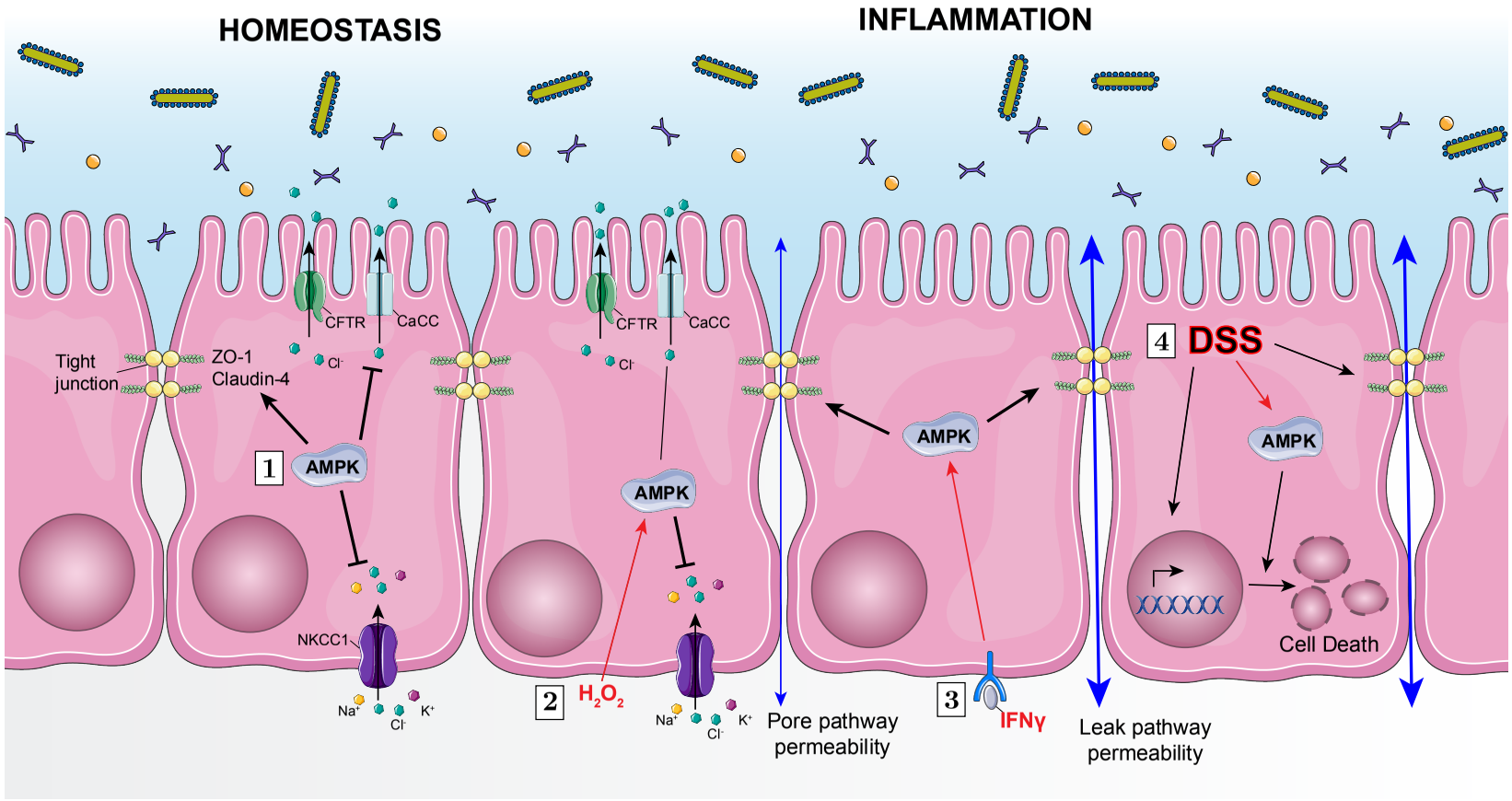

Figure 6.1: AMPK Modulates Intestinal Epithelial Functions during Health and Disease

During homeostasis AMPK promotes barrier function and regulates fluid secretion. 1) AMPK promotes Claudin-4 expression and ZO-1 localization to the membrane. AMPK inhibits NKCC1 expression, contributing to reduced calcium-dependent ion transport. 2) Oxidative stress induces AMPK activation leading to inhibition of NKCC1 activity and repression of calcium-dependent ion secretion. 3) In contrast, the pro-inflammatory cytokine IFNγ activates AMPK which promotes intestinal permeability. 4) Experimental colitis increases AMPK activation which may promote cell death in a caspase-independent manner.

isoform and not β2. In addition, loss of AMPKα expression led to reduced expression of AMPKβ1 in knockout mice. Similarly, mice that retained low expression of AMPKα had less expression of the β1 isoform.

Further examination of AMPKα$^{\Delta IEC\ KO}$ mice determined these mice had reduced transepithelial electrical resistance in the proximal colon associated with reduced colonic expression of Claudin-4. Expression of other tight junction proteins such as E-cadherin, Occludin, Zonula Occludens-1, and Claudins 2 and 15, was unaltered in these mice. I did not observe an increase in macromolecular paracellular permeability in the intestine of these mice. This was consistent with the unaltered expression of occludin and ZO-1, which are known to regulate this pathway. Although I have yet to confirm if occludin and/or ZO-1 localization are altered in these mice, others have observed AMPK inhibition results in mis-localization during calcium-swtich experiments. When large intestine from AMPKα$^{fl/fl}$ and AMPKα$^{\Delta IEC\ KO}$ mice was mounted in Ussing chambers, I saw that responses to Carbachol, and therefore calcium-dependent, electrogenic ion transport was increased in knockout mice. In addition, expression of the $Na^+/K^+/2Cl^-$ cotransporter (NKCC1) was increased in the large intestine of AMPKα$^{\Delta IEC\ KO}$ mice. These data indicate AMPK is a basal inhibitor of calcium-dependent electrogenic ion secretion and this could be mediated at least partially by regulation of NKCC1.

6.2 AMPK in Oxidative Stress

Our laboratory has confirmed that homeostatic inhibition of calcium-dependent electrogenic ion secretion is also mediated by AMPK during oxidative stress. We demonstrated that

hydrogen peroxide reduced ion transport responses without any alteration in transepithelial electrical resistance. This was associated with increased AMPK phosphorylation, indicative of its activation. We confirmed that inhibition of ion transport was dependent on AMPK as treatment with an AMPK inhibitor relieved this effect. In addition, we determined AMPK inhibition of calcium-dependent electrogenic ion transport was mediated by repression of NKCC1 activity and not by changes in its membrane localization. AMPK promoted phosphorylation of NKCC1, although this was contrary to the reduced activity of NKCC1 we observed. Finally, we observed AMPKα2 knockout mice have reduced calcium-dependent ion transport downstream of hydrogen peroxide treatment, an unexpected finding due to our previous data. As AMPKα1 is expressed in AMPKα2 knockout mice, there may be a compensatory increase in its expression and/or activity, potentially indicating that AMPKα1 is the predominant isoform responsible for inhibition of calcium-dependent electrogenic ion transport.

6.3 AMPK in Colitis

To test if basal activity of AMPK is protective against experimental colitis, I treated AMPKα$^{fl/fl}$ and AMPKα$^{\Delta IEC\ KO}$ mice with 2.5% and 5% DSS. These mice developed severe colitis that was similar for both concentrations and between both groups of mice. These data indicated basal AMPK activity is not protective and loss of AMPK activity did not exacerbate symptoms of colitis. Interestingly, I observed reduced expression of apoptosis markers in the proximal colon of DSS-treated mice. Further, the number of TUNEL-positive cells was decreased in the cecum of DSS-treated AMPKα$^{\Delta IEC\ KO}$ mice, suggesting AMPK sup-

presses cell death during colitis. Despite these differences, AMPK$\alpha^{fl/fl}$ and AMPK$\alpha^{\Delta IEC\ KO}$ mice displayed similar levels of disease as observed by loss of body weight, colon shortening, increased intestinal permeability, and histological features of chemically-induced colitis. I also tested if AMPK$\alpha^{fl/fl}$ and AMPK$\alpha^{\Delta IEC\ KO}$ mice would differ in their responses to a pathogenic enteric infection using the murine *Citrobacter rodentium* model, similar to EPEC and EHEC. While mice exhibited increased fecal bacterial burden of *C. rodentium* indicating they were successfully infected, these mice did not develop colitis. I did not observe a significant change in body weight, intestinal permeability, or bacterial dissemination. In addition, AMPK$\alpha^{fl/fl}$ and AMPK$\alpha^{\Delta IEC\ KO}$ mice displayed similar trends during infection. These data suggest basal AMPK activity does not protect against nor does loss of AMPK activity exacerbate pathogenic enteric infection.

6.4 Future Directions

6.4.1 Complete Characterization of AMPK$\alpha^{\Delta IEC\ KO}$ Mice

While I have confirmed a number of important findings through initial characterization of AMPK$\alpha^{\Delta IEC\ KO}$ Mice in Chapter 4, much work remains. Firstly, as previously mentioned although the expression of a number of tight junction proteins is unchanged, their localization at the cell membrane should also be confirmed as other groups have demonstrated this is an important mechanism of tight junction complex regulation. In addition, how AMPK regulates claudin expression has not been established. I also demonstrated AMPK$\alpha^{\Delta IEC\ KO}$ mice have increased calcium-dependent electrogenic ion transport, however a number of transporters can contribute to this effect. AMPK has been shown to regulate K^+ channels,

ENaC, and the Na^+/K^+-ATPase, all of which could potentially be altered by loss of AMPK activity [1–4]. Therefore additional studies of the activity and expression of these transporters would complete our understanding of how AMPK regulates this process. Other groups have suggested AMPK can modulate expression of nutrient transporters involved in absorption [5–10]. I believe this would also be an important aspect to test in these mice as the canonical function of AMPK is to promote nutrient uptake during energetic stress. While I did not observe any change in epithelial structure indicative of altered proliferation and/or differentiation, it would still be interesting to determine if subpopulations of cells are changed such as Paneth cells, goblet cells, and intestinal stem cells. These results were unexpected as AMPK is a highly conserved protein with critical functions during cellular stress. The AMPK kinase LKB1 is known to activate a number of other kinases in the AMPK family. It is possible that their functions provide some redundancy in the epithelium to prevent complete loss of a cell's ability to control responses to energetic stress. Therefore a genome-wide analysis of gene expression could provide useful insights to such redundant pathways in the intestine.

6.4.2 Oxidative Stress Activation of AMPK and its Downstream Effects

In Chapter 3, I described how AMPK activation during oxidative stress mediates inhibition of calcium-dependent electrogenic ion transport through NKCC1. In addition to AMPK, a number of other signaling pathways are activated in response to oxidative stress which may explain some discrepancies in how NKCC1 is inhibited. Further work could confirm if AMPK directly phosphorylates NKCC1 or blocks association of another regulating protein. In addition, differences in responses to oxidative stress based on dose of hydrogen peroxide

exist. Whether AMPK also contributes to these effects is not known. The mechanism of AMPK activation in our experiments has also yet to be confirmed. While other studies suggest this is probably mediated by LKB1 in response to decreased cellular ATP, it has also been shown that AMPK itself can be oxidized leading to S-glutathionylation of the α catalytic subunit and increased activity [11]. Most work on AMPK regulation has focused on Threonine-172 phosphorylation and AMP/ADP binding to the γ subunit. Therefore, oxidative stress would provide another avenue to investigate how other molecular modifications could result in AMPK activation or inhibition.

6.4.3 Role of AMPK in Intestinal Inflammation

In Chapter 5, I described the observed responses of AMPK$\alpha^{\Delta \text{IEC KO}}$ mice to 5% Dextran Sodium Sulfate and *Citrobacter rodentium* infection. In both contexts, AMPK$\alpha^{\text{fl/fl}}$ and AMPK$\alpha^{\Delta \text{IEC KO}}$ mice displayed similar responses and degrees of severity or bacterial burden. While I did observe reduced cell death in DSS-treated AMPK$\alpha^{\Delta \text{IEC KO}}$ mice, this did not ultimately affect disease progression. These results were unexpected as many groups have suggested AMPK is protective against colitis. However, this was not directly tested in my system using an AMPK agonist and would indicate if the protection resulting in those experiments is AMPK-independent. In addition, as discussed in Chapter 5 the administration of 5% and 2.5% DSS resulted in very severe acute colitis that may have masked effects of AMPK. Therefore future studies should utilize a titrated concentration of DSS, or utilize an additional and less destructive colitis model in order to better observe the role of AMPK. A previous study from our laboratory demonstrated AMPK mediates the effects of interferon-γ in intestinal epithelial cells, promoting barrier dysfunction [12]. Another

model which could be useful is cytokine-mediated intestinal inflammation to better test the results of that study in an *in vivo* setting. Further, as others have observed AMPK regulation of electrogenic ion secretion and suggested AMPK activation is protective of net fluid secretion in pathological conditions, responses to other types of infection that more directly target ion transport would be useful [13, 14]. For example, *Vibrio cholerae* infection which directly targets cyclic AMP-dependent ion transport and rotavirus infection that induces pathological calcium-dependent ion transport. These models would act as further evidence of bacterial and viral enteric infections and the effects of AMPK on ion transport in inflammation.

Another aspect of intestinal inflammation not addressed in this dissertation is intestinal restitution and recovery. As AMPK has been shown to promote tight junction assembly and metabolic processes important in cell proliferation, division, and differentiation, it is possible AMPK$\alpha^{\Delta \text{IEC KO}}$ mice may have altered restitution. Indeed Sun et al. observed mice lacking α1 catalytic subunit expression in intestinal epithelial cells had impaired recovery after 3% DSS treatment measured by stool consistency, gross bleeding, disease activity index, and failure to gain body weight 5 days after DSS withdrawal [15].

6.5 Conclusion

While this dissertation sheds some light to the importance of AMP-Activated Protein Kinase in the intestinal epithelium, we are only beginning to understand how this protein fits into the complex network of regulation necessary to maintain homeostasis and promote mucosal healing. We now understand that AMPK promotes barrier function through regulation of

components of the tight junction complex. In addition, AMPK modulates intestinal ion secretion during homeostasis and cellular stress such as oxidative stress. During intestinal inflammation, AMPK may promote cell death although the mechanism remains to be elucidated. Future studies of AMPK in the intestinal epithelium will focus on understanding how AMPK alters expression and localization of tight junction proteins, further characterize AMPK-dependent expression and activity of membrane transporters, determine the role of AMPK in other models of intestinal disease and in metabolic control of intestinal epithelial cells.

References

Chapter 1

1. Hedbacker K, C. M. SNF1/AMPK pathways in yeast. *Frontiers in Bioscience* **13,** 2408–2420 (2008).
2. Johnson, E. C. *et al.* Altered metabolism and persistent starvation behaviors caused by reduced AMPK function in Drosophila. en. *PLoS One* **5** (Sept. 2010).
3. Narbonne, P. & Roy, R. Caenorhabditis elegans dauers need LKB1/AMPK to ration lipid reserves and ensure long-term survival. en. *Nature* **457,** 210–214 (Jan. 2009).
4. Baena-González, E., Rolland, F., Thevelein, J. M. & Sheen, J. A central integrator of transcription networks in plant stress and energy signalling. en. *Nature* **448,** 938–942 (Aug. 2007).
5. Day, E. A., Ford, R. J. & Steinberg, G. R. AMPK as a Therapeutic Target for Treating Metabolic Diseases. en. *Trends Endocrinol. Metab.* **28,** 545–560 (Aug. 2017).
6. Khan, A. S. & Frigo, D. E. A spatiotemporal hypothesis for the regulation, role, and targeting of AMPK in prostate cancer. en. *Nat. Rev. Urol.* (Feb. 2017).
7. Dasgupta, B. & Chhipa, R. R. Evolving Lessons on the Complex Role of AMPK in Normal Physiology and Cancer. en. *Trends Pharmacol. Sci.* **37,** 192–206 (Mar. 2016).
8. Hawley, S. A. *et al.* 5'-AMP activates the AMP-activated protein kinase cascade, and Ca2+/calmodulin activates the calmodulin-dependent protein kinase I cascade, via three independent mechanisms. en. *J. Biol. Chem.* **270,** 27186–27191 (Nov. 1995).
9. Lizcano, J. M. *et al.* LKB1 is a master kinase that activates 13 kinases of the AMPK subfamily, including MARK/PAR-1. en. *EMBO J.* **23,** 833–843 (Feb. 2004).
10. Kullmann, L. & Krahn, M. P. Controlling the master-upstream regulation of the tumor suppressor LKB1. en. *Oncogene* **37,** 3045–3057 (June 2018).
11. Sakamoto, K. *et al.* Deficiency of LKB1 in skeletal muscle prevents AMPK activation and glucose uptake during contraction. en. *EMBO J.* **24,** 1810–1820 (May 2005).
12. Sakamoto, K. *et al.* Deficiency of LKB1 in heart prevents ischemia-mediated activation of AMPKalpha2 but not AMPKalpha1. en. *Am. J. Physiol. Endocrinol. Metab.* **290,** E780–8 (May 2006).

13. Sanders, M. J., Grondin, P. O., Hegarty, B. D., Snowden, M. A. & Carling, D. Investigating the mechanism for AMP activation of the AMP-activated protein kinase cascade. en. *Biochem. J* **403,** 139–148 (Apr. 2007).

14. Suter, M. *et al.* Dissecting the Role of 5-AMP for Allosteric Stimulation, Activation, and Deactivation of AMP-activated Protein Kinase. *J. Biol. Chem.* **281,** 32207–32216 (Oct. 2006).

15. Gowans, G. J., Hawley, S. A., Ross, F. A. & Hardie, D. G. AMP is a true physiological regulator of AMP-activated protein kinase by both allosteric activation and enhancing net phosphorylation. en. *Cell Metab.* **18,** 556–566 (Oct. 2013).

16. Zhang, Y.-L. *et al.* AMP as a low-energy charge signal autonomously initiates assembly of AXIN-AMPK-LKB1 complex for AMPK activation. en. *Cell Metab.* **18,** 546–555 (Oct. 2013).

17. Xiao, B. *et al.* Structure of mammalian AMPK and its regulation by ADP. en. *Nature* **472,** 230–233 (Apr. 2011).

18. Davies, S. P., Helps, N. R., Cohen, P. T. & Hardie, D. G. 5'-AMP inhibits dephosphorylation, as well as promoting phosphorylation, of the AMP-activated protein kinase. Studies using bacterially expressed human protein phosphatase-2C alpha and native bovine protein phosphatase-2AC. en. *FEBS Lett.* **377,** 421–425 (Dec. 1995).

19. Woods, A. *et al.* Ca2+/calmodulin-dependent protein kinase kinase-beta acts upstream of AMP-activated protein kinase in mammalian cells. en. *Cell Metab.* **2,** 21–33 (July 2005).

20. Hawley, S. A. *et al.* Calmodulin-dependent protein kinase kinase-beta is an alternative upstream kinase for AMP-activated protein kinase. en. *Cell Metab.* **2,** 9–19 (July 2005).

21. Hurley, R. L. *et al.* The Ca2+/calmodulin-dependent protein kinase kinases are AMP-activated protein kinase kinases. en. *J. Biol. Chem.* **280,** 29060–29066 (Aug. 2005).

22. Abbott, M. J., Edelman, A. M. & Turcotte, L. P. CaMKK is an upstream signal of AMP-activated protein kinase in regulation of substrate metabolism in contracting skeletal muscle. en. *Am. J. Physiol. Regul. Integr. Comp. Physiol.* **297,** R1724–32 (Dec. 2009).

23. Fogarty, S. *et al.* Calmodulin-dependent protein kinase kinase-beta activates AMPK without forming a stable complex: synergistic effects of Ca2+ and AMP. en. *Biochem. J* **426,** 109–118 (Jan. 2010).

24. Mungai, P. T. *et al.* Hypoxia triggers AMPK activation through reactive oxygen species-mediated activation of calcium release-activated calcium channels. en. *Mol. Cell. Biol.* **31,** 3531–3545 (Sept. 2011).

25. Sallé-Lefort, S. *et al.* Hypoxia upregulates Malat1 expression through a CaMKK/AMPK/HIF-1α axis. en. *Int. J. Oncol.* **49,** 1731–1736 (Oct. 2016).

26. Sundararaman, A., Amirtham, U. & Rangarajan, A. Calcium-Oxidant Signaling Network Regulates AMP-activated Protein Kinase (AMPK) Activation upon Matrix Deprivation. en. *J. Biol. Chem.* **291,** 14410–14429 (July 2016).

27. Ghislat, G., Patron, M., Rizzuto, R. & Knecht, E. Withdrawal of essential amino acids increases autophagy by a pathway involving Ca2+/calmodulin-dependent kinase kinase-β (CaMKK-β). en. *J. Biol. Chem.* **287,** 38625–38636 (Nov. 2012).

28. Birk, J. & Wojtaszewski, J. Predominant alpha2/beta2/gamma3 AMPK activation during exercise in human skeletal muscle. en. *J. Physiol.* **577,** 1021–1032 (Dec. 2006).

29. Treebak, J. T. *et al.* AS160 phosphorylation is associated with activation of alpha2beta2gamma1- but not alpha2beta2gamma3-AMPK trimeric complex in skeletal muscle during exercise in humans. en. *Am. J. Physiol. Endocrinol. Metab.* **292,** E715–22 (Mar. 2007).

30. Wojtaszewski, J. F. P. *et al.* Regulation of 5'AMP-activated protein kinase activity and substrate utilization in exercising human skeletal muscle. en. *Am. J. Physiol. Endocrinol. Metab.* **284,** E813–22 (Apr. 2003).

31. Ross, F. A., MacKintosh, C. & Hardie, D. G. AMP-activated protein kinase: a cellular energy sensor that comes in 12 flavours. en. *FEBS J.* **283,** 2987–3001 (Aug. 2016).

32. Chen, L. *et al.* Structural insight into the autoinhibition mechanism of AMP-activated protein kinase. en. *Nature* **459,** 1146–1149 (June 2009).

33. Chen, L. *et al.* Conserved regulatory elements in AMPK. en. *Nature* **498,** E8–10 (June 2013).

34. Xin, F.-J., Wang, J., Zhao, R.-Q., Wang, Z.-X. & Wu, J.-W. Coordinated regulation of AMPK activity by multiple elements in the α-subunit. en. *Cell Res.* **23,** 1237–1240 (Oct. 2013).

35. Viollet, B. *et al.* Activation of AMP-activated protein kinase in the liver: a new strategy for the management of metabolic hepatic disorders. en. *J. Physiol.* **574,** 41–53 (July 2006).

36. Jäger, S., Handschin, C., St-Pierre, J. & Spiegelman, B. M. AMP-activated protein kinase (AMPK) action in skeletal muscle via direct phosphorylation of PGC-1alpha. en. *Proc. Natl. Acad. Sci. U. S. A.* **104,** 12017–12022 (July 2007).

37. Kazgan, N., Williams, T., Forsberg, L. J. & Brenman, J. E. Identification of a nuclear export signal in the catalytic subunit of AMP-activated protein kinase. en. *Mol. Biol. Cell* **21,** 3433–3442 (Oct. 2010).

38. Hallows, K. R., Kobinger, G. P., Wilson, J. M., Witters, L. A. & Foskett, J. K. Physiological modulation of CFTR activity by AMP-activated protein kinase in polarized T84 cells. *Am. J. Physiol. Cell Physiol.* **284,** C1297–308 (May 2003).

39. Rajamohan, F. *et al.* Probing the enzyme kinetics, allosteric modulation and activation of α1- and α2-subunit-containing AMP-activated protein kinase (AMPK) heterotrimeric complexes by pharmacological and physiological activators. en. *Biochem. J* **473,** 581–592 (Mar. 2016).

40. Oakhill, J. S. *et al.* β-Subunit myristoylation is the gatekeeper for initiating metabolic stress sensing by AMP-activated protein kinase (AMPK). *Proc. Natl. Acad. Sci. U. S. A.* **107,** 19237–19241 (Nov. 2010).

41. Scott, J. W. *et al.* Thienopyridone drugs are selective activators of AMP-activated protein kinase beta1-containing complexes. en. *Chem. Biol.* **15,** 1220–1230 (Nov. 2008).

42. Warden, S. M. *et al.* Post-translational modifications of the beta-1 subunit of AMP-activated protein kinase affect enzyme activity and cellular localization. en. *Biochem. J* **354,** 275–283 (Mar. 2001).

43. Zhang, C.-S. *et al.* The lysosomal v-ATPase-Ragulator complex is a common activator for AMPK and mTORC1, acting as a switch between catabolism and anabolism. en. *Cell Metab.* **20,** 526–540 (Sept. 2014).

44. Liang, J. *et al.* Myristoylation confers noncanonical AMPK functions in autophagy selectivity and mitochondrial surveillance. en. *Nat. Commun.* **6,** 7926 (Aug. 2015).

45. Koay, A., Rimmer, K. A., Mertens, H. D. T., Gooley, P. R. & Stapleton, D. Oligosaccharide recognition and binding to the carbohydrate binding module of AMP-activated protein kinase. en. *FEBS Lett.* **581,** 5055–5059 (Oct. 2007).

46. Koay, A. *et al.* AMPK beta subunits display isoform specific affinities for carbohydrates. en. *FEBS Lett.* **584,** 3499–3503 (Aug. 2010).

47. McBride, A., Ghilagaber, S., Nikolaev, A. & Hardie, D. G. The glycogen-binding domain on the AMPK beta subunit allows the kinase to act as a glycogen sensor. en. *Cell Metab.* **9,** 23–34 (Jan. 2009).

48. McBride, A. & Hardie, D. G. AMP-activated protein kinase–a sensor of glycogen as well as AMP and ATP? en. *Acta Physiol.* **196,** 99–113 (May 2009).

49. Polekhina, G. *et al.* AMPK beta subunit targets metabolic stress sensing to glycogen. en. *Curr. Biol.* **13,** 867–871 (May 2003).

50. Polekhina, G. *et al.* Structural basis for glycogen recognition by AMP-activated protein kinase. en. *Structure* **13,** 1453–1462 (Oct. 2005).

51. Calabrese, M. F. *et al.* Structural basis for AMPK activation: natural and synthetic ligands regulate kinase activity from opposite poles by different molecular mechanisms. en. *Structure* **22,** 1161–1172 (Aug. 2014).

52. Li, X. *et al.* Structural basis of AMPK regulation by adenine nucleotides and glycogen. en. *Cell Res.* **25,** 50–66 (Jan. 2015).

53. Xiao, B. *et al.* Structural basis of AMPK regulation by small molecule activators. en. *Nat. Commun.* **4,** 3017 (2013).

54. Xiao, B. *et al.* Structural basis for AMP binding to mammalian AMP-activated protein kinase. en. *Nature* **449,** 496–500 (Sept. 2007).

55. Steinberg, G. R. & Kemp, B. E. AMPK in Health and Disease. *Physiol. Rev.* **89,** 1025–1078 (July 2009).

56. Cheung, P. C., Salt, I. P., Davies, S. P., Hardie, D. G. & Carling, D. Characterization of AMP-activated protein kinase gamma-subunit isoforms and their role in AMP binding. en. *Biochem. J* **346 Pt 3,** 659–669 (Mar. 2000).

57. Viollet, B. *et al.* AMPK: Lessons from transgenic and knockout animals. *Front. Biosci.* **14,** 19–44 (Jan. 2009).

58. O'Neill, H. M. *et al.* AMP-activated protein kinase (AMPK) beta1beta2 muscle null mice reveal an essential role for AMPK in maintaining mitochondrial content and glucose uptake during exercise. en. *Proc. Natl. Acad. Sci. U. S. A.* **108,** 16092–16097 (Sept. 2011).

59. Viollet, B. *et al.* The AMP-activated protein kinase alpha2 catalytic subunit controls whole-body insulin sensitivity. en. *J. Clin. Invest.* **111,** 91–98 (Jan. 2003).

60. Foretz, M. *et al.* Maintenance of red blood cell integrity by AMP-activated protein kinase alpha1 catalytic subunit. en. *FEBS Lett.* **584,** 3667–3671 (Aug. 2010).

61. Wang, S., Dale, G. L., Song, P., Viollet, B. & Zou, M.-H. AMPK alpha 1 deletion shortens erythrocyte lifespan in mice: role of oxidative stress. *J. Biol. Chem.* (Apr. 2010).

62. Jørgensen, S. B. *et al.* Knockout of the alpha2 but not alpha1 5'-AMP-activated protein kinase isoform abolishes 5-aminoimidazole-4-carboxamide-1-beta-4-ribofuranoside but not contraction-induced glucose uptake in skeletal muscle. en. *J. Biol. Chem.* **279,** 1070–1079 (Jan. 2004).

63. Lieberthal, W. *et al.* Susceptibility to ATP depletion of primary proximal tubular cell cultures derived from mice lacking either the α1 or the α2 isoform of the catalytic domain of AMPK. en. *BMC Nephrol.* **14,** 251 (Nov. 2013).

64. Yang, C., Li, Z., Lai, P., Bai, X. & Jin, D. Chondrocyte-Specific Ablation of AMPKα1 Does Not Affect Bone Development or Pathogenesis of Osteoarthritis in Mice. en. *DNA Cell Biol.* **35,** 156–162 (Mar. 2016).

65. Schaffer, B. E. *et al.* Identification of AMPK Phosphorylation Sites Reveals a Network of Proteins Involved in Cell Invasion and Facilitates Large-Scale Substrate Prediction. en. *Cell Metab.* **22,** 907–921 (Nov. 2015).

66. El-Mir, M. Y. *et al.* Dimethylbiguanide inhibits cell respiration via an indirect effect targeted on the respiratory chain complex I. en. *J. Biol. Chem.* **275,** 223–228 (Jan. 2000).

67. Owen, M. R., Doran, E. & Halestrap, A. P. Evidence that metformin exerts its anti-diabetic effects through inhibition of complex 1 of the mitochondrial respiratory chain. en. *Biochem. J* **348 Pt 3,** 607–614 (June 2000).

68. Hawley, S. A. *et al.* Use of cells expressing gamma subunit variants to identify diverse mechanisms of AMPK activation. en. *Cell Metab.* **11,** 554–565 (June 2010).

69. Foretz, M., Guigas, B., Bertrand, L., Pollak, M. & Viollet, B. Metformin: from mechanisms of action to therapies. en. *Cell Metab.* **20,** 953–966 (Dec. 2014).

70. Jenkins, Y. *et al.* AMPK activation through mitochondrial regulation results in increased substrate oxidation and improved metabolic parameters in models of diabetes. en. *PLoS One* **8,** e81870 (Dec. 2013).

71. Marcinko, K. *et al.* The AMPK activator R419 improves exercise capacity and skeletal muscle insulin sensitivity in obese mice. en. *Mol Metab* **4,** 643–651 (Sept. 2015).

72. Foretz, M. *et al.* Metformin inhibits hepatic gluconeogenesis in mice independently of the LKB1/AMPK pathway via a decrease in hepatic energy state. en. *J. Clin. Invest.* **120,** 2355–2369 (July 2010).

73. Miller, R. A. *et al.* Biguanides suppress hepatic glucagon signalling by decreasing production of cyclic AMP. en. *Nature* **494,** 256–260 (Feb. 2013).

74. Chen, S. C. *et al.* Metformin suppresses adipogenesis through both AMP-activated protein kinase (AMPK)-dependent and AMPK-independent mechanisms. en. *Mol. Cell. Endocrinol.* **440,** 57–68 (Jan. 2017).

75. Rao, E. *et al.* AMPK-dependent and independent effects of AICAR and compound C on T-cell responses. en. *Oncotarget* **7,** 33783–33795 (June 2016).

76. Glund, S. *et al.* Role of adenosine 5'-monophosphate-activated protein kinase in interleukin-6 release from isolated mouse skeletal muscle. en. *Endocrinology* **150,** 600–606 (Feb. 2009).

77. Zhou, G. *et al.* Role of AMP-activated protein kinase in mechanism of metformin action. en. *J. Clin. Invest.* **108,** 1167–1174 (Oct. 2001).

78. Bain, J. *et al.* The selectivity of protein kinase inhibitors: a further update. en. *Biochem. J* **408,** 297–315 (Dec. 2007).

79. Vogt, J., Traynor, R. & Sapkota, G. P. The specificities of small molecule inhibitors of the TGFß and BMP pathways. en. *Cell. Signal.* **23,** 1831–1842 (Nov. 2011).

80. Dasgupta, B. & Seibel, W. Compound C/Dorsomorphin: Its Use and Misuse as an AMPK Inhibitor. en. *Methods Mol. Biol.* **1732,** 195–202 (2018).

81. Cheruiyot, A. *et al.* Compound C inhibits nonsense-mediated RNA decay independently of AMPK. en. *PLoS One* **13,** e0204978 (Oct. 2018).

82. in. *Gastrointestinal Physiology* (ed Barrett, K. E.) 1–17 (The McGraw-Hill Companies, Inc., 2006).

83. Moor, A. E. *et al.* Spatial Reconstruction of Single Enterocytes Uncovers Broad Zonation along the Intestinal Villus Axis. en. *Cell* **175,** 1156–1167.e15 (Nov. 2018).

84. Clevers, H. C. & Bevins, C. L. Paneth cells: maestros of the small intestinal crypts. en. *Annu. Rev. Physiol.* **75,** 289–311 (2013).

85. Stappenbeck, T. S. Paneth cell development, differentiation, and function: new molecular cues. en. *Gastroenterology* **137,** 30–33 (July 2009).

86. Hawker, P. C., McKay, J. S. & Turnberg, L. A. Electrolyte transport across colonic mucosa from patients with inflammatory bowel disease. en. *Gastroenterology* **79,** 508–511 (Sept. 1980).

87. Sandle, G. I. *et al.* Cellular basis for defective electrolyte transport in inflamed human colon. en. *Gastroenterology* **99,** 97–105 (July 1990).

88. Musch, M. W. *et al.* Na+ K+ Cl co-transport in the intestine of a marine teleost. *Nature* **300,** 351–353 (Nov. 1982).

89. Dharmsathaphorn, K., Mandel, K. G., Masui, H. & McRoberts, J. A. Vasoactive intestinal polypeptide-induced chloride secretion by a colonic epithelial cell line. Direct participation of a basolaterally localized Na+,K+,Cl- cotransport system. en. *J. Clin. Invest.* **75,** 462–471 (Feb. 1985).

90. Garcia-Hernandez, V., Quiros, M. & Nusrat, A. Intestinal epithelial claudins: expression and regulation in homeostasis and inflammation. en. *Ann. N. Y. Acad. Sci.* **1397,** 66–79 (June 2017).

91. Turner, J. R. *et al.* Physiological regulation of epithelial tight junctions is associated with myosin light-chain phosphorylation. en. *Am. J. Physiol.* **273,** C1378–85 (Oct. 1997).

92. Yu, A. S. L. *et al.* Knockdown of occludin expression leads to diverse phenotypic alterations in epithelial cells. en. *Am. J. Physiol. Cell Physiol.* **288,** C1231–41 (June 2005).

93. Al-Sadi, R. *et al.* Occludin regulates macromolecule flux across the intestinal epithelial tight junction barrier. en. *Am. J. Physiol. Gastrointest. Liver Physiol.* **300,** G1054–64 (June 2011).

94. Knoop, K. A., McDonald, K. G., McCrate, S., McDole, J. R. & Newberry, R. D. Microbial sensing by goblet cells controls immune surveillance of luminal antigens in the colon. en. *Mucosal Immunol.* **8,** 198–210 (Jan. 2015).

95. Miyata, N. *et al.* Microbial Sensing by Intestinal Myeloid Cells Controls Carcinogenesis and Epithelial Differentiation. en. *Cell Rep.* **24,** 2342–2355 (Aug. 2018).

96. Price, A. E. *et al.* A Map of Toll-like Receptor Expression in the Intestinal Epithelium Reveals Distinct Spatial, Cell Type-Specific, and Temporal Patterns. en. *Immunity* (Aug. 2018).

97. Rescigno, M. *et al.* Dendritic cells express tight junction proteins and penetrate gut epithelial monolayers to sample bacteria. en. *Nat. Immunol.* **2,** 361–367 (Apr. 2001).

98. Ding, S. *et al.* Mucosal healing and fibrosis after acute or chronic inflammation in wild type FVB-N mice and C57BL6 procollagen α1(I)-promoter-GFP reporter mice. en. *PLoS One* **7,** e42568 (Aug. 2012).

99. Kurashima, Y. & Kiyono, H. Mucosal Ecological Network of Epithelium and Immune Cells for Gut Homeostasis and Tissue Healing. en. *Annu. Rev. Immunol.* **35,** 119–147 (Apr. 2017).

100. Caruso, R. *et al.* A specific gene-microbe interaction drives the development of Crohn's disease–like colitis in mice. en. *Science Immunology* **4,** eaaw4341 (Apr. 2019).

101. Hugot, J. P. *et al.* Association of NOD2 leucine-rich repeat variants with susceptibility to Crohn's disease. en. *Nature* **411,** 599–603 (May 2001).

102. Kühn, R., Löhler, J., Rennick, D., Rajewsky, K. & Müller, W. Interleukin-10-deficient mice develop chronic enterocolitis. en. *Cell* **75,** 263–274 (Oct. 1993).

103. Sellon, R. K. *et al.* Resident enteric bacteria are necessary for development of spontaneous colitis and immune system activation in interleukin-10-deficient mice. en. *Infect. Immun.* **66,** 5224–5231 (Nov. 1998).

104. Jostins, L. *et al.* Host-microbe interactions have shaped the genetic architecture of inflammatory bowel disease. *Nature* **491,** 119–124 (Nov. 2012).

105. McCole, D. F. IBD candidate genes and intestinal barrier regulation. *Inflamm. Bowel Dis.* **20,** 1829–1849 (Oct. 2014).

106. Miao, W. *et al.* Sodium Butyrate Promotes Reassembly of Tight Junctions in Caco-2 Monolayers Involving Inhibition of MLCK/MLC2 Pathway and Phosphorylation of PKCβ2. en. *Int. J. Mol. Sci.* **17** (Oct. 2016).

107. Pongkorpsakol, P., Buasakdi, C., Chantivas, T., Chatsudthipong, V. & Muanprasat, C. An agonist of a zinc-sensing receptor GPR39 enhances tight junction assembly in intestinal epithelial cells via an AMPK-dependent mechanism. en. *Eur. J. Pharmacol.* **842,** 306–313 (Oct. 2018).

108. Rowart, P., Wu, J., Caplan, M. J. & Jouret, F. Implications of AMPK in the Formation of Epithelial Tight Junctions. en. *Int. J. Mol. Sci.* **19** (July 2018).

109. Wu, W., Wang, S., Liu, Q., Shan, T. & Wang, Y. Metformin Protects against LPS-Induced Intestinal Barrier Dysfunction by Activating AMPK Pathway. en. *Mol. Pharm.* **15,** 3272–3284 (Aug. 2018).

110. Zhu, M.-J., Sun, X. & Du, M. AMPK in regulation of apical junctions and barrier function of intestinal epithelium. en. *Tissue Barriers,* 1–13 (Aug. 2018).

111. Bai, A. *et al.* Novel anti-inflammatory action of 5-aminoimidazole-4-carboxamide ribonucleoside with protective effect in dextran sulfate sodium-induced acute and chronic colitis. en. *J. Pharmacol. Exp. Ther.* **333,** 717–725 (June 2010).

112. Afrin, M. R. *et al.* Le Carbone, a charcoal supplement, modulates DSS-induced acute colitis in mice through activation of AMPKα and downregulation of STAT3 and caspase 3 dependent apoptotic pathways. en. *Int. Immunopharmacol.* **43,** 70–78 (Feb. 2017).

113. Wei, W. *et al.* Protective effects of wedelolactone on dextran sodium sulfate induced murine colitis partly through inhibiting the NLRP3 inflammasome activation via AMPK signaling. en. *Biomed. Pharmacother.* **94,** 27–36 (July 2017).

114. Xu, B. *et al.* Geniposide ameliorates TNBS-induced experimental colitis in rats via reducing inflammatory cytokine release and restoring impaired intestinal barrier function. en. *Acta Pharmacol. Sin.* (Mar. 2017).

115. Chen, L. *et al.* Activating AMPK to Restore Tight Junction Assembly in Intestinal Epithelium and to Attenuate Experimental Colitis by Metformin. *Front. Pharmacol.* **9,** 761 (2018).

116. Deng, J. *et al.* Metformin protects against intestinal barrier dysfunction via AMPKα1-dependent inhibition of JNK signalling activation. en. *J. Cell. Mol. Med.* **22,** 546–557 (Jan. 2018).

117. Scharl, M., Paul, G., Barrett, K. E. & McCole, D. F. AMP-activated protein kinase mediates the interferon-gamma-induced decrease in intestinal epithelial barrier function. en. *J. Biol. Chem.* **284,** 27952–27963 (Oct. 2009).

118. Talero, E. *et al.* Expression patterns of sirtuin 1-AMPK-autophagy pathway in chronic colitis and inflammation-associated colon neoplasia in IL-10-deficient mice. en. *Int. Immunopharmacol.* **35,** 248–256 (June 2016).

119. Yang, G., Wang, H., Kang, Y. & Zhu, M.-J. Grape seed extract improves epithelial structure and suppresses inflammation in ileum of IL-10-deficient mice. en. *Food Funct.* **5,** 2558–2563 (Oct. 2014).

Chapter 2

1. Bouyer, P. G. *et al.* Capsaicin induces NKCC1 internalization and inhibits chloride secretion in colonic epithelial cells independently of TRPV1. en. *Am. J. Physiol. Gastrointest. Liver Physiol.* **304,** G142–56 (Jan. 2013).

2. Hastie, C. J., McLauchlan, H. J. & Cohen, P. Assay of protein kinases using radiolabeled ATP: a protocol. en. *Nat. Protoc.* **1,** 968–971 (2006).

3. Viollet, B. *et al.* The AMP-activated protein kinase alpha2 catalytic subunit controls whole-body insulin sensitivity. en. *J. Clin. Invest.* **111,** 91–98 (Jan. 2003).

4. Chappell, A. E. *et al.* Hydrogen peroxide inhibits Ca2+-dependent chloride secretion across colonic epithelial cells via distinct kinase signaling pathways and ion transport proteins. *FASEB J.* **22,** 2023–2036 (June 2008).

5. Wirtz, S. *et al.* Chemically induced mouse models of acute and chronic intestinal inflammation. en. *Nat. Protoc.* **12,** 1295–1309 (July 2017).

6. Erben, U. *et al.* A guide to histomorphological evaluation of intestinal inflammation in mouse models. *Int. J. Clin. Exp. Pathol.* **7,** 4557–4576 (July 2014).

Chapter 3

1. Cooke, H. J. Neuroimmune signaling in regulation of intestinal ion transport. en. *Am. J. Physiol.* **266,** G167–78 (Feb. 1994).

2. Sidhu, M. & Cooke, H. J. Role for 5-HT and ACh in submucosal reflexes mediating colonic secretion. en. *Am. J. Physiol.* **269,** G346–51 (Sept. 1995).

3. Barrett, K. E. & Keely, S. J. Chloride secretion by the intestinal epithelium: molecular basis and regulatory aspects. en. *Annu. Rev. Physiol.* **62,** 535–572 (2000).

4. Grubb, B. R. & Gabriel, S. E. Intestinal physiology and pathology in gene-targeted mouse models of cystic fibrosis. en. *Am. J. Physiol.* **273,** G258–66 (Aug. 1997).

5. Kerem, E. *et al.* The relation between genotype and phenotype in cystic fibrosis–analysis of the most common mutation (delta F508). en. *N. Engl. J. Med.* **323,** 1517–1522 (Nov. 1990).

6. Zeisel, M. B., Dhawan, P. & Baumert, T. F. Tight junction proteins in gastrointestinal and liver disease. en. *Gut* (Oct. 2018).

7. Cunningham, S. A. *et al.* Cloning of an epithelial chloride channel from bovine trachea. en. *J. Biol. Chem.* **270,** 31016–31026 (Dec. 1995).

8. Gruber, A. D., Schreur, K. D., Ji, H. L., Fuller, C. M. & Pauli, B. U. Molecular cloning and transmembrane structure of hCLCA2 from human lung, trachea, and mammary gland. en. *Am. J. Physiol.* **276,** C1261–70 (June 1999).

9. Gruber, A. D. *et al.* Genomic cloning, molecular characterization, and functional analysis of human CLCA1, the first human member of the family of Ca2+-activated Cl- channel proteins. en. *Genomics* **54,** 200–214 (Dec. 1998).

10. Nanda Kumar, N. S., Singh, S. K. & Rajendran, V. M. Mucosal potassium efflux mediated via Kcnn4 channels provides the driving force for electrogenic anion secretion in colon. en. *Am. J. Physiol. Gastrointest. Liver Physiol.* **299,** G707–14 (Sept. 2010).

11. Payne, J. A. *et al.* Primary structure, functional expression, and chromosomal localization of the bumetanide-sensitive Na-K-Cl cotransporter in human colon. en. *J. Biol. Chem.* **270,** 17977–17985 (July 1995).

12. D'Andrea, L. *et al.* Na:K:2Cl cotransporter (NKCC) of intestinal epithelial cells. Surface expression in response to cAMP. en. *J. Biol. Chem.* **271,** 28969–28976 (Nov. 1996).

13. Torchia, J., Lytle, C., Pon, D. J., Forbush 3rd, B. & Sen, A. K. The Na-K-Cl cotransporter of avian salt gland. Phosphorylation in response to cAMP-dependent and calcium-dependent secretogogues. en. *J. Biol. Chem.* **267,** 25444–25450 (Dec. 1992).

14. Lytle, C. & Forbush 3rd, B. The Na-K-Cl cotransport protein of shark rectal gland. II. Regulation by direct phosphorylation. en. *J. Biol. Chem.* **267,** 25438–25443 (Dec. 1992).

15. Lytle, C. & Forbush, B. *Na-K-Cl cotransport in the shark rectal gland. II. Regulation in isolated tubules* 1992.

16. Matthews, J. B., Awtrey, C. S. & Madara, J. L. Microfilament-dependent activation of Na+/K+/2Cl- cotransport by cAMP in intestinal epithelial monolayers. en. *J. Clin. Invest.* **90,** 1608–1613 (Oct. 1992).

17. Matthews, J. B., Smith, J. A. & Hrnjez, B. J. Effects of F-actin stabilization or disassembly on epithelial Cl- secretion and Na-K-2Cl cotransport. en. *Am. J. Physiol.* **272,** C254–62 (Jan. 1997).

18. Piechotta, K., Lu, J. & Delpire, E. Cation chloride cotransporters interact with the stress-related kinases Ste20-related proline-alanine-rich kinase (SPAK) and oxidative stress response 1 (OSR1). en. *J. Biol. Chem.* **277,** 50812–50819 (Dec. 2002).

19. Dowd, B. F. X. & Forbush, B. PASK (proline-alanine-rich STE20-related kinase), a regulatory kinase of the Na-K-Cl cotransporter (NKCC1). en. *J. Biol. Chem.* **278,** 27347–27353 (July 2003).

20. Moriguchi, T. *et al.* WNK1 regulates phosphorylation of cation-chloride-coupled cotransporters via the STE20-related kinases, SPAK and OSR1. en. *J. Biol. Chem.* **280,** 42685–42693 (Dec. 2005).

21. Gagnon, K. B. E., England, R. & Delpire, E. A single binding motif is required for SPAK activation of the Na-K-2Cl cotransporter. en. *Cell. Physiol. Biochem.* **20,** 131–142 (2007).

22. Ponce-Coria, J., Gagnon, K. B. & Delpire, E. Calcium-binding protein 39 facilitates molecular interaction between Ste20p proline alanine-rich kinase and oxidative stress response 1 monomers. en. *Am. J. Physiol. Cell Physiol.* **303,** C1198–205 (Dec. 2012).

23. Ponce-Coria, J. *et al.* A novel Ste20-related proline/alanine-rich kinase (SPAK)-independent pathway involving calcium-binding protein 39 (Cab39) and serine threonine kinase with no lysine member 4 (WNK4) in the activation of Na-K-Cl cotransporters. en. *J. Biol. Chem.* **289,** 17680–17688 (June 2014).

24. Del Castillo, I. C. *et al.* Dynamic regulation of Na+-K+-2Cl cotransporter surface expression by PKC-ϵ in Cl-secretory epithelia. en. *American Journal of Physiology - Cell Physiology* **289,** C1332–C1343 (Nov. 2005).

25. Chappell, A. E. & Barrett, K. E. *Direct and indirect signaling through the epidermal growth factor receptor (EGFr) exerts distinct effects on surface expression of Na+, K+, 2 Cl- cotransporter-1 (NKCC1) in colonic epithelial cells* in. **23** (FASEB, Apr. 2009), 796.29–796.29.

26. Tang, J. *et al.* Activated PKC{delta} and PKC{epsilon} inhibit epithelial chloride secretion response to cAMP via inducing internalization of the Na+-K+-2Cl- cotransporter NKCC1. en. *J. Biol. Chem.* **285,** 34072–34085 (Oct. 2010).

27. Bouyer, P. G. *et al.* Capsaicin induces NKCC1 internalization and inhibits chloride secretion in colonic epithelial cells independently of TRPV1. en. *Am. J. Physiol. Gastrointest. Liver Physiol.* **304,** G142–56 (Jan. 2013).

28. Otamiri, T. & Sjödahl, R. Oxygen radicals: their role in selected gastrointestinal disorders. en. *Dig. Dis.* **9,** 133–141 (1991).

29. Ray, P. D., Huang, B.-W. & Tsuji, Y. Reactive oxygen species (ROS) homeostasis and redox regulation in cellular signaling. en. *Cell. Signal.* **24,** 981–990 (May 2012).

30. Biasi, F., Leonarduzzi, G., Oteiza, P. I. & Poli, G. Inflammatory bowel disease: mechanisms, redox considerations, and therapeutic targets. en. *Antioxid. Redox Signal.* **19,** 1711–1747 (Nov. 2013).

31. Test, S. T. & Weiss, S. J. Quantitative and temporal characterization of the extracellular H2O2 pool generated by human neutrophils. en. *J. Biol. Chem.* **259,** 399–405 (Jan. 1984).

32. Yamada, T. & Grisham, M. B. Role of neutrophil-derived oxidants in the pathogenesis of intestinal inflammation. en. *Klin. Wochenschr.* **69,** 988–994 (Dec. 1991).

33. Nielsen, O. H., Berild, D. & Ahnfelt-Rønne, I. In vitro Superoxide Production by Peripheral Neutrophils from Patients with Inflammatory Bowel Disease. en. *Mediators Inflamm.* **3,** 161–164 (1994).

34. Keshavarzian, A. *et al.* Excessive production of reactive oxygen metabolites by inflamed colon: analysis by chemiluminescence probe. en. *Gastroenterology* **103,** 177–185 (July 1992).

35. Simmonds, N. J. *et al.* Chemiluminescence assay of mucosal reactive oxygen metabolites in inflammatory bowel disease. en. *Gastroenterology* **103,** 186–196 (July 1992).

36. Sedghi, S. *et al.* Increased production of luminol enhanced chemiluminescence by the inflamed colonic mucosa in patients with ulcerative colitis. en. *Gut* **34,** 1191–1197 (Sept. 1993).

37. Grisham, M. B. Oxidants and free radicals in inflammatory bowel disease. en. *Lancet* **344,** 859–861 (Sept. 1994).

38. Lih-Brody, L. *et al.* Increased oxidative stress and decreased antioxidant defenses in mucosa of inflammatory bowel disease. en. *Dig. Dis. Sci.* **41,** 2078–2086 (Oct. 1996).

39. Keshavarzian, A., Morgan, G., Sedghi, S., Gordon, J. H. & Doria, M. Role of reactive oxygen metabolites in experimental colitis. en. *Gut* **31,** 786–790 (July 1990).

40. Keshavarzian, A. *et al.* Agents capable of eliminating reactive oxygen species. Catalase, WR-2721, or Cu(II)2(3,5-DIPS)4 decrease experimental colitis. en. *Dig. Dis. Sci.* **37,** 1866–1873 (Dec. 1992).

41. Choudhary, S. *et al.* Novel antioxidants zolimid and AEOL11201 ameliorate colitis in rats. en. *Dig. Dis. Sci.* **46,** 2222–2230 (Oct. 2001).

42. Oz, H. S., Chen, T. S., McClain, C. J. & de Villiers, W. J. S. Antioxidants as novel therapy in a murine model of colitis. en. *J. Nutr. Biochem.* **16,** 297–304 (May 2005).

43. Barrett, K. E. & McCole, D. F. The Hydrogen Peroxide Scavenger, Catalase, Alleviates Ion Transport Dysfunction in Murine Colitis. en. *Clin. Exp. Pharmacol. Physiol.* (Aug. 2016).

44. Sandle, G. I. *et al.* Cellular basis for defective electrolyte transport in inflamed human colon. en. *Gastroenterology* **99,** 97–105 (July 1990).

45. Schmitz, H. *et al.* Epithelial barrier and transport function of the colon in ulcerative colitis. en. *Ann. N. Y. Acad. Sci.* **915,** 312–326 (2000).

46. Amasheh, S. *et al.* Cytokine-dependent transcriptional down-regulation of epithelial sodium channel in ulcerative colitis. en. *Gastroenterology* **126,** 1711–1720 (June 2004).

47. Schultheiss, G., Hennig, B. & Diener, M. Sites of action of hydrogen peroxide on ion transport across rat distal colon. en. *Br. J. Pharmacol.* **154,** 991–1000 (July 2008).

48. Chappell, A. E. *et al.* Hydrogen peroxide inhibits Ca2+-dependent chloride secretion across colonic epithelial cells via distinct kinase signaling pathways and ion transport proteins. *FASEB J.* **22,** 2023–2036 (June 2008).

49. Hirota, C. L. & McKay, D. M. Loss of Ca2+-mediated ion transport during colitis correlates with reduced ion transport responses to a Ca2+-activated K+ channel opener. *Br. J. Pharmacol.* **156,** 1085–1097 (2009).

50. Lynch, S. V. *et al.* Cystic fibrosis transmembrane conductance regulator knockout mice exhibit aberrant gastrointestinal microbiota. en. *Gut Microbes* **4,** 41–47 (Jan. 2013).

51. Walker, J., Jijon, H. B., Churchill, T., Kulka, M. & Madsen, K. L. Activation of AMP-activated protein kinase reduces cAMP-mediated epithelial chloride secretion. *Am. J. Physiol. Gastrointest. Liver Physiol.* **285,** G850–60 (Nov. 2003).

52. Ratcliff, R. *et al.* Production of a severe cystic fibrosis mutation in mice by gene targeting. *Nature Genetics* **4,** 35–41 (May 1993).

53. Snouwaert, J. N. *et al.* An animal model for cystic fibrosis made by gene targeting. en. *Science* **257,** 1083–1088 (Aug. 1992).

54. Van Doorninck, J. H. *et al.* A mouse model for the cystic fibrosis delta F508 mutation. en. *EMBO J.* **14,** 4403–4411 (Sept. 1995).

55. Zeiher, B. G. *et al.* A mouse model for the delta F508 allele of cystic fibrosis. en. *J. Clin. Invest.* **96,** 2051–2064 (Oct. 1995).

56. Delaney, S. J. *et al.* Cystic fibrosis mice carrying the missense mutation G551D replicate human genotype-phenotype correlations. en. *EMBO J.* **15,** 955–963 (Mar. 1996).

57. Cuthbert, A. W. *et al.* Ion-transporting activity in the murine colonic epithelium of normal animals and animals with cystic fibrosis. en. *Pflugers Arch.* **428,** 508–515 (Oct. 1994).

58. Choi, S.-L. *et al.* The Regulation of AMP-Activated Protein Kinase by H2O2. *Biochem. Biophys. Res. Commun.* **287,** 92–97 (Sept. 2001).

59. Kar, R., Kellogg 3rd, D. L. & Roman, L. J. Oxidative stress induces phosphorylation of neuronal NOS in cardiomyocytes through AMP-activated protein kinase (AMPK). en. *Biochem. Biophys. Res. Commun.* **459,** 393–397 (Apr. 2015).

60. Ju, T.-C. *et al.* AMPK-α1 functions downstream of oxidative stress to mediate neuronal atrophy in Huntington's disease. en. *Biochim. Biophys. Acta* **1842,** 1668–1680 (Sept. 2014).

61. Pongkorpsakol, P. *et al.* Flufenamic acid protects against intestinal fluid secretion and barrier leakage in a mouse model of Vibrio cholerae infection through NF-κB inhibition and AMPK activation. en. *Eur. J. Pharmacol.* (Jan. 2017).

62. Soltoff, S. P. & Hedden, L. Regulation of ERK1/2 by ouabain and Na-K-ATPase-dependent energy utilization and AMPK activation in parotid acinar cells. en. *Am. J. Physiol. Cell Physiol.* **295,** C590–9 (Sept. 2008).

63. Flemmer, A. W., Gimenez, I., Dowd, B. F. X., Darman, R. B. & Forbush, B. Activation of the Na-K-Cl cotransporter NKCC1 detected with a phospho-specific antibody. en. *J. Biol. Chem.* **277,** 37551–37558 (Oct. 2002).

64. Marin, T. L. *et al.* Identification of AMP-activated protein kinase targets by a consensus sequence search of the proteome. *BMC Syst. Biol.* **9,** 13 (Mar. 2015).

65. Nguyen, T. D. & Canada, A. T. Modulation of human colonic T84 cell secretion by hydrogen peroxide. en. *Biochem. Pharmacol.* **47,** 403–410 (Jan. 1994).

66. DuVall, M. D., Guo, Y. & Matalon, S. Hydrogen peroxide inhibits cAMP-induced Cl secretion across colonic epithelial cells. en. *American Journal of Physiology - Cell Physiology* **275,** C1313–C1322 (Nov. 1998).

67. Scharl, M., Paul, G., Barrett, K. E. & McCole, D. F. AMP-activated protein kinase mediates the interferon-gamma-induced decrease in intestinal epithelial barrier function. en. *J. Biol. Chem.* **284,** 27952–27963 (Oct. 2009).

68. Auciello, F. R., Ross, F. A., Ikematsu, N. & Hardie, D. G. Oxidative stress activates AMPK in cultured cells primarily by increasing cellular AMP and/or ADP. en. *FEBS Lett.* **588,** 3361–3366 (Sept. 2014).

69. Liangpunsakul, S. *et al.* Effect of ethanol on hydrogen peroxide-induced AMPK phosphorylation. en. *Am. J. Physiol. Gastrointest. Liver Physiol.* **295,** G1173–81 (Dec. 2008).

70. López-Cotarelo, P. *et al.* A novel MEK-ERK-AMPK signaling axis controls chemokine receptor CCR7-dependent survival in human mature dendritic cells. en. *J. Biol. Chem.* **290,** 827–840 (Jan. 2015).

71. Zmijewski, J. W. *et al.* Exposure to hydrogen peroxide induces oxidation and activation of AMP-activated protein kinase. en. *J. Biol. Chem.* **285,** 33154–33164 (Oct. 2010).

72. Fraser, S. A. *et al.* Activation of AMPK reduces the co-transporter activity of NKCC1. en. *Mol. Membr. Biol.* **31,** 95–102 (Mar. 2014).

Chapter 4

1. Günzel, D. & Yu, A. S. L. Claudins and the modulation of tight junction permeability. en. *Physiol. Rev.* **93,** 525–569 (Apr. 2013).

2. Foretz, M. *et al.* Metformin inhibits hepatic gluconeogenesis in mice independently of the LKB1/AMPK pathway via a decrease in hepatic energy state. en. *J. Clin. Invest.* **120,** 2355–2369 (July 2010).

3. Miller, R. A. *et al.* Biguanides suppress hepatic glucagon signalling by decreasing production of cyclic AMP. en. *Nature* **494,** 256–260 (Feb. 2013).

4. Rao, E. *et al.* AMPK-dependent and independent effects of AICAR and compound C on T-cell responses. en. *Oncotarget* **7,** 33783–33795 (June 2016).

5. Glund, S. *et al.* Role of adenosine 5'-monophosphate-activated protein kinase in interleukin-6 release from isolated mouse skeletal muscle. en. *Endocrinology* **150,** 600–606 (Feb. 2009).

6. Bain, J. *et al.* The selectivity of protein kinase inhibitors: a further update. en. *Biochem. J* **408,** 297–315 (Dec. 2007).

7. Vogt, J., Traynor, R. & Sapkota, G. P. The specificities of small molecule inhibitors of the TGFß and BMP pathways. en. *Cell. Signal.* **23,** 1831–1842 (Nov. 2011).

8. Viollet, B. *et al.* The AMP-activated protein kinase alpha2 catalytic subunit controls whole-body insulin sensitivity. en. *J. Clin. Invest.* **111,** 91–98 (Jan. 2003).

9. Jørgensen, S. B. *et al.* Knockout of the alpha2 but not alpha1 5'-AMP-activated protein kinase isoform abolishes 5-aminoimidazole-4-carboxamide-1-beta-4-ribofuranoside but not contraction-induced glucose uptake in skeletal muscle. en. *J. Biol. Chem.* **279,** 1070–1079 (Jan. 2004).

10. Chappell, A. E. *et al.* Hydrogen peroxide inhibits Ca2+-dependent chloride secretion across colonic epithelial cells via distinct kinase signaling pathways and ion transport proteins. *FASEB J.* **22,** 2023–2036 (June 2008).

11. Blackmore, K., Zhou, W. & Dailey, M. J. LKB1-AMPK modulates nutrient-induced changes in the mode of division of intestinal epithelial crypt cells in mice. en. *Exp. Biol. Med.* 1535370217724427 (Jan. 2017).

12. Turer, E. *et al.* Creatine maintains intestinal homeostasis and protects against colitis. en. *Proc. Natl. Acad. Sci. U. S. A.* (Jan. 2017).

13. Heller, S. *et al.* Reduced mitochondrial activity in colonocytes facilitates AMPKα2-dependent inflammation. en. *FASEB J.* **31,** 2013–2025 (May 2017).

14. Sun, X., Yang, Q., Rogers, C. J., Du, M. & Zhu, M.-J. AMPK improves gut epithelial differentiation and barrier function via regulating Cdx2 expression. en. *Cell Death Differ.* (Feb. 2017).

15. Chen, L. *et al.* Activating AMPK to Restore Tight Junction Assembly in Intestinal Epithelium and to Attenuate Experimental Colitis by Metformin. *Front. Pharmacol.* **9,** 761 (2018).

16. Villanueva-Paz, M. *et al.* AMPK Regulation of Cell Growth, Apoptosis, Autophagy, and Bioenergetics. en. *EXS* **107,** 45–71 (2016).

17. Blagih, J. *et al.* The energy sensor AMPK regulates T cell metabolic adaptation and effector responses in vivo. en. *Immunity* **42,** 41–54 (Jan. 2015).

18. Williamson, D. L., Butler, D. C. & Alway, S. E. AMPK inhibits myoblast differentiation through a PGC-1alpha-dependent mechanism. en. *Am. J. Physiol. Endocrinol. Metab.* **297,** E304–14 (Aug. 2009).

19. Zhang, L., Li, J., Young, L. H. & Caplan, M. J. AMP-activated protein kinase regulates the assembly of epithelial tight junctions. *Proc. Natl. Acad. Sci. U. S. A.* **103,** 17272–17277 (Nov. 2006).

20. Zheng, B. & Cantley, L. C. Regulation of epithelial tight junction assembly and disassembly by AMP-activated protein kinase. *Proc. Natl. Acad. Sci. U. S. A.* **104,** 819–822 (Jan. 2007).

21. Zhang, L. *et al.* AMP-activated Protein Kinase (AMPK) Activation and Glycogen Synthase Kinase-3β (GSK-3β) Inhibition Induce Ca 2+ -independent Deposition of Tight Junction Components at the Plasma Membrane. *J. Biol. Chem.* **286,** 16879–16890 (May 2011).

22. Yano, T., Matsui, T., Tamura, A., Uji, M. & Tsukita, S. The association of microtubules with tight junctions is promoted by cingulin phosphorylation by AMPK. en. *J. Cell Biol.* **203,** 605–614 (Nov. 2013).

23. Xiang, R.-L. *et al.* Claudin-4 is required for AMPK-modulated paracellular permeability in submandibular gland cells. en. *J. Mol. Cell Biol.* **6,** 486–497 (Dec. 2014).

24. Peng, L., Li, Z.-R., Green, R. S., Holzman, I. R. & Lin, J. Butyrate enhances the intestinal barrier by facilitating tight junction assembly via activation of AMP-activated protein kinase in Caco-2 cell monolayers. *J. Nutr.* **139,** 1619–1625 (Sept. 2009).

25. Miao, W. *et al.* Sodium Butyrate Promotes Reassembly of Tight Junctions in Caco-2 Monolayers Involving Inhibition of MLCK/MLC2 Pathway and Phosphorylation of PKCβ2. en. *Int. J. Mol. Sci.* **17** (Oct. 2016).

26. Horman, S. *et al.* AMP-activated protein kinase phosphorylates and desensitizes smooth muscle myosin light chain kinase. en. *J. Biol. Chem.* **283,** 18505–18512 (July 2008).

27. Pongkorpsakol, P., Buasakdi, C., Chantivas, T., Chatsudthipong, V. & Muanprasat, C. An agonist of a zinc-sensing receptor GPR39 enhances tight junction assembly in intestinal epithelial cells via an AMPK-dependent mechanism. en. *Eur. J. Pharmacol.* **842,** 306–313 (Oct. 2018).

28. Park, H.-Y., Kunitake, Y., Hirasaki, N., Tanaka, M. & Matsui, T. Theaflavins enhance intestinal barrier of Caco-2 Cell monolayers through the expression of AMP-activated protein kinase-mediated Occludin, Claudin-1, and ZO-1. *Biosci. Biotechnol. Biochem.* **79,** 130–137 (2015).

29. Hallows, K. R., Raghuram, V., Kemp, B. E., Witters, L. A. & Foskett, J. K. Inhibition of cystic fibrosis transmembrane conductance regulator by novel interaction with the metabolic sensor AMP-activated protein kinase. en. *J. Clin. Invest.* **105,** 1711–1721 (June 2000).

30. Hallows, K. R., McCane, J. E., Kemp, B. E., Witters, L. A. & Foskett, J. K. Regulation of channel gating by AMP-activated protein kinase modulates cystic fibrosis transmembrane conductance regulator activity in lung submucosal cells. en. *J. Biol. Chem.* **278,** 998–1004 (Jan. 2003).

31. Hallows, K. R., Kobinger, G. P., Wilson, J. M., Witters, L. A. & Foskett, J. K. Physiological modulation of CFTR activity by AMP-activated protein kinase in polarized T84 cells. *Am. J. Physiol. Cell Physiol.* **284,** C1297–308 (May 2003).

32. Walker, J., Jijon, H. B., Churchill, T., Kulka, M. & Madsen, K. L. Activation of AMP-activated protein kinase reduces cAMP-mediated epithelial chloride secretion. *Am. J. Physiol. Gastrointest. Liver Physiol.* **285,** G850–60 (Nov. 2003).

33. Myerburg, M. M. *et al.* AMPK agonists ameliorate sodium and fluid transport and inflammation in cystic fibrosis airway epithelial cells. en. *Am. J. Respir. Cell Mol. Biol.* **42,** 676–684 (June 2010).

34. Collins, D. *et al.* Hypoxia inhibits colonic ion transport via activation of AMP kinase. en. *Ann. Surg.* **254,** 957–963 (Dec. 2011).

35. Hallows, K. R. *et al.* Up-regulation of AMP-activated Kinase by Dysfunctional Cystic Fibrosis Transmembrane Conductance Regulator in Cystic Fibrosis Airway Epithelial Cells Mitigates Excessive Inflammation. en. *J. Biol. Chem.* **281,** 4231–4241 (Feb. 2006).

36. Rogers, A. C. *et al.* Activation of AMPK inhibits cholera toxin stimulated chloride secretion in human and murine intestine. *PLoS One* **8,** e69050 (July 2013).

37. Kongsuphol, P. *et al.* Regulation of Cl(-) secretion by AMPK in vivo. en. *Pflugers Arch.* **457,** 1071–1078 (Mar. 2009).

38. King, S. J. *et al.* AMPK mediates inhibition of electrolyte transport and NKCC1 activity by reactive oxygen species. en. *Am. J. Physiol. Gastrointest. Liver Physiol.* (May 2019).

39. Kongsuphol, P. *et al.* Mechanistic insight into control of CFTR by AMPK. en. *J. Biol. Chem.* **284,** 5645–5653 (Feb. 2009).

40. Csanády, L. *et al.* Preferential phosphorylation of R-domain Serine 768 dampens activation of CFTR channels by PKA. en. *J. Gen. Physiol.* **125,** 171–186 (Feb. 2005).

41. Fraser, S. A. *et al.* Activation of AMPK reduces the co-transporter activity of NKCC1. en. *Mol. Membr. Biol.* **31,** 95–102 (Mar. 2014).

42. Bhalla, V. *et al.* AMP-activated kinase inhibits the epithelial Na+ channel through functional regulation of the ubiquitin ligase Nedd4-2. en. *J. Biol. Chem.* **281,** 26159–26169 (Sept. 2006).

43. Almaça, J. *et al.* AMPK controls epithelial Na(+) channels through Nedd4-2 and causes an epithelial phenotype when mutated. en. *Pflügers Archiv-European Journal of Physiology* **458,** 713–721 (Aug. 2009).

Chapter 5

1. Afrin, M. R. *et al.* Le Carbone, a charcoal supplement, modulates DSS-induced acute colitis in mice through activation of AMPKα and downregulation of STAT3 and caspase 3 dependent apoptotic pathways. en. *Int. Immunopharmacol.* **43,** 70–78 (Feb. 2017).

2. Bai, A. *et al.* Novel anti-inflammatory action of 5-aminoimidazole-4-carboxamide ribonucleoside with protective effect in dextran sulfate sodium-induced acute and chronic colitis. en. *J. Pharmacol. Exp. Ther.* **333,** 717–725 (June 2010).

3. Bai, A. *et al.* AMPK agonist downregulates innate and adaptive immune responses in TNBS-induced murine acute and relapsing colitis. en. *Biochem. Pharmacol.* **80,** 1708–1717 (Dec. 2010).

4. Chang, K.-W. & Kuo, C.-Y. 6-Gingerol modulates proinflammatory responses in dextran sodium sulfate (DSS)-treated Caco-2 cells and experimental colitis in mice through adenosine monophosphate-activated protein kinase (AMPK) activation. *Food Funct.* **6,** 3334–3341 (July 2015).

5. Mattaveewong, T. *et al.* Chitosan oligosaccharide suppresses tumor progression in a mouse model of colitis-associated colorectal cancer through AMPK activation and suppression of NF-κB and mTOR signaling. *Carbohydr. Polym.* **145,** 30–36 (July 2016).

6. Koh, S.-J., Kim, J. M., Kim, I.-K., Ko, S. H. & Kim, J. S. Anti-inflammatory mechanism of metformin and its effects in intestinal inflammation and colitis-associated colon cancer. *J. Gastroenterol. Hepatol.* **29,** 502–510 (Mar. 2014).

7. Xue, Y., Zhang, H., Sun, X. & Zhu, M.-J. Metformin Improves Ileal Epithelial Barrier Function in Interleukin-10 Deficient Mice. en. *PLoS One* **11,** e0168670 (Dec. 2016).

8. Foretz, M. *et al.* Metformin inhibits hepatic gluconeogenesis in mice independently of the LKB1/AMPK pathway via a decrease in hepatic energy state. en. *J. Clin. Invest.* **120,** 2355–2369 (July 2010).

9. Miller, R. A. *et al.* Biguanides suppress hepatic glucagon signalling by decreasing production of cyclic AMP. en. *Nature* **494,** 256–260 (Feb. 2013).

10. Chen, S. C. *et al.* Metformin suppresses adipogenesis through both AMP-activated protein kinase (AMPK)-dependent and AMPK-independent mechanisms. en. *Mol. Cell. Endocrinol.* **440,** 57–68 (Jan. 2017).

11. Chassaing, B., Aitken, J. D., Malleshappa, M. & Vijay-Kumar, M. en. in *Current Protocols in Immunology* (eds Coligan, J. E., Bierer, B. E., Margulies, D. H., Shevach, E. M. & Strober, W.) 15.25.1–15.25.14 (John Wiley & Sons, Inc., Hoboken, NJ, USA, Feb. 2014).

12. Hernández-Chirlaque, C. *et al.* Germ-free and Antibiotic-treated Mice are Highly Susceptible to Epithelial Injury in DSS Colitis. en. *J. Crohns. Colitis* **10,** 1324–1335 (Nov. 2016).

13. Dieleman, L. A. *et al.* Dextran sulfate sodium-induced colitis occurs in severe combined immunodeficient mice. en. *Gastroenterology* **107,** 1643–1652 (Dec. 1994).

14. Laroui, H. *et al.* Dextran sodium sulfate (DSS) induces colitis in mice by forming nano-lipocomplexes with medium-chain-length fatty acids in the colon. *PLoS One* **7,** e32084 (Mar. 2012).

15. Kenny, B. & Jepson, M. Targeting of an enteropathogenic Escherichia coli (EPEC) effector protein to host mitochondria. en. *Cell. Microbiol.* **2,** 579–590 (Dec. 2000).

16. Ma, C. *et al.* Citrobacter rodentium infection causes both mitochondrial dysfunction and intestinal epithelial barrier disruption in vivo: role of mitochondrial associated protein (Map). *Cell. Microbiol.* **8,** 1669–1686 (2006).

17. Mundy, R. *et al.* Identification of a novel type IV pilus gene cluster required for gastrointestinal colonization of Citrobacter rodentium. en. *Mol. Microbiol.* **48,** 795–809 (May 2003).

18. Deng, W. *et al.* Dissecting virulence: systematic and functional analyses of a pathogenicity island. en. *Proc. Natl. Acad. Sci. U. S. A.* **101,** 3597–3602 (Mar. 2004).

19. Sun, X., Yang, Q., Rogers, C. J., Du, M. & Zhu, M.-J. AMPK improves gut epithelial differentiation and barrier function via regulating Cdx2 expression. en. *Cell Death Differ.* (Feb. 2017).

20. Gongol, B. *et al.* AMPKα2 exerts its anti-inflammatory effects through PARP-1 and Bcl-6. *Proc. Natl. Acad. Sci. U. S. A.* **110,** 3161–3166 (Feb. 2013).

21. Meares, G. P., Qin, H., Liu, Y., Holdbrooks, A. T. & Benveniste, E. N. AMP-activated protein kinase restricts IFN-γ signaling. en. *J. Immunol.* **190,** 372–380 (Jan. 2013).

22. Zhang, B., Lakshmanan, J., Du, Y., Smith, J. W. & Harbrecht, B. G. Cell-specific regulation of iNOS by AMP-activated protein kinase in primary rat hepatocytes. en. *J. Surg. Res.* **221,** 104–112 (Jan. 2018).

23. Simeoli, R. *et al.* An orally administered butyrate-releasing derivative reduces neutrophil recruitment and inflammation in dextran sulphate sodium-induced murine colitis. en. *Br. J. Pharmacol.* **174,** 1484–1496 (June 2017).

24. Koroleva, E. P. *et al.* Citrobacter rodentium-induced colitis: A robust model to study mucosal immune responses in the gut. *J. Immunol. Methods* **421,** 61–72 (June 2015).

25. Scharl, M., Paul, G., Barrett, K. E. & McCole, D. F. AMP-activated protein kinase mediates the interferon-gamma-induced decrease in intestinal epithelial barrier function. en. *J. Biol. Chem.* **284,** 27952–27963 (Oct. 2009).

26. Sun, X., Du, M., Navarre, D. A. & Zhu, M.-J. Purple Potato Extract Promotes Intestinal Epithelial Differentiation and Barrier Function by Activating AMP-activated Protein Kinase. en. *Mol. Nutr. Food Res.* (Nov. 2017).

27. Villanueva-Paz, M. *et al.* AMPK Regulation of Cell Growth, Apoptosis, Autophagy, and Bioenergetics. en. *EXS* **107,** 45–71 (2016).

28. Viollet, B. *et al.* The AMP-activated protein kinase alpha2 catalytic subunit controls whole-body insulin sensitivity. en. *J. Clin. Invest.* **111,** 91–98 (Jan. 2003).

29. Rakoff-Nahoum, S., Paglino, J., Eslami-Varzaneh, F., Edberg, S. & Medzhitov, R. Recognition of commensal microflora by toll-like receptors is required for intestinal homeostasis. en. *Cell* **118,** 229–241 (July 2004).

30. Round, J. L. & Mazmanian, S. K. The gut microbiota shapes intestinal immune responses during health and disease. *Nat. Rev. Immunol.* **9,** 313–323 (May 2009).

31. Wei, W. *et al.* Protective effects of wedelolactone on dextran sodium sulfate induced murine colitis partly through inhibiting the NLRP3 inflammasome activation via AMPK signaling. en. *Biomed. Pharmacother.* **94,** 27–36 (July 2017).

32. Turer, E. *et al.* Creatine maintains intestinal homeostasis and protects against colitis. en. *Proc. Natl. Acad. Sci. U. S. A.* (Jan. 2017).

33. Kasper, S. H. *et al.* Deficiency of Protein Tyrosine Phosphatase Non-Receptor Type 2 in Intestinal Epithelial Cells Has No Appreciable Impact on Dextran Sulphate Sodium Colitis Severity But Promotes Wound Healing. en. *Digestion* **93,** 249–259 (Apr. 2016).

34. Sag, D., Carling, D., Stout, R. D. & Suttles, J. Adenosine 5'-monophosphate-activated protein kinase promotes macrophage polarization to an anti-inflammatory functional phenotype. en. *J. Immunol.* **181,** 8633–8641 (Dec. 2008).

35. Araki, Y., Mukaisyo, K.-I., Sugihara, H., Fujiyama, Y. & Hattori, T. Increased apoptosis and decreased proliferation of colonic epithelium in dextran sulfate sodium-induced colitis in mice. en. *Oncol. Rep.* **24,** 869–874 (Oct. 2010).

36. Sheng, Y. H. *et al.* The MUC13 cell-surface mucin protects against intestinal inflammation by inhibiting epithelial cell apoptosis. en. *Gut* **60,** 1661–1670 (Dec. 2011).

37. Su, L. *et al.* TNFR2 activates MLCK-dependent tight junction dysregulation to cause apoptosis-mediated barrier loss and experimental colitis. en. *Gastroenterology* **145,** 407–415 (Aug. 2013).

38. Le, D.-D. T. *et al.* Inhibitory role of AMP-activated protein kinase in necroptosis of HCT116 colon cancer cells with p53 null mutation under nutrient starvation. en. *Int. J. Oncol.* (Nov. 2018).

39. Wen, S. *et al.* Necroptosis is a key mediator of enterocytes loss in intestinal ischaemia/reperfusion injury. en. *J. Cell. Mol. Med.* **21,** 432–443 (Mar. 2017).

40. Wang, Y.-S. *et al.* AMP-activated protein kinase protects against necroptosis via regulation of Keap1-PGAM5 complex. en. *Int. J. Cardiol.* **259,** 153–162 (May 2018).

41. Maiti, A. K. *et al.* IL-4 Protects the Mitochondria Against TNFα and IFNγ Induced Insult During Clearance of Infection with Citrobacter rodentium and Escherichia coli. en. *Sci. Rep.* **5,** 15434 (Oct. 2015).

42. Berger, C. N. *et al.* Citrobacter rodentium Subverts ATP Flux and Cholesterol Homeostasis in Intestinal Epithelial Cells In Vivo. en. *Cell Metab.* **26,** 738–752.e6 (Nov. 2017).

43. Inoue, J. *et al.* Autophagy in the intestinal epithelium regulates Citrobacter rodentium infection. *Arch. Biochem. Biophys.* **521,** 95–101 (May 2012).

Chapter 6

1. Bhalla, V. *et al.* AMP-activated kinase inhibits the epithelial Na+ channel through functional regulation of the ubiquitin ligase Nedd4-2. en. *J. Biol. Chem.* **281,** 26159–26169 (Sept. 2006).

2. Almaça, J. *et al.* AMPK controls epithelial Na(+) channels through Nedd4-2 and causes an epithelial phenotype when mutated. en. *Pflügers Archiv-European Journal of Physiology* **458,** 713–721 (Aug. 2009).

3. Benziane, B. *et al.* AMP-activated protein kinase activator A-769662 is an inhibitor of the Na(+)-K(+)-ATPase. en. *Am. J. Physiol. Cell Physiol.* **297,** C1554–66 (Dec. 2009).

4. Ingwersen, M. S. *et al.* Na,K-ATPase activity in mouse muscle is regulated by AMPK and PGC-1α. en. *J. Membr. Biol.* **242,** 1–10 (July 2011).

5. Pieri, M., Christian, H. C., Wilkins, R. J., Boyd, C. A. R. & Meredith, D. The apical (hPepT1) and basolateral peptide transport systems of Caco-2 cells are regulated by AMP-activated protein kinase. en. *Am. J. Physiol. Gastrointest. Liver Physiol.* **299,** G136–43 (July 2010).

6. Sakar, Y. *et al.* Metformin-induced regulation of the intestinal D-glucose transporters. en. *J. Physiol. Pharmacol.* **61,** 301–307 (June 2010).

7. Sopjani, M. *et al.* Regulation of Na+-coupled glucose carrier SGLT1 by AMP-activated protein kinase. en. *Mol. Membr. Biol.* **27,** 137–144 (Apr. 2010).

8. Krimi, R. B. *et al.* Resistin-like molecule-beta inhibits SGLT-1 activity and enhances GLUT2-dependent jejunal glucose transport. *Diabetes* **58,** 2032–2038 (Sept. 2009).

9. Gabler, N. K., Radcliffe, J. S., Spencer, J. D., Webel, D. M. & Spurlock, M. E. Feeding long-chain n-3 polyunsaturated fatty acids during gestation increases intestinal glucose absorption potentially via the acute activation of AMPK. en. *J. Nutr. Biochem.* **20,** 17–25 (Jan. 2009).
10. Walker, J. *et al.* 5-aminoimidazole-4-carboxamide riboside (AICAR) enhances GLUT2-dependent jejunal glucose transport: a possible role for AMPK. *Biochem. J* **385,** 485–491 (Jan. 2005).
11. Zmijewski, J. W. *et al.* Exposure to hydrogen peroxide induces oxidation and activation of AMP-activated protein kinase. en. *J. Biol. Chem.* **285,** 33154–33164 (Oct. 2010).
12. Scharl, M., Paul, G., Barrett, K. E. & McCole, D. F. AMP-activated protein kinase mediates the interferon-gamma-induced decrease in intestinal epithelial barrier function. en. *J. Biol. Chem.* **284,** 27952–27963 (Oct. 2009).
13. Rogers, A. C. *et al.* Activation of AMPK inhibits cholera toxin stimulated chloride secretion in human and murine intestine. *PLoS One* **8,** e69050 (July 2013).
14. Pongkorpsakol, P. *et al.* Flufenamic acid protects against intestinal fluid secretion and barrier leakage in a mouse model of Vibrio cholerae infection through NF-κB inhibition and AMPK activation. en. *Eur. J. Pharmacol.* (Jan. 2017).
15. Sun, X., Yang, Q., Rogers, C. J., Du, M. & Zhu, M.-J. AMPK improves gut epithelial differentiation and barrier function via regulating Cdx2 expression. en. *Cell Death Differ.* (Feb. 2017).

.1 List of acronyms

ACC Acetyl-CoA Carboxylase

ADP Adenosine diphosphate

AICAR 5-Aminoimidazole-4-carboxamide ribonucleotide

AID Auto-inhibitory domain

AMP Adenosine monophosphate

AMP Antimicrobial peptide

AMPK AMP-activated protein kinase

AMPK$\alpha^{fl/fl}$ AMPKα floxed mice

AMPK$\alpha^{\Delta IEC\ KO}$ AMPKα intestinal epithelial-specific knockout

ATP Adenosine triphosphate

CaCC Calcium-activated chloride channels

CaMKKβ Ca^{2+}/Calmodulin-Kinase Kinase β

cAMP Cyclic adenosine monophosphate

CC Compound C

CCh Carbachol

CCL2 C-C motif chemokine ligand 2

CD Crohn's Disease

Cdx2 Caudal type homeobox 2 transcription factor

CFTR Cystic Fibrosis transmembrane conductance regulator

DNA Deoxyribonucleic acid

DSS Dextran sodium sulfate or Dextran sulfate sodium

EDTA Ethylenediaminetetraacetic acid

EHEC Enterohemorrhagic *Escherichia coli*

ENaC Epithelial Na^+ channel

EPEC Enteropathogenic *Escherichia coli*

ERK1/2 Extracellular signal-regulated kinase 1/2

FITC-dextran Fluorescein isothiocyanate-dextran

Fsk Forskolin

GALT Gut-associated lymphoid tissue

H_2O_2 Hydrogen peroxide

IBD Inflammatory Bowel Disease

IECs Intestinal epithelial cells

IFNγ Interferon-γ

IL-1β Interleukin-1β

IL-10 Interleukin-10

IL-6 Interleukin-6

iNOS Inducible nitric oxide synthase

Isc Short-circuit current

KBR Kreb's Ringer's buffer

LB Lysogeny broth

LKB1 Liver kinase beta 1

LPS Lipopolysaccharide

MAPK Mitogen-activated protein kinase

MLC Myosin light chain

MLCK Myosin light-chain II kinase

mTOR Mammalian target of Rapamycin

Na^+/K^+-ATPase Sodium-Potassium Adenosine triphosphatase

NADPH Nicotinamide adenine dinucleotide phosphate

NF-$\varkappa$B Nuclear factor-kappa B transcription factor

NKCC1 $Na^+/K^+/2Cl^-$ Cotransporter

NOD-like receptor Nucleotide-binding oligomerization domain-like receptor

Nos2 Gene encoding mouse inducible nitric oxide synthase

OSR1 Oxidative stress response kinase 1

PARP Poly (ADP-ribose) polymerase

PBS Phosphate-buffered saline

PI3K Phosphoinositide-3 kinase

PKA Protein kinase A

PKC Protein kinase C

PP2αC Protein Phosphatase 2αC

Prkaa1 Mouse gene encoding AMPK catalytic alpha 1 subunit

Prkaa2 Mouse gene encoding AMPK catalytic alpha 2 subunit

Pyk2 Protein Tyrosine Kinase 2 Beta

RIM Regulatory interacting motifs

RNA Ribonucleic acid

ROS Reactive oxygen species

p70-S6K Ribosomal protein S6 kinase β1

Ser Serine

SCID Severe-combined immunodeficiency

sIgA Secretory Immunoglobulin A

SPAK STE20-related proline-alanine-rich kinase

Src Proto-oncogene tyrosine-protein kinase Src

STK11 Human gene encoding Liver Kinase B1

TAMPs Tight junction-associated Marvel proteins

TBST Tris-buffered saline + Tween-20

TEER Transepithelial electrical resistance

Thr Threonine

TGF-β Transforming growth factor-β

Th T-helper cell

TLR Toll-like receptor

TMCH Transmissible murine crypt hyperplasia

TNF-α Tumor necrosis factor-α

Treg T-regulatory cell

TUNEL Terminal deoxynucleotidyl transferase dUTP nick end labeling

UC Ulcerative colitis

ZMP AICAR 5'-monophosphate

ZO-1 Zonula occludens-1

.2 PCR primer sequences

PCR Primer Sequences	
Ccl2 Forward	5'-ATCAATGCCCCAGTCACCTG-3'
Ccl2 Reverse	5'-TCTCCTTGGCCACAATGGTC-3'
Nos2 Forward	5'-TCCCGAAGTTCTCAAGGCAC-3'
Nos2 Reverse	5'-TCCAAGGACAGGCCATCTCT-3'
Gapdh Forward	5'-GTTTGTGATGGGTGTGAACCACG-3'
Gapdh Reverse	5'-GTGGCAGTGATGGCATGGAC-3'

.3 Buffer solutions

1X Phosphate-buffered saline: 137 mM NaCl, 10 mM Phosphate, 2.7 mM KCl, pH 7.4

1X Running buffer: 250 mM Tris, 1.92 M glycine, 0.1% Sodium Dodecyl Sulfate, pH 8.3

1X Transfer buffer: 25 mM Tris, 190 mM glycine, 20% methanol, pH 8.3

1X Transfer buffer for high molecular weight proteins: 25 mM Tris, 190 mM glycine, 10% methanol, pH 8.3

1X Tris-buffered saline with Tween-20: 20 mM Tris pH 7.5, 150 mM NaCl, 0.1% Tween 20

1X PBS-Tween-20: 137 mM NaCl, 10 mM Phosphate, 2.7 mM KCl, 0.1% Tween 20, pH 7.4